Opération Cadre Régional Beachmed-e

Projet OpTIMAL

Optimisation des Techniques Intégrées de Monitorage Appliquées aux Littoraux

Cahier Technique de Phase B

Décembre 2007

Chef de File: Enzo Pranzini

Partnership:

1. Dip. Sc. della Terra, Università degli Studi di Firenze
2. DISTART, Università degli Studi di Bologna
3. DIPTERIS, Università degli Studi di Genova
4. Dip. Sc. della Terra, Università degli Studi di Roma “La Sapienza”
5. ARPA, Ingegneria Ambientale
6. EID Méditerranée
7. OANAK
8. IACM, FORTH
9. School of Engineering, Democritus University of Thrace
10. ICM

Key-words: Coastal Evolution, Mediterranean, Monitoring Techniques

Table of Contents

Presentation

During the preceding Phase A of Interreg IIIc sud "Opération Cadre Régional Beachmed-e", we have reviewed the scientific literature about beach monitoring techniques, which has been presented in the I (Phase A) Cahier Technique of operation Beachmed-e. Following the end of Phase A, each partner has developed methodological tests, in order to choose the method they will be applying in the pilot studies of Phase C of the project. Tests and the resulting methods chosen by each partner are presented in this II (Phase B) Cahier Technique. Some preliminary results of the methodological application are shown.

The following techniques and approaches to the study of beach evolution have been considered during this phase of the project by partners of OpTIMAL (the description of each subject can be found in the phase A *First Cahier Technique of Opération Beachmed-e* (Beachmed-e, 2007):

- Satellite remote sensing techniques
- Video systems/Webcams
- ALB/LIDAR
- High Resolution Seismic
- Intrinsic variability of beaches
- Network of Sea Control Points
- Numerical models

These approaches to beach monitoring will be applied together (for example, satellite images and numerical modelling), and/or in association with other techniques, such as photogrammetry, Multibeam, GPS, sedimentological analysis. This will allow to calibrate their use and application, and evaluate their accuracy.

P1 - Dip. Sc. della Terra, Università degli Studi di Firenze

Enzo Pranzini (epranzini@unifi.it); Sara Carli (sara.carli@unifi.it); Dan Bowman (dbowman@bgu.ac.il); Lilian Wetzel (lilian.wetzel@unifi.it)

This partner conducts their research on 3 lines: (A) the study of intrinsic variability of beaches; (B) the development and test of bathymetric control points (Sea Control Points); and (C) the development of techniques for optimising the definition of shoreline position using satellite images.

Intrinsic beach variability

The state-of-the-art of "monitoring long-term trends of shoreline migration versus event and seasonal short-term behaviour" indicated the following major topics and guidelines to be applied as part of our recommended methodology for monitoring shorelines:

- Long term trends may become masked in the light of dynamic short-term changes, including those triggered by engineering activity. It is of interest to examine how far do shoreline changes reflect trends in the beach sedimentary budget, and how far do vertical changes in the backshore morphology, including the coastal foredune, fit the trends of the shoreline fluctuations.

- Shoreline and the subaerial beach behaviour may reflect less the long term trends, compared to the more dynamic subaqueous changes. Profiles may show antinodes of maximum change onshore and offshore of the waterline, which may behave as a nodal zone.

- It is recommended to avoid or filter out any phenomena which may be in phase with any spatial/temporal rhythmic shoreline behaviour. The measurement resolution should be greater than the relevant analysed shoreline fluctuation.

Hot spots

Hot spots are coastal segments with the highest shoreline shift due to combinations of processes, including energy concentration by refraction. Storm effects may last here beyond seasonal periods and the duration of healing may also be very fast. Hot spots are of the highest hazard potential. An effort should be made to examine to what degree are the extreme shoreline fluctuations at hot spots site-specific - what their spatial long-term trend of migration as well as their variability are. Examination of historical repetitions of maximum run up penetration by grass boundary is relevant. The change in the mean inland limit of overwash penetration + STD or in the extreme wave run up line may be most significant for estimating the probability of the future coastal erosion.

Extreme erosion shorelines and the periods of accretion that follow can lead to erroneous calculations of long term trends. It is recommended that such extreme shorelines, which do not represent the long-range processes, should be removed from data sets attempting to determine long-term trends. However, storms are the most dramatic agent of shoreline change and may cause tens of meters of shoreline migration over days, equivalent to tens of years of gradual shoreline change. We intend to examine this issue on part of the Toscana shoreline data.

Rates

We shall recommend to regard shoreline changes of < 0.1 m/y as micro, and shoreline migration rates in the range of 0.1- 0.9 m/y as meso. The meso range is the dominating migration rate along most of the world shorelines. Short-term meso-rates may be found in beaches with a balanced sediment budget. Shoreline migration rates of 1 m/y and larger indicate rapid to extreme high rates. Interannual / interdecadal variations can deviate for at least a limited time by an amount larger than the long-term mean rate of shoreline change.

Monitoring periods

Shoreline beach trends will be evaluated according to the following temporal monitoring scale: single storm events; seasonal/annual scale of months to a few single years; short historic scale of a time slice of multi-decadal years; and long- term monitoring of historic periods of multi-centennial years. Former studies proved that the temporal variance of shoreline migration is 3-4 times greater than the spatial one. The time span of coverage should be a few times longer than the time span interested. To capture short term variation the temporal resolution should be at least two orders of magnitude finer than the interested variation.

Spatial sampling

Erosion and accumulation are variable alongshore. The spatial sampling intervals determine the standard deviation of the shoreline changes. The variance is positively linked to the spatial spacing. Sampling intervals of < 5km are recommended. Regular sampling should not be caught in any along-coast periodicity.

Following the positive relation between spacing of beach profiles and the variability between the transects, we shall define an "optimal transect spacing" that will minimize the variability between adjacent transects without composing a too dense net of profiles.

Sea Control Points

Since the accuracy of bathymetric data is limited in respect to the needs of the analysis of coastal sediment stock budget, both in natural conditions and after beach nourishments, Sea Control Points (SCPs) were created and tested to calibrate acoustics soundings.

SCPs consist in a reflector located on 3-meter-long poles which can be infixed into the seafloor for 2 ÷ 2.5 m using traditional coring techniques; in our case the Polaris s.r.l. corer onboard a 15 m long boat was used. Reflector size varies from is 1m x 1m to 1.5m x 1.5m according to the installation depth. This stable surface, once their echo is recognised on analogical or digital data, allows ecosounder calibration or profile-fitting if during each survey an overpass on the SCP is verified. One steel ring was slipped on each SCP pole to evaluate the disturbance depth and to validate the computed depth of closure.

A first series of 3 SCPs was installed into the sea bottom at -4, -6 and -10 m in front of the Arno River mouth and profiles intercepting them were acquired by Geo Coste s.r.l. at different times; they allowed to evaluate the improvement in the nearshore evolution analysis given by this system.

In Figures 1 and 2 uncalibrated and SCP-calibrated profile evolution is represented showing an approximately 3.5 - 4 cm displacement.

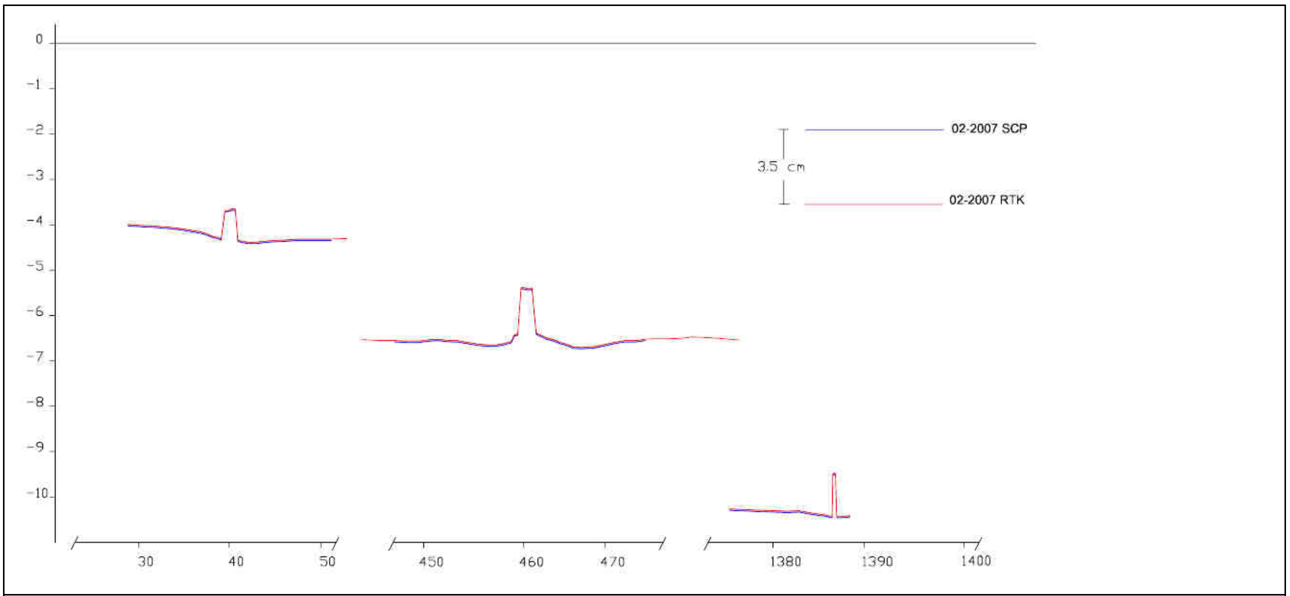

Figure 1: Uncalibrated (RTK) and calibrated (SCP) profiles at Bocca d’Arno acquired on February 2007.

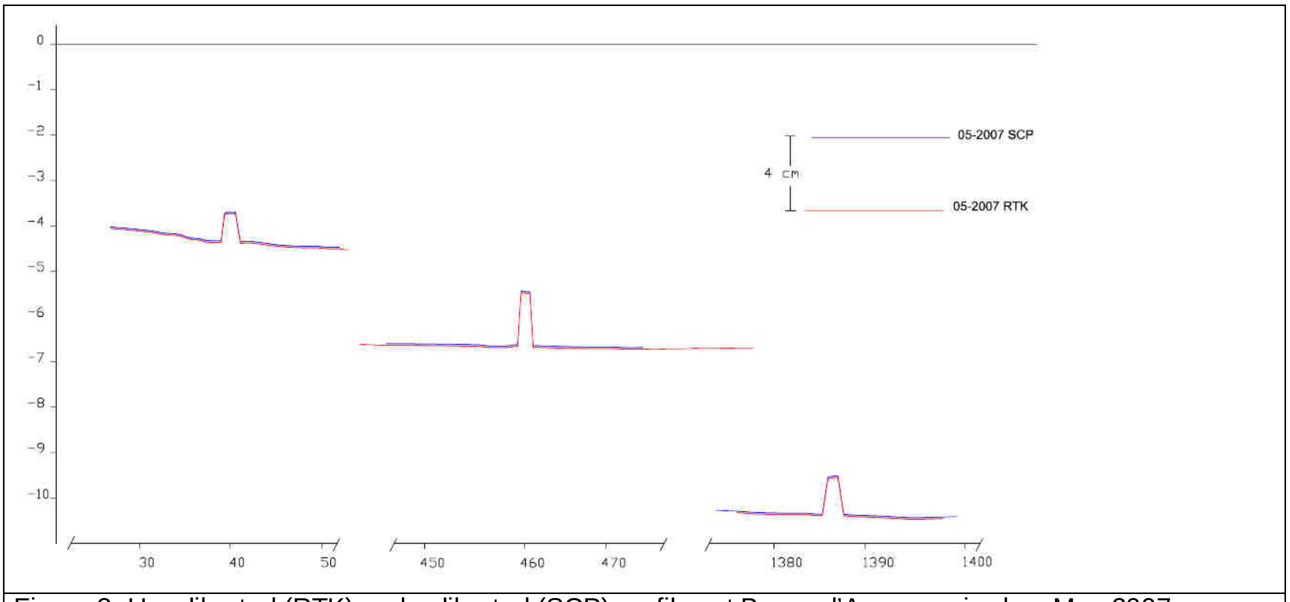

Figure 2: Uncalibrated (RTK) and calibrated (SCP) profiles at Bocca d’Arno acquired on May 2007.

Further, one SCP was placed at 3 m depth offshore the low-crested breakwater facing the town of Follonica, which will be used to improve the accuracy of nearshore evolution monitoring after the construction of this defence structure.

In Figure 3 a 3D model of the nearshore is represented showing the SCP, together with a nearshore profile crossing the SCP.

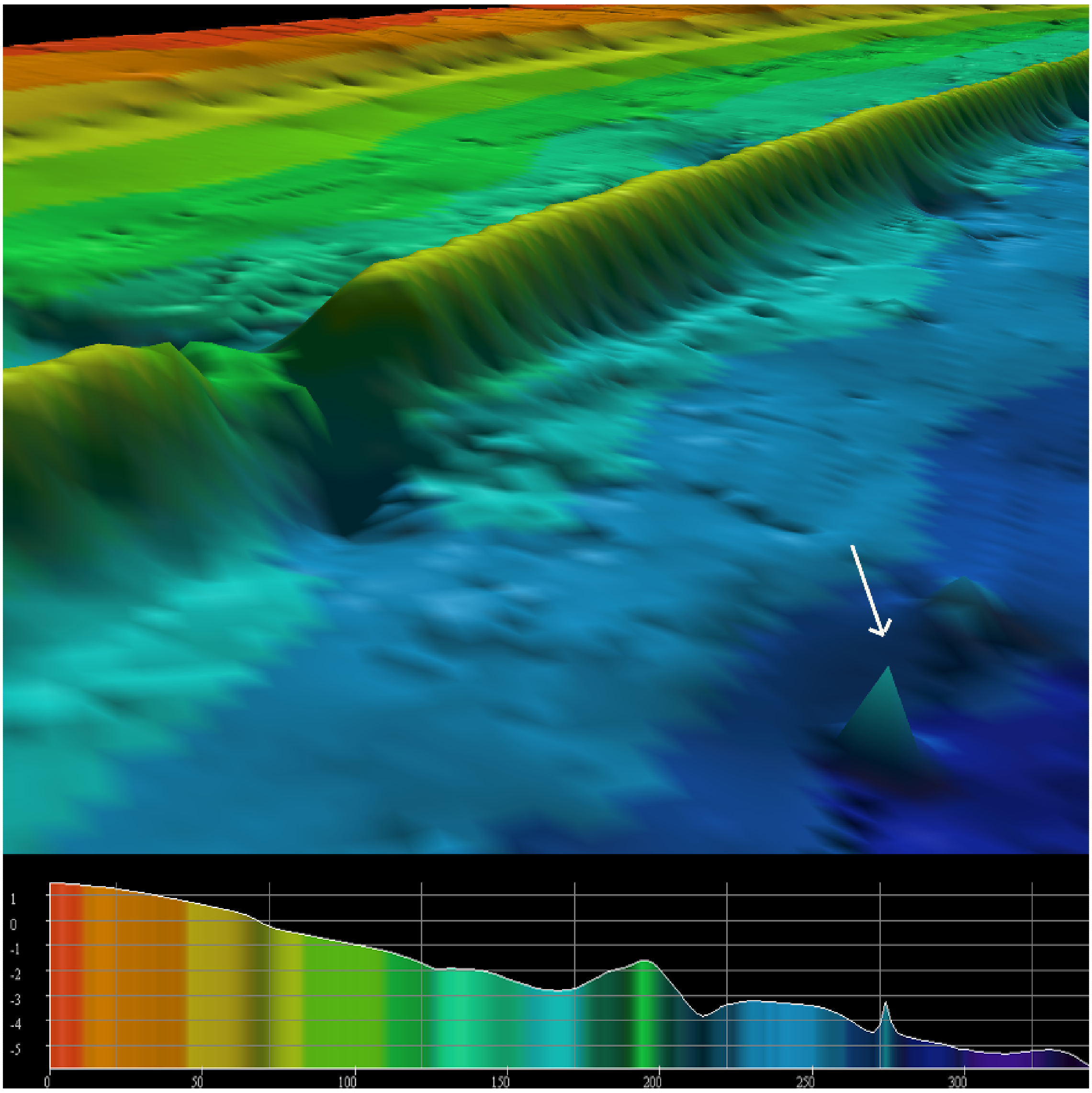

Figure 3: 3D model of the nearshore showing the SCP (arrow) (top), and beach profile crossing the SCP (bottom).

Satellite Remote Sensing

During this phase of the project, we have applied some of the procedures that we had identified in the previous phase of the project, which put into evidence the important role that remote sensing has in the study and monitoring of coastal evolution. The first step of this research was carried in collaboration with subcontractor CNR-IIA (Remote Sensing Laboratory) measuring sand reflectivity at the beach of Prato Ranieri (Golfo di Follonica, Grosseto, Italy).

A portable field spectral-radiometer (FieldSpeck FR) was used for direct *in situ* measurements of the electromagnetic radiation that is reflected by sand at wavelength intervals within the range of 350 nm (ultraviolet) and 2500 nm (infrared). The transect was 27 m long, extending from the dune toe to the step zone; the reflectivity measurements of rugged sand were taken every 3-5 meters, after instrument calibration with a white panel of *Spectralon*. Near the swash zone, measurements along the transect were taken at shorter intervals of beach width, in order to emphasise the differences between wet sand and sand that is covered only by a shallow layer of water.

Figure 4 shows spectral signatures of sand at different wave lengths at control points. We can observe the difference between the upper four spectral signatures, representing the four points of dry sand measured, and the following three points representing sand with different degrees of wetness. The last spectral signature identifies sand covered by a shallow layer of water. From the spectral signatures, we can see different reflectivity also among the dry sand group; these differences are more evident in the infrared wavelengths, compared to the visible one. These differences of reflectivity are due to intrinsic properties of the sand, such us: rough surface, petrography, detritus. In wet sand we can note differences also in sands at different degrees of wetness, this means that if one should use spectral signatures for the identification of the limit between wet sand and water, their reflectivity values could be used as a separation index for mixed pixel. Figure 5 shows the average spectral signature of three different zones: dry sand, wet sand, and sand saturated by water.

At this step, it was not possible to have the acquisition of a satellite image at the exact time of the tests carried on the beach, and therefore we were not able to extract spectral signatures on the image in order to compare them with those obtained by the spectral-radiometer.

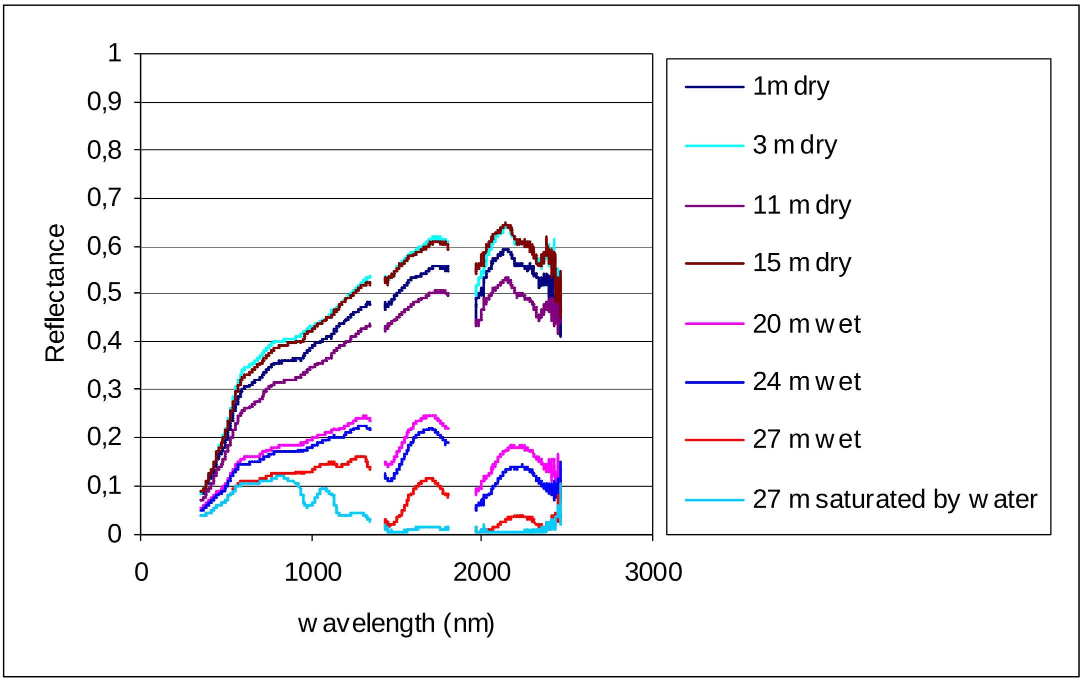

Figure 4: Spectral signatures of sand at control points

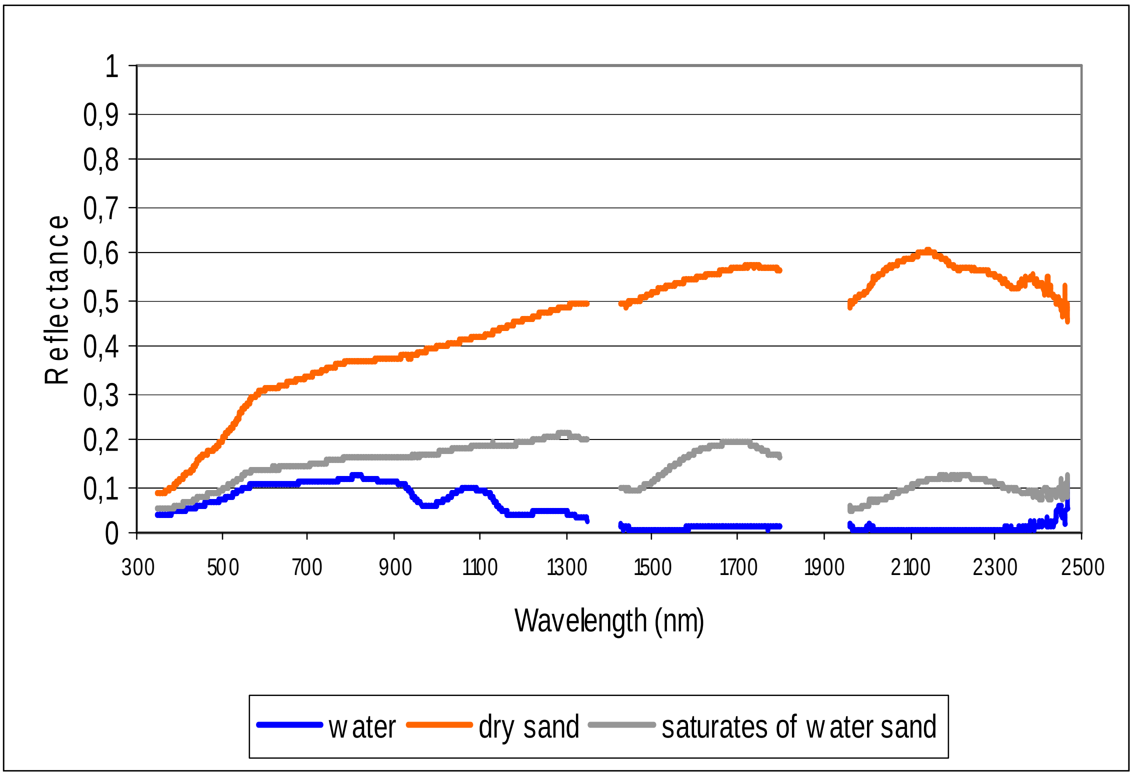

Figure 5: Average spectral signatures of the 3 sampling zones

An Ikonos image was though acquired on 18 April 2007 which covered the whole Golfo di Follonica. The official Italian distributor of Ikonos images (Planetek Italia s.r.l) has previously informed us the date and exact time of satellite passage, and therefore it was possible to plan and perform a contemporaneous GPS survey of: a) the position of the instantaneous waterline and b) the line separating dry sand and wet sand. Due to fortuitous logistic problems, it was not possible to organize a land survey at the same time of the satellite passage.

The ortho-rectified true colour image of Golfo di Follonica was overlaid on top of the 1:10.000 regional technical chart (*Carta Tecnica Regionale*) in order to verify the accuracy of georeferencing. This was followed by manual digitalisation of the instantaneous waterline identified by photointerpretation.

The digitalised waterline was also overlaid on top of the Ikonos image at the infrared band, where white pixels from wave foam are not observable and therefore do not cause interferences. The use of such wave length proved useful in order to verify the accuracy of photointerpretation of the instantaneous waterline position. Further verification was carried importing points that had been surveyed with GPS, which represent the waterline surveyed in the field. The waterline derived from the satellite image results slightly displaced towards the land in relation to the waterline position obtained by GPS. The comparison between these two waterlines has turned out satisfactory for the scope of verifying the correct positioning of the digitalised waterline.

Afterwards, we have imported also the points that represent the zero isoipse which had been used as reference for translating the waterline digitalised by hand: it was possible in this way to assimilate the remote waterline to the shoreline with quota zero on the sea level. After such translation the remote waterline can be used for the comparison with historical shoreline datasets.

Data show that in average the latter is displaced 2,7 m inland. This value was obtained from the average of distances between the zero isoipse points and the waterline resulting from photointerpretation. In order to understand this difference, we have calculated the quote error that such distances may have along the emerged beach profile. In fact, the longest distance measured between point zero and the shoreline is of 9,39 m and its quote error is of 0,37 m. This value is compatible with the emerged beach profile.

During the GPS survey, the distance between the waterline and the limit of wet sand was also measured. In the elaboration of the spectral transect along such distances, on the image at infrared wave length, the reflectivity intervals of pixels, in the different zones of the emerged beach profile, have been emphasised. For profile 1 (Fig. 6) we can also observe the limits between two different degrees of sand wetness, before the dry sand pixels which are highly reflective. Figure 7 shows the values that the transect presents at the different wave lengths of the acquired image. The line that represents the DN (Digital Number) profile in the infrared is the one which best identifies the limit between water pixel and pixel of wet sand, identifying also the run-up zone. This narrow pixel band is not influenced by the presence of wave foam since the reflectivity values of the corresponding pixel do not alter the spectral response in this wave length. It is likely that such pixel values can be used as a limit in order to identify the exact position of the shoreline, which can be further corrected with tidal and pressure data from the time when the satellite image was acquired in order to obtain the zero isobate.

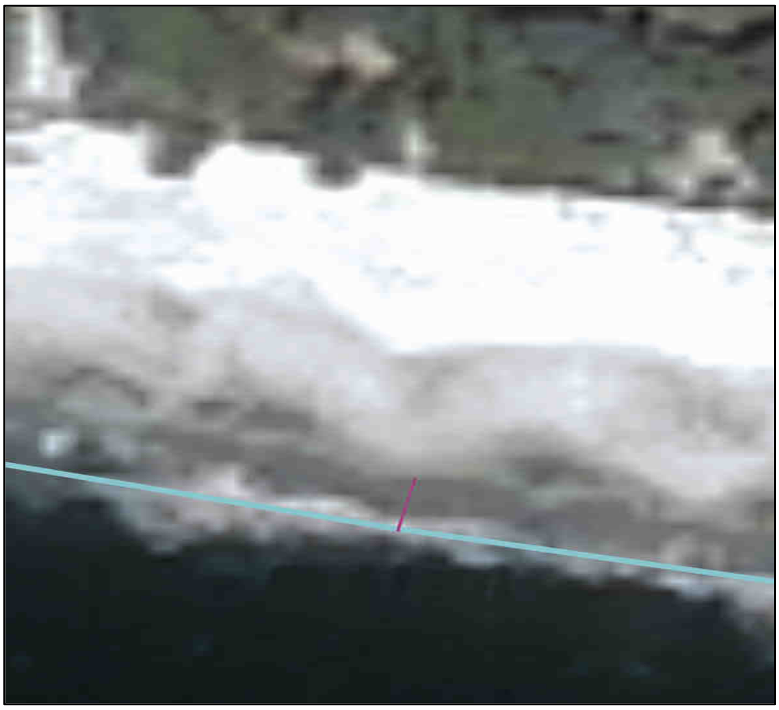

Figure 6: Transect of sand spectral profile

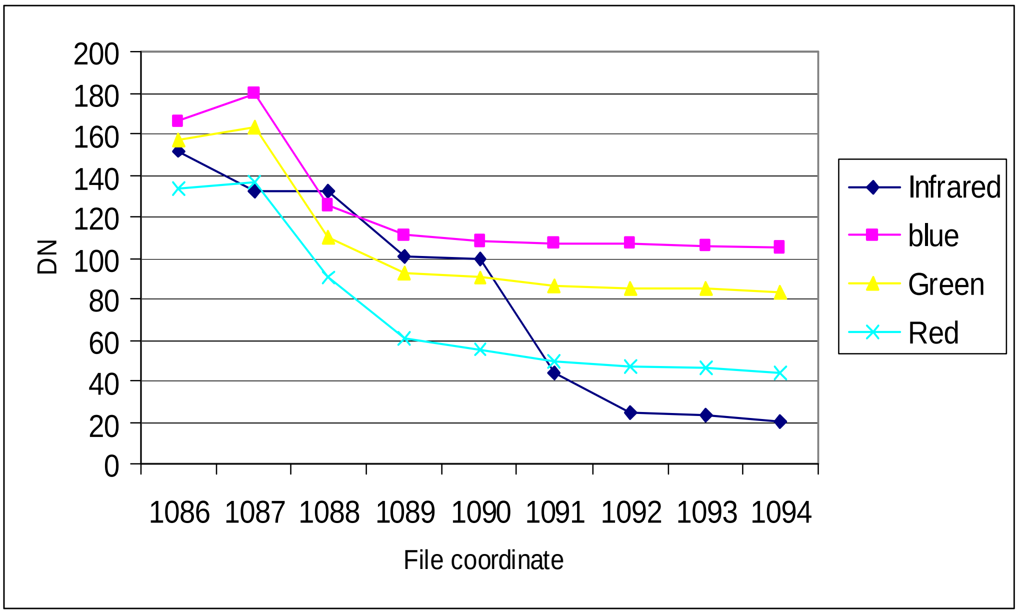

Figure 7: DN value of different wave lengths (visible and infrared) on the emerged beach

P2 - DISTART, Università degli Studi di Bologna

Renata Archetti (renata.archetti@unibo.it); Eleonora Torricelli (eleonora.torricelli2@unibo.it)

Remote monitoring of coastal conditions in locations of high public usage is a fast growing application of information technology. Video camera systems provide a relatively cheap and potentially rich source of information on the state of the intertidal beach zone. The present report presents the chosen methodologies of video monitoring system for appropriate feature extraction and integration with other sources of weather and wave data for the purpose of assessing and predicting the beach width threshold value for tourist demand and for flooding risk. The feasibility of combined image processing and feature extraction routines for providing real-time input to estimate a level of beach safety is demonstrated.

The installation of a new video monitoring station in Igea Marina and in general a description of the SVM video station are presented. The Argus video station of Lido di Dante is also described, and a comparison analysis between different video station technologies is presented. We also present the technique for the shoreline and intertidal beach bathymetry position detection and the technique for the error estimation.

Video monitoring station in Igea Marina

Due to the innovative character of the intervention in Igea Marina (Preti et al., 2005) a monitoring program aimed to observe the effects of the defence works on the beach has been planned and is now on going. Besides traditional techniques to measure shoreline positions, bathymetry, waves and currents, a new technology was chosen in order to observe the beach in Igea Marina: the technique is based on video analysis. The installation of the video station in Igea Marina was implemented in order to monitor the coastline evolution and the hydrodynamics at the groin heads and at the barrier gaps beyond the area of the intervention.

The SVM video system

The SVM system is a hi-resolution digital camera system used to take pictures, archive them, and upload them to the Internet. Designed for construction and environmental monitoring and documentation, the system has a number of features and characteristics such as: photo quality images, automatic creation of time lapse movies, extensive image archiving, weather station support, easy installation. The system is controlled by an embedded Pentium computer running Windows. The control software has been designed over eight years to be very flexible and easy to programmed for handling both the Webcam and image archiving needs you may have.

The Video Monitoring Station Software for Windows XP™ (VM95) is at the heart of Video Monitoring Stations. The software offers many sophisticated operations not available in other software packages.

VM95 allows for unattended image acquisition, labelling, archiving, and optionally uploading to the Internet at programmable intervals. Available features include exposure time, image quality/dimension, daily on/off times, graphic overlays, and many more. Setting up the software to capture images, graph weather data, and make slideshows to upload to the Internet is done by setting up scenes. Up to 80 different scenes may be programmed. All scenes have a daily on/off hour and sample interval.

The installation at Igea Marina

The video station has been installed on the roof of a building in the front of the beach. The station is composed of two video systems. The first video system consists of a high resolution video camera Super HAD CCD 1/2" with zoom 3,6-18 mm, looking to the north (Fig. 8). The second video system looking towards the south, is composed of two 8 megapixel digital still cameras Olympus SP500UZ (maximum resolution 2816 X 2112) mounted in a single housing. One of the digital cameras is set to take snapshot pictures at daylight and long time exposures during the night, the other, covered by a suitable filter, is set to collect long time-exposures (15 s) during the day.

The camera control software permits a remote operator to schedule image collection of specified types of images at arbitrary desired intervals. Thus, for example, with the video camera we plan on collecting on an hourly basis, a continuous stream of video images that are then averaged together to form a single averaged image (called a "timex" image). With the digital camera, timex images will be obtained by averaging many of the 15 second (exposure time) images, covering 600 seconds. The associated PC based controller performs camera control and image collection, creates the time-averaged images (thereby sharply reducing data transmission overhead) and transmits the result to the remote data collection centre. Images are available on the web site: http://videomonitoring.eu.org/igea.

Figure 8: Aerial view of Igea Marina. Picture taken by the video camera (left) and by the digital still camera

The video monitoring station of Igea Marina beach observes the shoreline evolution, related to storms events and nourishments. The lens distortion has been corrected trough lens calibration and tools have been developed (in the matlab environment) in order to ortho-rectify and to geo-reference the images.

An example of calibrated and ortho-rectified images is shown in Figure 9.

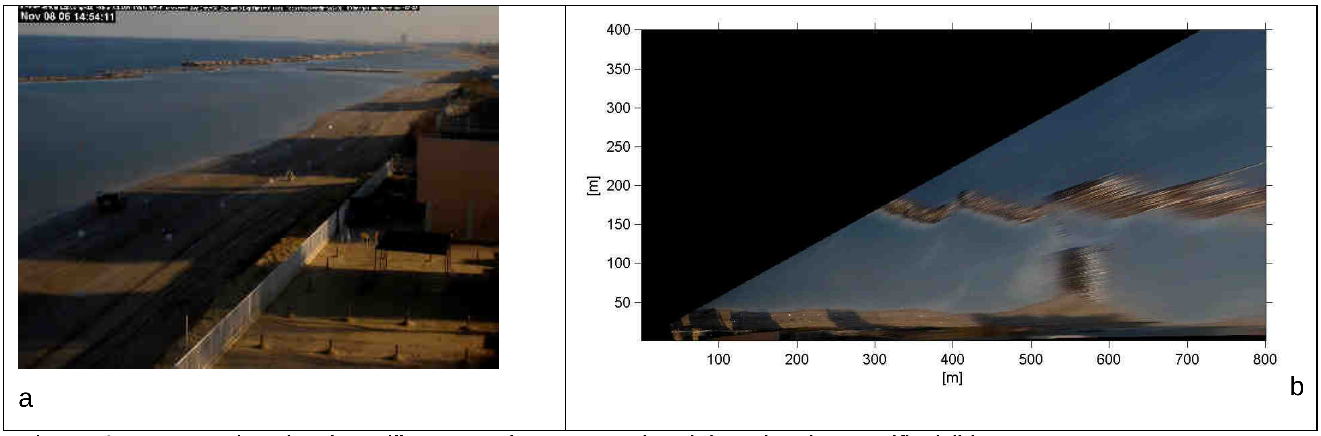

Figure 9: Image taken by the still camera in Igea Marina (a) and ortho-rectified (b)

In Figure 10b it is interesting to observe how emerged structures (the groin and the parallel emerged structures located at the right side of the groins) are wide. This is due to the fact that the high objects are projected on the image.

Video monitoring station in Lido di Dante

ARGUS station at Lido di Dante

The video monitoring station installed in 2003 at Lido di Dante is a 3rd generation ARGUS station (Holman and Stanley, 2007) and consists of a system of four digital video cameras placed on a 18 m high wooden tower. The image pixel resolution is 1024 x 768.

Pictures taken by the four cameras are not simultaneous: the first camera (C1 directed to the south) takes pictures during the first ten minutes of every daytime hour, C2 during the minutes from 10' to 20' and so on. The last 20 minutes in the hour are used to collect timestacks (Archetti and Lamberti, 2006). Images are collected during every daylight hour and are available for public view via the web (www.wldelft.nl/argus).

The video camera oriented south films the non-protected beach, and the other three acquire images of the beach and the sea protected by the LCS (Davidson et al, 2007; Albertazzi et al., 2003). Images taken by the cameras are shown in Figure 10. The merged image data provides full 180° coverage of the coastline. Examples of a panoramic view (merged image) and a plan view (rectified image) are shown in Figure 10. The abscissa (y axis) represents the longitudinal direction, the x axis runs across the shore, and the video station is the origin. The ARGUS reference is rotated a few degrees versus the geographical reference system in order to keep the detached barrier along the y axis.

Figure 10: Images taken by the ARGUS station in Lido di Dante

In Figure 11, it is easy to recognise the two cells representing the structures, the north cell on the left hand and the south cell on the right-hand, and the right side of the image shows the southern coast.

The video monitoring station is programmed to take pictures according to the ARGUS protocol, described in the OpTIMAL report of Phase A.

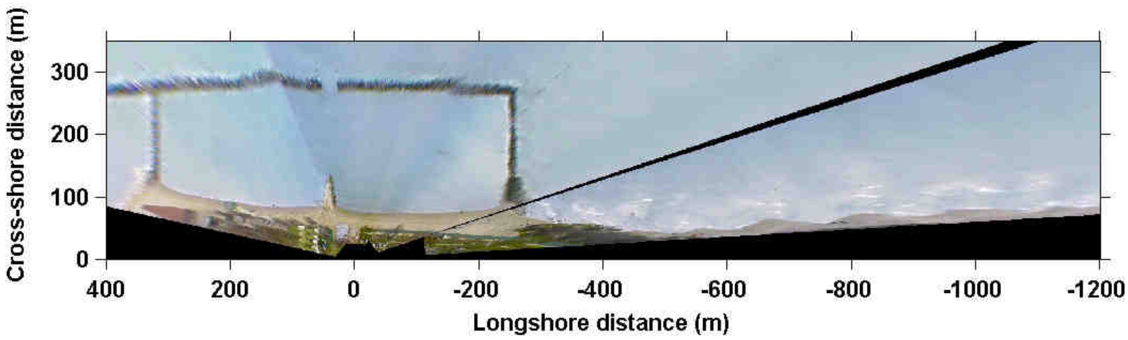

Figure 11: Local geographic reference in Lido di Dante on merged and rectified image. X is the cross-shore direction and y the long-shore direction.

<u>Comparison analysis</u>

Besides the two video systems installed by the University of Bologna and described in the previous sessions, another video system for coastal monitoring was developed by a joint research group from University of Pau and University of Santander (Spain). A synthetic comparison among the systems for the coastal video monitoring is presented in the Table 1.

Table 1: Comparison among coastal video monitoring systems

Established, well known and internationally accepted system for video acquisition and analysis.	System developed since 1998 mainly used for environmental control	System developed in 2006 for coastal monitoring
More then 50 ARGUS Station in USA Europa and Australia	Some installation equivalent to Argus are available: Puleo at Delaware Univ. USA. Igea Marina UNIBO. Installation for beach monitoring: Boca Raton FL Boca Inlet Boynton Inlet Lake Worth Inlet Jupiter Inlet Monty county FL Saint Lucie Inlet Sebastian Inlet Pocomac River Monmouth Beach Santa Cruz CA San Francisco CA USGS Lerici I Sarzana I	Adour (September 2006) Mundaka / Espagne (February 2007) Sain Juan de Luz France (February 2007) Biarritz France (2007).
Software for database management Software for image rectification and merging, shoreline identification	Software for Timex and variance images Post processing software Lens calibration Ortho-rectification Geo-referencing * Shoreline detection Intertidal beach bathymetry * In progress	Software for Timex and variance images Post processing software Lens calibration Ortho-rectification Geo-referencing
Max resolution:1024 x 768 pixels	Max resolution 10MPixel (3264x2488)	Max resolution:1024 x 768 pixels.
Timestack images	Timestack images	Information not available
	Acquisition possible during the night	Information not available
Rigid	Flexible	Flexible
Type of cameras: Digital cameras (Low resolution)	Type of cameras: Video-cameras and still-cameras (up to 10 MP resolution)	Type of cameras: Digital cameras
Cost rather high	Cost rather cheap	Cost rather cheap
Real time remote control not possible	Real time remote control possible	Information not available
	easy to change setup system and scheduling by remote control	Information not available
	Watch – dogs presents to monitoring system functionality	Information not available

Methodology

Error estimation in the shoreline detection

The accuracy of the image-derived survey method is assessed by comparison with a beach survey obtained with a DGPS. The error of the topographical survey of the shoreline and of the IBB is attributable to the following factors:

- the horizontal uncertainty induced by the ortho-rectification process;
- the uncertainty due to the shoreline detection process;

An accurate analysis of the uncertainty in the detection of the shoreline using video was carried out for the images taken by the Argus station in Lido di Dante and is in progress for the images taken at Igea Marina.

A data set of 29 shoreline measurements was collected at Lido di Dante from 15 to 22 July 2004. The shoreline surveys were carried out by moving a DGPS in the kinematics mode over a distance of about 800 meters alongshore, in the protected area delimited by the external groins, at the centre of the swash zone. The climate conditions during the survey were extremely calm: measured offshore waves were lower than 0.15 m, the water in the protected zone was extremely still and the tidal level spanned a range between -0.5 m and +0.3 m with respect to the mean sea water level.

The survey was carried out on an hourly basis, simultaneously with the recording of time-averaged (timex) video images by the four cameras of the ARGUS station in Lido di Dante. The post-processing correction of the single frequency DGPS (model SR510 by LEICA Geosystems) data through the data collected simultaneously by a close Continuously Operating Reference Station (CORS) produced data with centimetre precision. The RINEX file used comes from the CORS managed by the Department of Geophysics of the University of Bologna located in Marina di Ravenna, about 8 Km from the survey area.

The shoreline was detected on merged and rectified image (Fig. 10) during each hourly survey, (methodology to detect the shoreline position on timex images is described in the OpTIMAL phase A Report) and the deviations between ARGUS video-based and DGPS-surveyed shorelines were defined as in Equation (1):

$$\delta_d(y,t) = x_A(y,t) - x_G(y,t) \qquad (1)$$

where $\delta_d(y,t)$ is the deviation between the ARGUS-based and DGPS-surveyed alongshore position y (Fig.11) at time t and $x_A(y,t)$, $x_G(y,t)$ represent the shoreline position at alongshore position y and time t as identified from the ARGUS video analysis and the GPS survey, respectively.

Two zones were selected: the north cell (320 < y < 60) and the south cell (40 > y > -270) $x_A(y,t)$, $x_G(y,t)$ were surveyed and interpolated in order to have data at 1 m spacing alongshore in the two selected zones, and the groins were excluded from the analysis.

Figure 12 shows an example of the procedure for estimating $\delta_d(y,t)$ as conducted on 7th July 2005 at 8:00 am: the DGPS measured shoreline and the video-derived shorelines are plotted in the top panel, and $\delta_d(y,t)$ at each alongshore coordinate is plotted in the bottom panel.

When $\delta_d(y,t)$ is negative, this means that the shoreline measured by ARGUS was landward with respect to the DGPS survey. The high deviation between the measurements close to the central groin (coordinate x = 50 m in Fig. 12) was due to the difficulty in the survey of the shoreline with ARGUS, as the groin masks the shoreline. Except for these outlier data, the $\delta_d(y,t)$ ranges between ±1.2 m within a distance of ± 300 m from the ARGUS station.

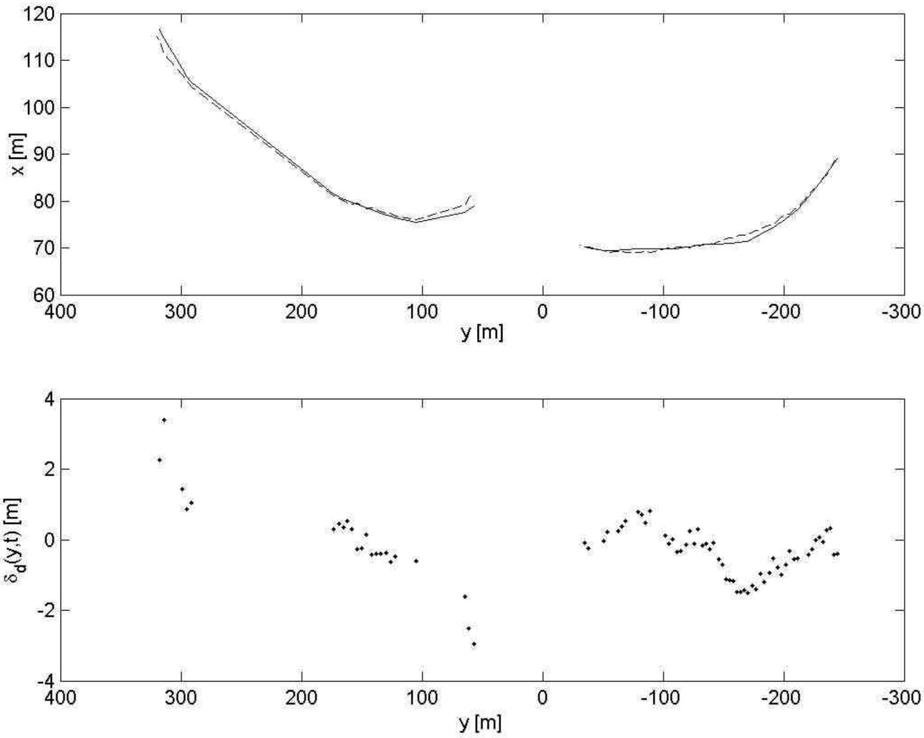

Figure 12: Example of comparison of DGPS and Video derived shoreline (top) and deviation between the two measures (bottom).

For each shoreline measurement collected during the survey at time t, the following statistics were evaluated: the mean of the absolute $\delta_d(y,t)$ over all alongshore positions y, the standard deviation of the absolute $\delta_d(y,t)$, and the root mean square (rms) estimated over all alongshore positions y.

The mean of $\delta_d(y,t)$ ranges between 0.39 m to 1.41 m, the mean of the absolute $\delta_d(y,t)$ is equal to 0.83 m, the standard deviation of the absolute $\delta_d(y,t)$ is 0.63 m and the mean of the rms is equal to 1.04 m. The greater errors are estimated in the shoreline comparison during the early morning, when the sunrise leads to difficulty in detecting the shoreline position.

The value of 0.83 m ± 0.63 m can be assumed as the horizontal uncertainty induced by the ortho-rectification process and due to the shoreline detection process (eHShoreline).

The uncertainty due to the shoreline detection process has been assessed comparing the shoreline identification of the same image executed by different operators. The subjectivity of the processing is important in some situations. The shorelines analysed by different operators turned out to be almost equal, and the comparison of the detected shoreline by two operators (authors) gave approximately the same values.

Methodology to describe the short and medium term trends of the beach

In order to describe the evolution of the beach width the following indicators can be detected on ortho-rectified images and monitored with the use of the video technique:

- Mean shoreline position
- Position in selected section of the beach
- Position of the mean intertidal beach bathymetry
- Mean shoreline position

The indicator selected to describe the shoreline position was defined as "the mean distance, from a fixed position (the Argus station) in the cross-shore direction, of the average shoreline position over the alongshore"; looking at Figure 12 the mean shoreline position (MSP) indicator at time $\bar{t}$ is estimated as in Equation (2):

$$MSP(\bar{t}) = mean\left[x\left(y,\bar{t}\right)\right]_{-yS<y<yN} \qquad (2)$$

where yS and yN are the boundaries of the mean at the southern coordinate y and the northern coordinate y, respectively.

Shoreline position in selected section of the beach

Another way to observe the dynamics of the shoreline position in time is to concentrate on some defined cross-section, and to follow the shoreline position. The main difference with the previous methodology is that before we estimated the mean shoreline position in an area, in this case the position in single section is observed. An example is given in the Figures 13a and 13b. Figure 13b shows a timestack (timeseries of intensity pixel on a predefined array) taken on section y=300 (white line in Fig. 13a). It is evident the approximate shoreline position and its behaviour during months from January to March 2007. This methodology was introduced by Elko et al (2005) in order to study the beach evolution after a nourishment and will be applied to study the beach nourishment at Igea Marina

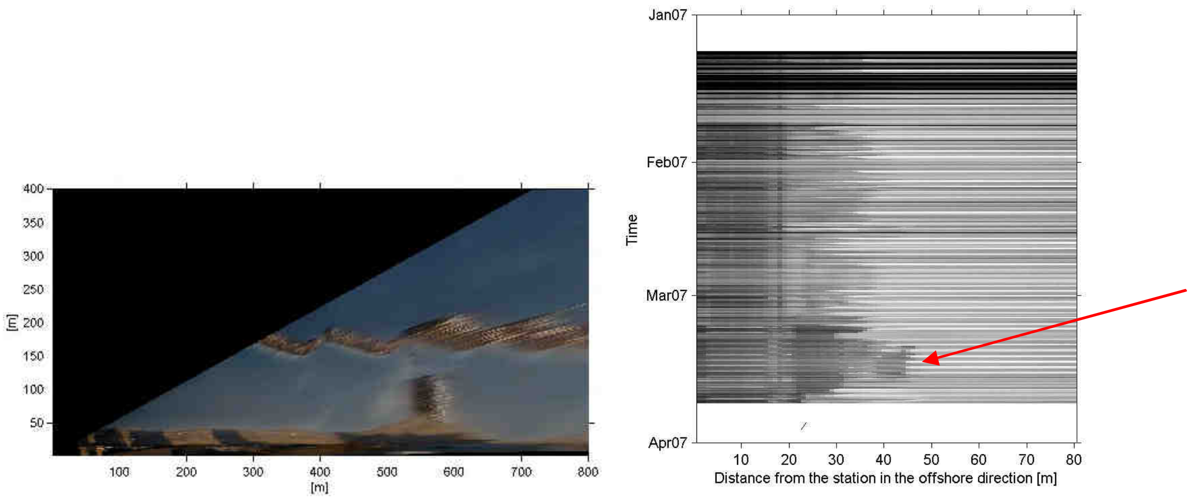

Figure 13: Ortho-rectified image at Igea marina and timestack of section 300. Shoreline position is evident and shown by the arrow.

Position of the mean intertidal beach bathymetry

The mean position of the intertidal beach bathymetry represents a more stable indicator compared to the MSP or the shoreline evolution in a single section and can offer the opportunity to estimate the volume changes in the intertidal zone.

The mean position of the IBB is the average position in both the alongshore direction and the cross-shore direction, and is a synthetic indicator of how the intertidal beach moves back and forward. The beach position must be estimated in reference to an initial configuration in order to estimate its behaviour over a long period of time, or in reference to a fixed date in order to study the effect of a single event such as a nourishment.

The mean IBB is similar to the consolidated indicator used in the Netherlands momentary intertidal coast line, MICL (Van Koningsveld and Mulder, 2004), defined as the mean position of the coastline between the dune foot and the lower limit of the intertidal beach. In the case of Lido di Dante, the MICL cannot be defined since there are no dunes in the back-beach.

In Lido di Dante, and in general on the beaches of the Romagna littoral, the intertidal beach has a tidal range of approximately 0.5[÷]1 m with an averaged intertidal slope of 1:15, and it extends in a cross-shore direction for approximately 7.5 m[÷]15 m.

An example on how the IBB is surveyed with video analysis and on how the beach bathymetry changes are estimated is shown here regarding the state of the beach in Lido di Dante on 9 June 2005 and on 25 July 2005, before and after a storm coming from the North.

The maximum significant wave height measured by the wave buoys of the Italian National Wave Recorder Network in Ancona (150 Km south of Ravenna) is HS = 1.50 m, TP = 6.4 s and dir = 17° N recorded on 15 July 2005. The buoy is moored in deep water (approximately at 70 m depth). The details of the locations of the buoys and the systems of measure are available on the website of APAT (www.apat.it). The analysed sea storm has a return period of approximately 1 year.

The IBBs before and after the sea storm (9 June 2005 and the 25 July 2005) are shown in Figure 14, and at first sight, a regression of the beach in the whole area can be observed.

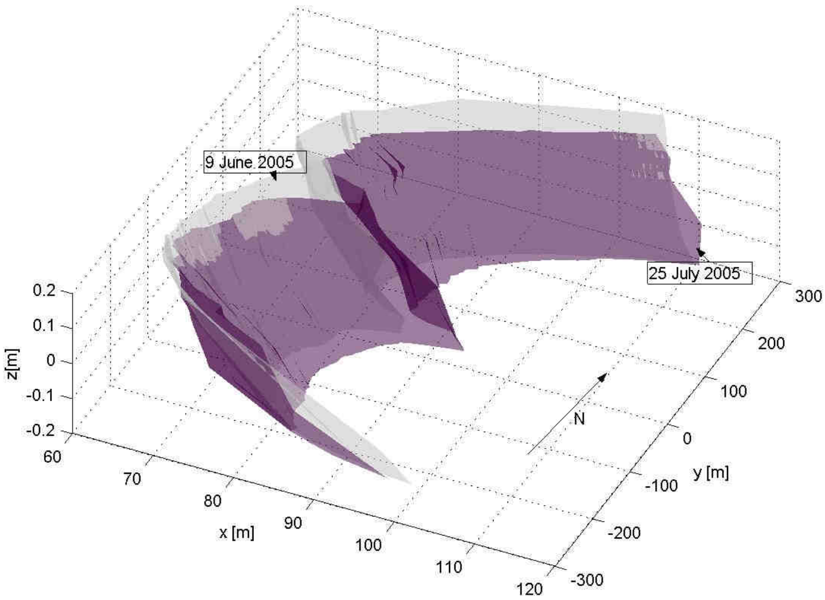

Figure 14: Video derived IBBs. Before the storm (light grey, 9 June 2005) and after the storm (dark grey, 25 July 2005).

The images in Figure 15 represent in chromatic terms the beach accretion and/or regression over the whole length of the intertidal beach. Colour blue represents the area with a negative difference between the first and second bathymetry, while yellow, orange and red colours show an advancement (positive difference) between the first and the second bathymetry.

Figure 15a shows the distances between the IBBs collected on 9 June and on 25 July 2005 in the cross-shore direction seen from an observing point that looks onto the beach frontally from the sea side. The vertical extension of the beach ranges between -0.20 m to +0.15 m. The cross-shore distance between the two IBBs is approximately 3 m (dark green in the legend) in the southern cell (-220 m < y < 20 m) and more than 5 m (light green in the legend) in the northern cell (30 m < y < 280 m).

Figure 15b shows the difference in the vertical direction between the two IBBs measured on 9 June and on 25 July 2005. A rising up to 0.2 m is observed on the upper part (landward) of the beach, and a lowering is seen in the seaward part of the beach (up to 0.35 m). The observed non-homogeneous transformation of the beach during the storm causes an increase in beach steepness.

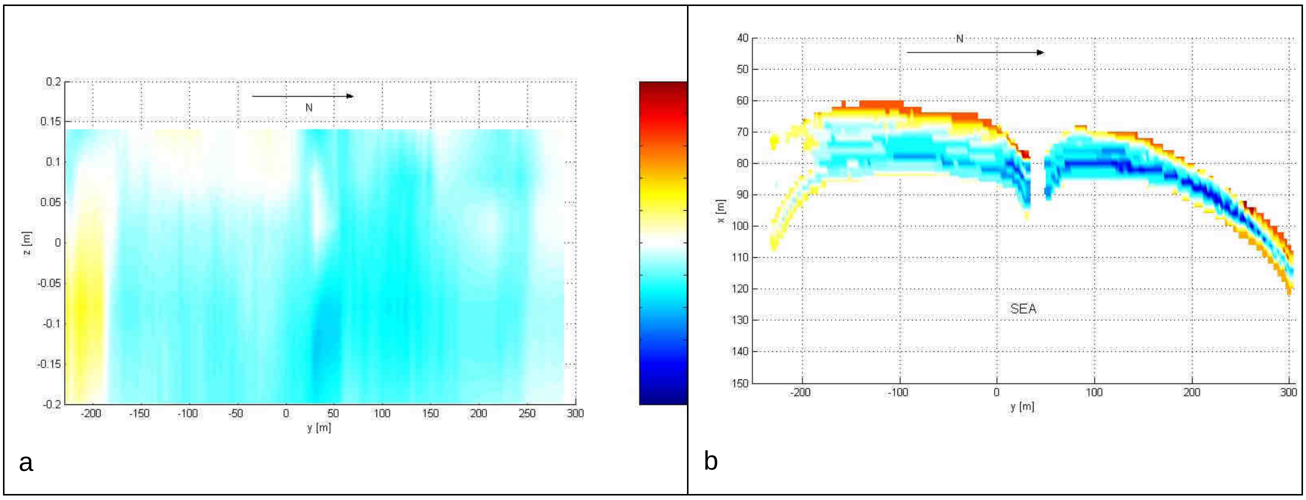

Figure 15: Comparison between IBBs detected on the 9 June 2005 and 25 July 2005: a) Frontal variational chromatic graph. b) Aerial variational chromatic graph.

Summarising, the variation of the intertidal bathymetric profile shows that there was a displacement of sand volume from the lower part (seashore) towards the upper part of the intertidal zone, resulting in an increase of the slope and a cross-shore regression.

A synthetic parameter is defined in order to describe the mean distance between two IBBs: ΔX is defined as the average distance in the cross-shore direction between the two bathymetries. The ΔX is a measure of how the IBB translates in the cross-shore direction.

P3 - DIPTERIS, Università degli Studi di Genova

Nicola Corradi (corradi@dipteris.unige.it); Marco Ferrari (ferrari@dipteris.unige.it); Chiara Francesca Schiaffino (chiaraschiaffino79@yahoo.it)

The use of webcams to monitor coastal processes is becoming increasingly popular internationally because it offers the possibility of acquiring qualitatively valid data automatically, continuously and in real time without the problems so often associated with field studies using classical methods (Davidson et al, 2004), which are then only required to confirm the reliability of the data. Technological advances in recent years have made it possible to use webcams to monitor the littoral continuously, even for prolonged periods of time. The data obtained in real time or after appropriate elaboration can then be used to provide information on the evolution of the coast.

The use of a webcam requires the elaboration of the images to provide morphological and hydrodynamic characteristics of the beach, which can be interpreted quickly and easily.

The project proposed by the Dipartimento per lo studio del Territorio e delle sue Risorse (Dip.Te.Ris.) dell'Università degli Studi di Genova involves monitoring an artificial nourishment using webcams.

The aim of the study is to verify and evaluate the suitability of indirect monitoring of a littoral morphology like that of Liguria, characterised by a very indented rocky coast cut by beaches of reduced dimensions that are more or less limited laterally by jutting promontories.

The study is applied to the beach of Levanto, in eastern Liguria (Fig. 16). The beach in question, about 900 metres long, is delimited by two promontories, Punta Mesco and Punta Levanto, and could be classified as a pocket beach. The continuity of the beach is interrupted by two groins that divide the littoral into three distinct sectors; the groins and two submerged breakwaters in the north-westernmost and central sector influence the overall morphological evolution of the beach. In February 2005 the two north-westernmost arcs were the subject of an artificial nourishment programme that involved the deposit of 16000 m3 of quarried material suitably crushed and treated.

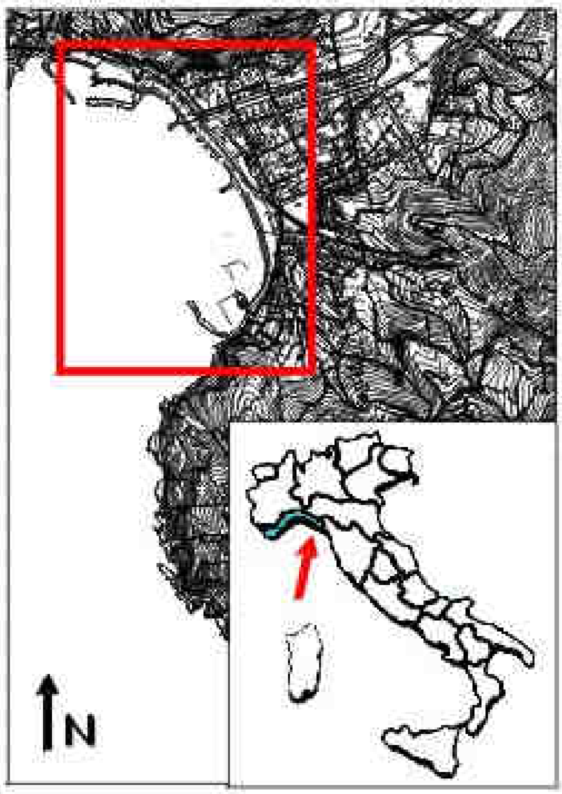

Figure 16: Study area.

The webcam study focuses on the sectors subject to the nourishment to try to define the evolutive trend of the littoral and the impact of diverse sedimentary fluxes that occurred under varying marine conditions following the construction of the defences. Sample images were acquired with the two webcams between June 2005 and June 2006. Subsequently a bibliographical study was conducted to obtain a picture of the most up-to-date techniques being used internationally for the management and elaboration of the images to determine the most suitable method for a later analysis of the trend of the coastline study area and analyse the angle of the waves to the coast (Holland et al, 1997; Holman et al, 2003).

As the scope is to evaluate the effectiveness and flexibility of the systems used, once we had acquired sufficient information from the webcams we began to experiment the various photo processing systems in order to determine which one provided the clearest picture of those morphological features that would otherwise be difficult to interpret.

As such webcam systems functioned well only in those cases where the littoral was characterised by beaches of substantial width and length, the systems currently in use were too cumbersome for our needs given the morphological characteristics of this pocket beach. On the basis of these morphological characteristics we tried to create an ad hoc system that used only two webcams, could provide images qualitatively comparable with commercially available systems, and would be suitable for morphological studies of specific coastal tracts distinguished by pocket beaches of reduced dimensions.

The monitoring station installed at Levanto by Ge.Co.s.r.l. consists of two fixed colour webcams linked to a switchboard for the transmission of the data to a server in real time via remote connection. The webcams are installed on the top of a building (16 metres above mean sea level) situated just to the east of the section of the beach being studied, to provide the best possible view of the two arcs being studied. The cameras provide two different pictures of the littoral; camera 1 providing a panoramic view of the entire beach and camera 2 providing a close-up view of the nourished sector. The webcams acquire photos of the littoral automatically in real time with a definition of 1280x960 pixels and take one photograph per minute for four minutes, three times a day, at 8.00 a.m., midday and 4.00 p.m. As digital webcams can be remotely programmed it is possible to modify any acquisition parameter and intervene when the camera fails to function or functions badly.

Dip.Te.Ris. and the Dipartimento di Matematica dell'Università di Genova, with a long history of collaboration in the digital field, were able to develop and test a specific photo management and elaboration software programme that provides three different types of images (timex, variance and day-timex) with different characteristics and purposes from the snapshots.

Snapshots (Fig. 17) are, as the name implies, instamatic photos of the study site; in these photos it is possible to distinguish the wave fronts (Fig. 18), which are useful for determining the characteristics and angle of the waves to the coast. Putting the snapshots in order it is possible to observe the temporal evolution of the area. By elaborating the snapshots of any specific acquisition cycle it is possible to produce time-exposure images (Fig. 19), that is images of four superimposed snapshots that make it possible to eliminate momentary random sea conditions.

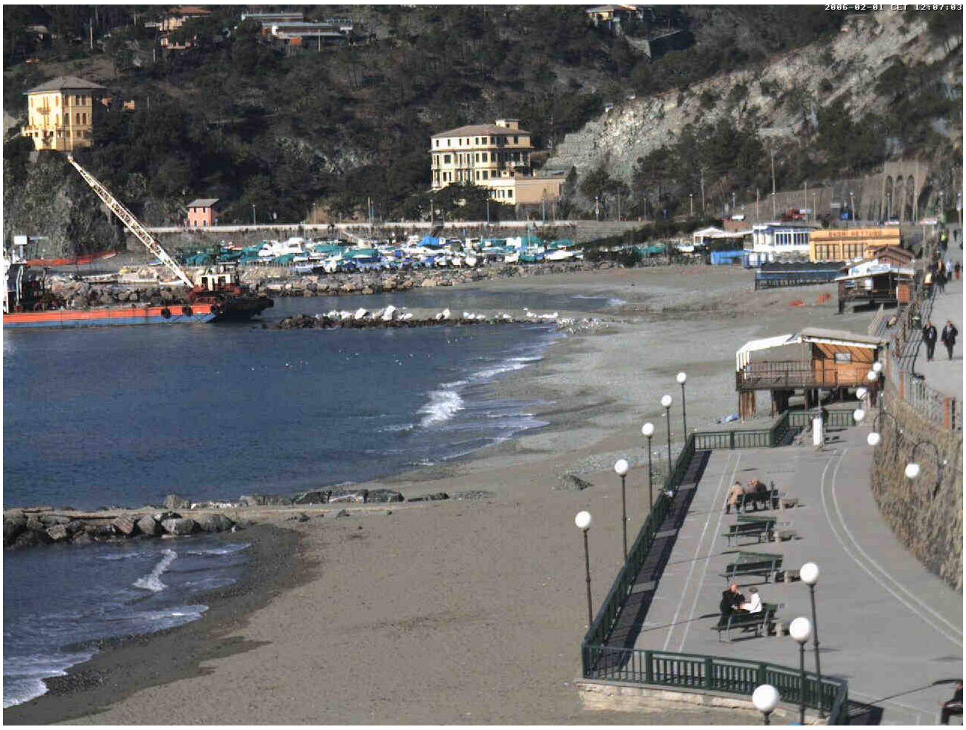

Figure 17: Snapshot taken at 12.07 p.m. 1st February 2006, Levanto.

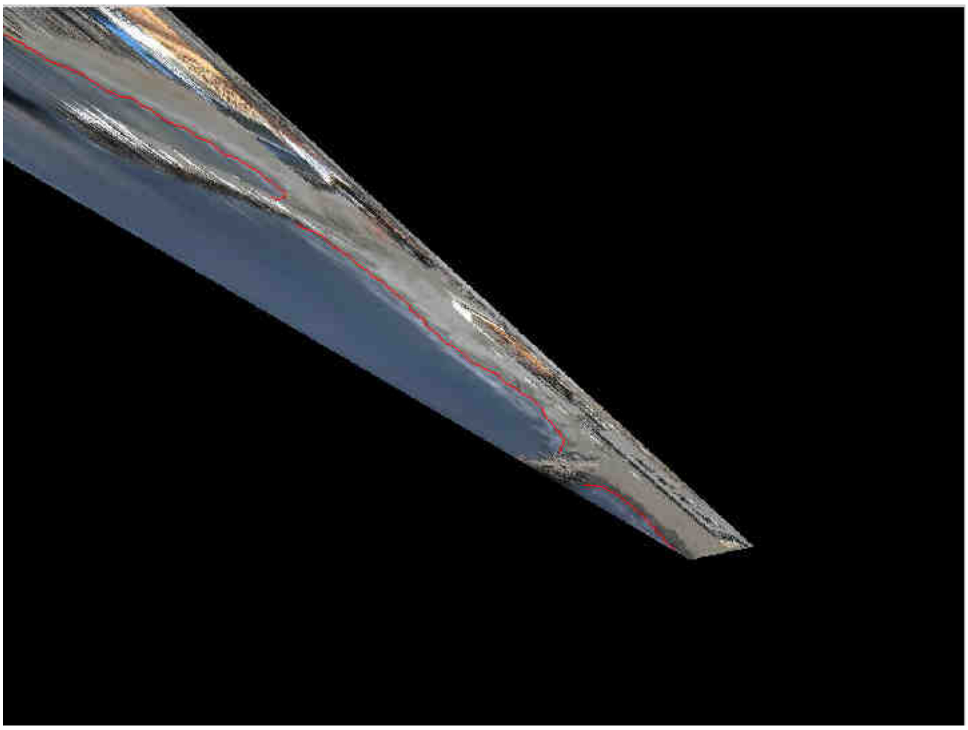

Figure 18: Rectified time-exposure image with coastline taken at midday 1st February 2006, Levanto.

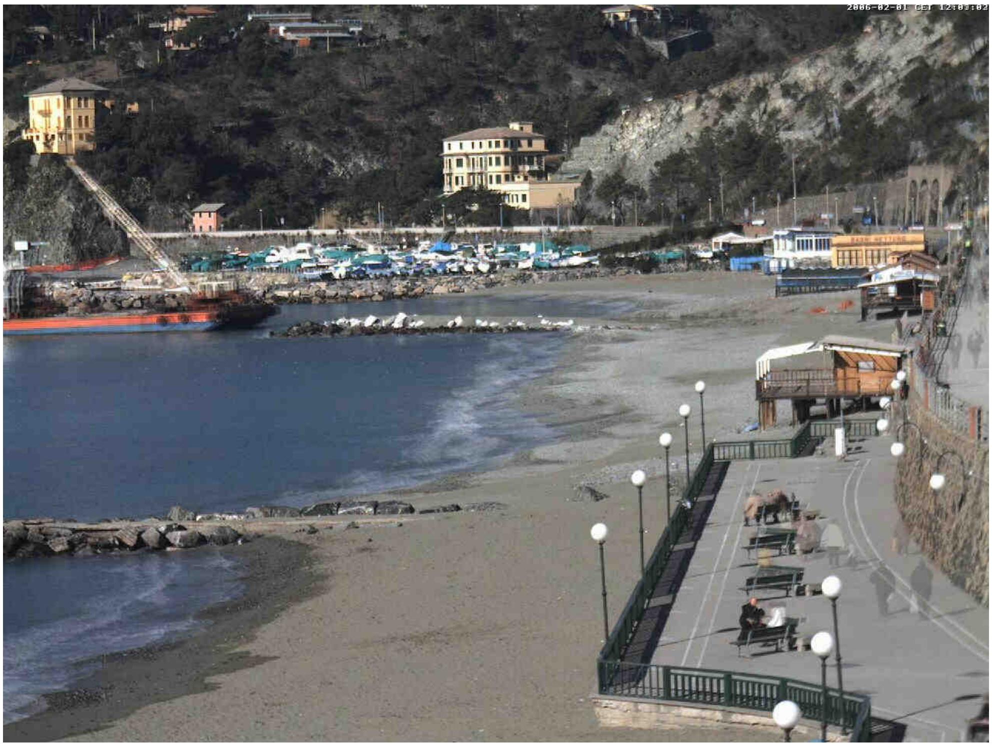

Figure 19: Time-exposure image taken at midday 1st February 2006, Levanto.

Thus it is possible to highlight and analyse characteristics that it would otherwise be difficult to distinguish and interpret, providing an excellent basis for the analysis of the area (Alexander and Holman, 2004). Timex images provide a real model of wave dispersal in the swash zone and therefore provide valuable information for the analysis of the evolution of the coastline over time and the determination of the impact that defence works in the area have had on the morphological evolution of the beach (Guillén et al, 2003). Furthermore, such images can be used to evaluate the short- and long-term impact of stormy seas on the coast (Cáceres, 2002; Van Konigsveld et al, 2003).

The elaboration of a cycle of snapshots can provide variance images (Fig. 20), the study of which, specifically the variation in the intensity of the pixels, makes it possible to distinguish static and dynamic areas and so better define the swash zone and underwater structures. The variance images can also be used to distinguish the coastline, particularly in those cases where the wave front is poorly visible in timex images because of a flat surf.

Figure 20: Variance image taken at midday 1st February 2006, Levanto.

Combining the three daily cycles of snapshots can produce a day-timex image (Fig. 21) that provides a daily image for medium- and long-term studies of the coastal morphodynamics and can be used to evaluate the impact of stormy seas on the beach.

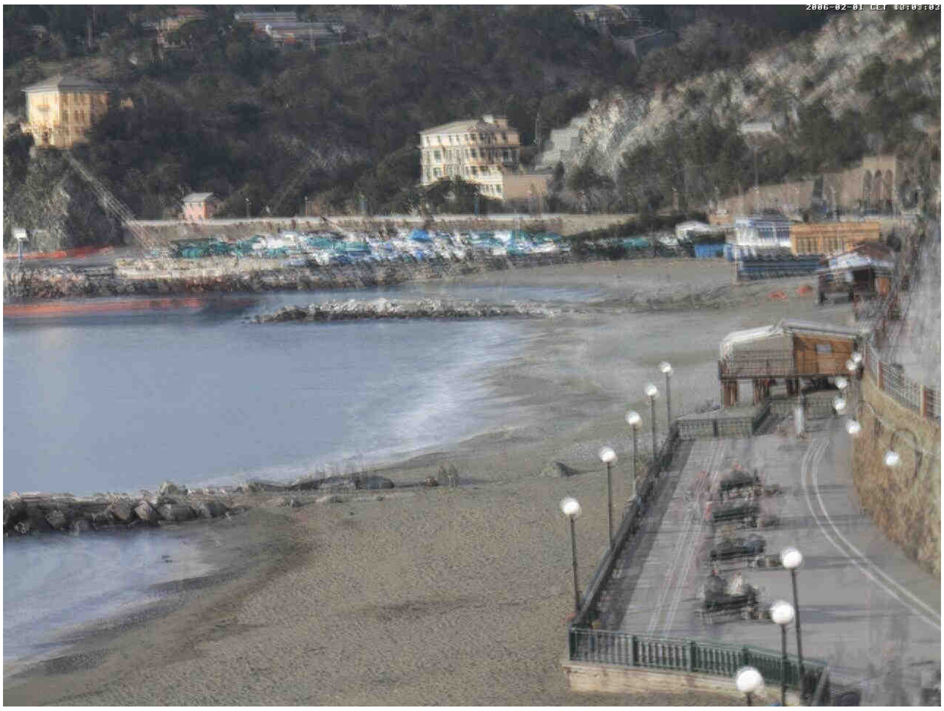

Figure 21: Day timex image taken on 1st February 2006, Levanto.

Therefore, so that the photos and images have scientific validity and in order to enable us to make both qualitative and quantitative measurements we developed a Matlab code for their georeferencing.

The Gauss Boaga geographical co-ordinates of eight fixed points on the beach were established with a GPS in a differential setting and subsequently used to establish the georeference. This process involved converting the real XYZ co-ordinates of the eight points into UV co-ordinates of the same points within the photo, which necessitated changing from a three-dimensional to a two-dimensional system. This projective geometrical problem was solved by using a specific linear system following the approach proposed by Abdel-Aziz et al (1971) and thanks to which it was possible to correlate the real and photographic co-ordinates (Monti et al, 1999). When this correlation was established it was possible to find the geographical co-ordinate of every single pixel in the images obtained with the webcam.

The results of this process were more than satisfactory. Figure 22 shows how the introduced co-ordinates fit well with the measured base points and Table 2 demonstrates the quantitative reliability of the results/data obtained through a numerical comparison of the co-ordinates obtained during a field study and those derived from the georeferencing of the images. It can be noted that programme errors increase with distance from the webcam due to image distortion caused by the angle of inclination of the surveillance camera. After georeferencing it is possible to further elaborate the images to orthorectify them.

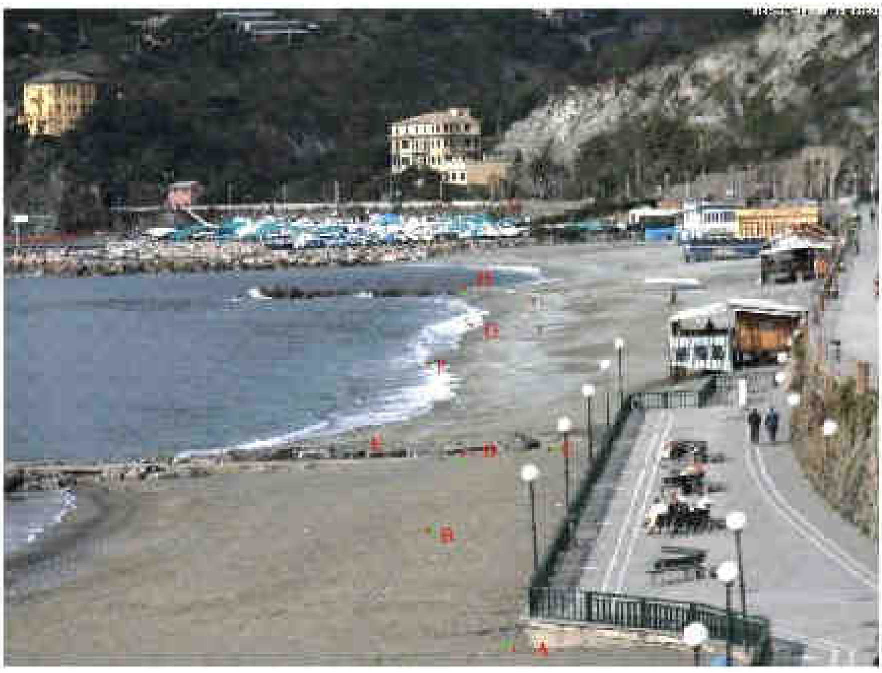

Figure 22: The base points for the geographical co-ordinates are shown in red, the points corresponding to the co-ordinates after georeferencing in green.

Table 2: Real and reconstructed co-ordinates.

PUNTO	Real GBN	Reconstructed GBN	Real GBE	Reconstructed GBE
A	4890814.986	4890814.364	1548772.350	1548773.232
B	4890842.557	4890842.839	1548741.024	1548740.512
C	4890874.285	4890874.643	1548718.215	1548717.652
D	4890870.895	4890873.687	1548714.808	1548712.127
E	4890885.940	4890885.903	1548690.389	1548690.520
F	4890943.444	4890942.067	1548639.525	1548640.593
G	4890995.261	4890987.075	1548592.314	1548600.819
H	4891052.217	4891059.494	1548535.275	1548527.947

The photos obtained with the webcam have an inclination that depends on the height of the camera monitoring that tract of the littoral. This angle of inclination could cause problems in interpreting the morphological characteristics of the beach and so it was necessary to develop software that would provide a bird's-eye view of the images (Fig. 23).

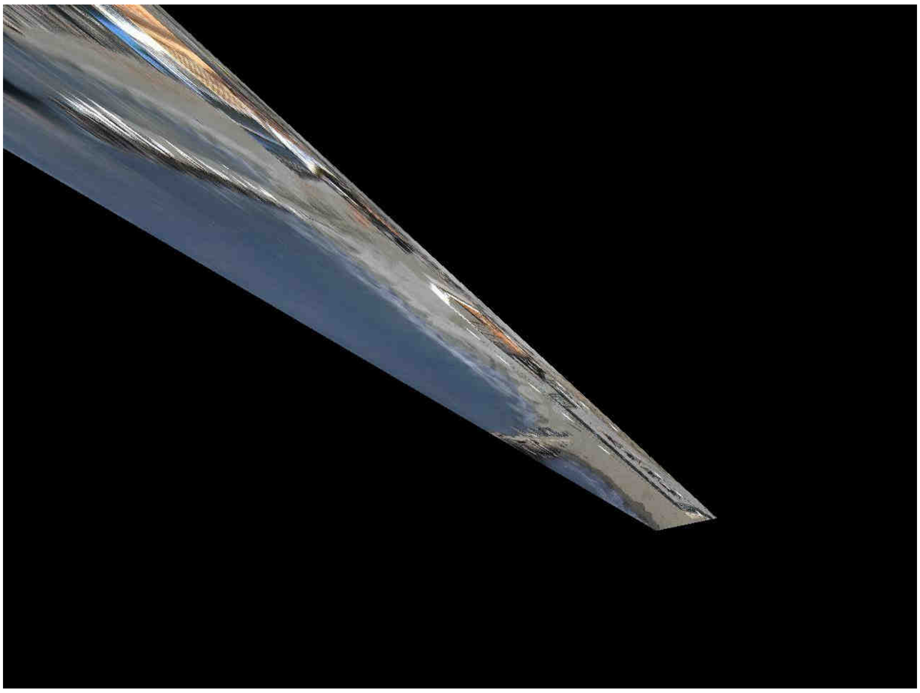

Figure 23: Rectified time-exposure image taken at 8.00 a.m. 4th February 2006, Levanto.

Instead of using the standard orthorectification methods described in the literature, which require a detailed understanding of the intrinsic parameters of photography (Holland et al, 1997), it was decided to develop a software programme based on georeferencing. Although the images thus obtained were not free of deformation, particularly in the areas furthest from the camera (a problem already noted during georeferencing) the resulting images could be considered of good quality because the deformation did not interfere with the beach morphology that it was intended to produce.

The software includes a special function to distinguish the coastline and the wave front (Fig. 18 and Fig. 24) in the snapshots and elaborated and rectified images to study the evolution of the coastal tract. These data make it possible to distinguish through comparisons of the various photos the morphology of the beach during one year and following any changes in the wave motion.

Figure 24: Snapshot with wave front taken at 3.57 p.m. 23rd August 2005, Levanto.

During the first period in which the backshore of Levanto was being surveyed a field study was conducted on the beach and wind-wave data for the entire surveillance period was obtained from the wave-meter buoy of La Spezia to validate the webcam data. During this monitoring two campaigns were also conducted to obtain bathymetric information on the foreshore trend and four campaigns were conducted to obtain backshore surveys to reconstruct the beach profile along five suitable benchmarks, to determine the trend of the coastline when the surveys were performed and provide a set of sedimentological data of both the back- and foreshores to define the sedimentary dynamics. The field studies described above not only add to the webcam data and provide a panorama of the morphosedimentary characteristics of the littoral system of Levanto but provide information to validate the technique.

P4 - Dip. Sc. della Terra, Università degli Studi di Roma “La Sapienza”

Ruggero Casacchia (ruggero.casacchia@cnr.it); Giovanni Battista La Monica (giovannibattista.lamonica@uniroma1.it); Elisabetta Petrocchi (elisabetta@petrocchi.net); Maria Cristina Salvatore (mariacristina.salvatore@uniroma1.it); Rosamaria Salvatori (salvatori@iia.cnr.it); Paolo Tortora (paolo.tortora@uniroma1.it)

Activities during Phase B regarded two themes: (A) innovative methods for determining the changes to shoreline position in time (for evolution purposes), and (B) development of a forecasting model for the morphological effects produced by beach nourishment interventions.

Innovative methods for definition of the shoreline position

Two images captured by the sensor fitted on DigitalGlobe’s Quickbird 2 satellite were analysed in order to establish a shoreline mapping protocol using satellite images and an automated or semi automated approach. The satellite was launched into orbit on 18 October 2001, it has a sun-synchronous orbit and captures its images from a distance of 450 km. The images taken on 11 June 2005 and 29 June 2005 relate to a part of Lazio’s coastline located between Sabaudia and Gaeta (Southern Lazio). Geometric resolution at Nadir is: 0.61 m for panchromatic (wavelength interval 0.45-0.90 µm), 2.44 m for multispectral (Blue 0.45–0.52 µm; Green 0.52 – 0.60 µm; Red 0.63 – 0.69 µm; NIR (near infrared) 0.76-0.9 µm) and a radiometric resolution of 11 bits. The images were supplied in GeoTiff format and mapped using the nearest neighbour method which does not alter the DN (Digital Number) value.

Processing

A sample area was selected west of the town of Terracina (Fig. 25) and some mapping tests were carried out on the shoreline using a number of techniques.

Figure 25: Location of test area

Two types of processing were carried out concurrently on the images. The first was of qualitative nature aimed mainly at photo interpretatation while the second was analytical in nature. The latter process was the result of image processing which was then also used for the photo interpretation stage.

As far as the first procedure was concerned multispectral analysis limits you to using three bands: a series of output images were produced in GeoTiff format using the various band compositions. Stretching was carried out on the histogram, improving contrast in order to produce an output which could be used for photo interpretation.

During the analytical processing phase the study was, through the use of masks, made to focus solely on the coastal area, taking into consideration spectral characteristics of sand, vegetation and water (Fig. 26).

From a spectral point of view, vegetation varies its behaviour according to type and state of health. However it has basically a typical reflectance curve, which can easily be recognised by the two blue and red absorption bands linked to the presence of chlorophyll and high reflectance values of the NIR (near infrared). The colour and reflectance of the ground depend on their physical and chemical composition and the presence of water. Water, on the other hand, completely absorbs NIR's incident energy and, as it is the only natural element with this feature, it can be identified immediately.

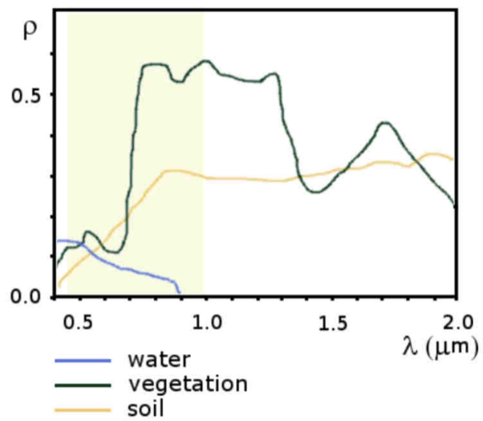

Fig.26: Water, sand and vegetation spectral curves

We decided to obtain the NDVI (Normalized Difference Vegetation Index) using the multispectral image as in Equation (3):

$$NDVI = \frac{\rho IR - \rho R}{\rho IR + \rho R} \qquad (3)$$

Where ρIR is reflectance in the near infrared band and ρR is reflectance in the red band. The NDVI is generally used to define the state of health of vegetation and to study the spatial distribution of vegetation and land features.

During another parallel study we applied a directional convolution filter to the image, parallel to the shoreline, so that it could be easily identified. This resulted is an image composed of 50% image and 50% filter. Some ROI (Regions of Interest) were chosen on this image in order to identify 5 classes (urban, vegetation, sand, water, and shoreline) which were used in the classification algorithms.

Analysis of Principal Components was also carried out: within the same picture different bands can often be strongly linked together which will result in information that is closely crammed together. The mathematical procedure contained in PCA (Principal Component Analysis) enables you to transform a certain number of correlated variables into a smaller set of non correlated variables. The first band contains the greatest possible variance, the bands that follow contain the next greatest possible variances.

As far as panchromatic data is concerned, its resolution is four times higher than that of multispectral data. However, although it has high geometrical resolution it does not allow any useful data to be extracted from it. The pan-sharpening process was therefore applied to the images (The Gram-Smith method provided the best results for the images in our possession). The pan-sharpening process uses a data fusion algorithm which enables you to associate the four lower resolution bands with the high geometric resolution of the panchromatic band.

Data Analysis

Five images were created for the photo interpretation phase, combining the different bands using additive synthesis: one image with natural colours (RGB=321), one with false-colours (RGB = 432), the NDVI image with 2.44 m resolution and two images with, respectively, natural colours and false-colours, and panchromatic resolution obtained using the pan-sharpening method.

A comparison was made between the different shorelines and the ones that correspond the most are the high resolution images (pan-sharpened RGB = 432 and pan-sharpened RGB = 321) while there is a wider gap in shoreline location with lower resolution images.

As far as image analysis is concerned we started off by using a RGB = 432 combination and studied the spatial profiles of the Digital Numbers (in proportion to reflectance values) using transepts which were orthogonal to the shoreline in order to identify the shoreline itself (Fig.27). In these profiles the abscissa axis shows the position of the transect pixels, the ordinate axis shows the DN values.

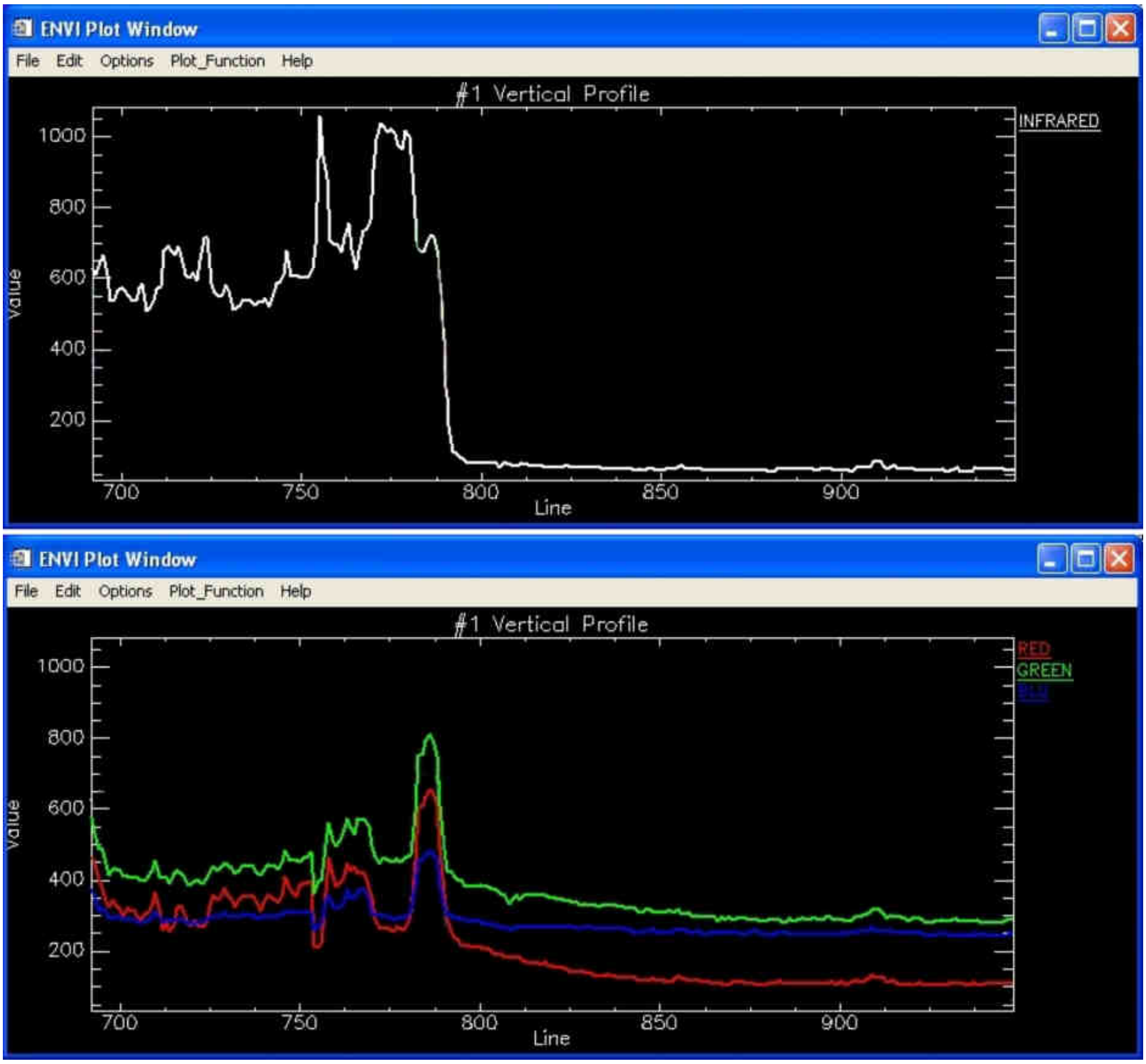

Figure 27: Spatial profiles along a transept for VISIBLE and NIR

In order to facilitate interpretation the NIR profile has been separated from the visible ones. Common feature of all the profiles is a sharp reduction in DN values as you get to the shore. As far as the NIR profile is concerned it can be used to adequately perform diagnostics, as the water's DN values are very low, enabling us to establish the shoreline with an uncertainty of one/two pixels. While the visible profiles on the other hand show a positive and very noticeable peak in DN values which correspond to beach location: this can be due to the chromatic characteristics of the sand (very light) while a darker beach would provide lower values. Another point is that while infrared completely absorbs radiation, with visible images there is always reflection present, which, although low, cannot be ignored as it means that there is a higher level of uncertainty in establishing the shoreline.

A profile was marked out on the NDVI image (Fig. 28) in the same way, analysing the DN values along a transept which was orthogonal to the shoreline: even here there was a sharp decrease in pixel value right where the shoreline is located. As water completely absorbs radiation, starting from infrared, the NDVI image always has a negative value, so the water/shore line is always easy to identify. The beach is also easy to identify: as no vegetation is present its DN values are constant (close to 0). A great advantage to using NDVI images is that, as this is a normalised value it can be compared with data obtained at other points in time.

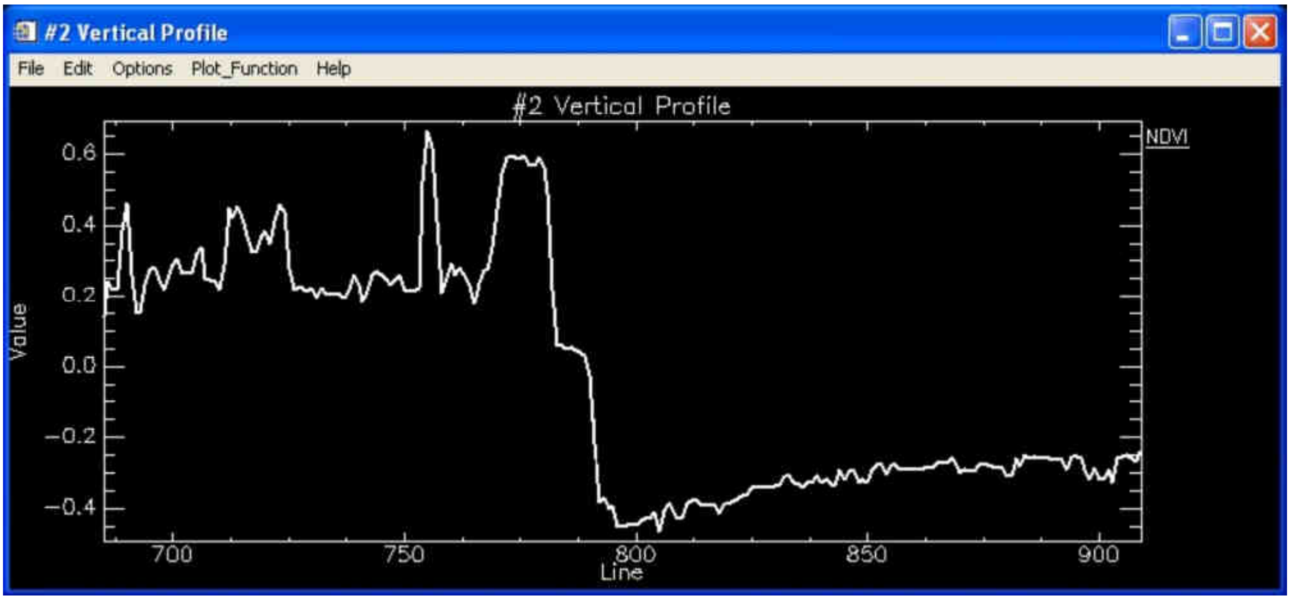

Figure 28: NDVI Spatial profiles

Even vertical profiles (in this case ascribable to spectral signatures) can be used as identification tools. In Figure 29 some profiles carried out along a transept are shown: the green profiles (y = 882-885) represent vegetation, the yellow ones (y = 886-887) show mixed pixel behaviour between vegetation and the beach, the lilac ones (y = 888-892) show the beach, the white ones (y = 893-894) show mixed pixel behaviour between the beach and the water (shore) and, finally, the blue ones (y = 895-901) represent water.

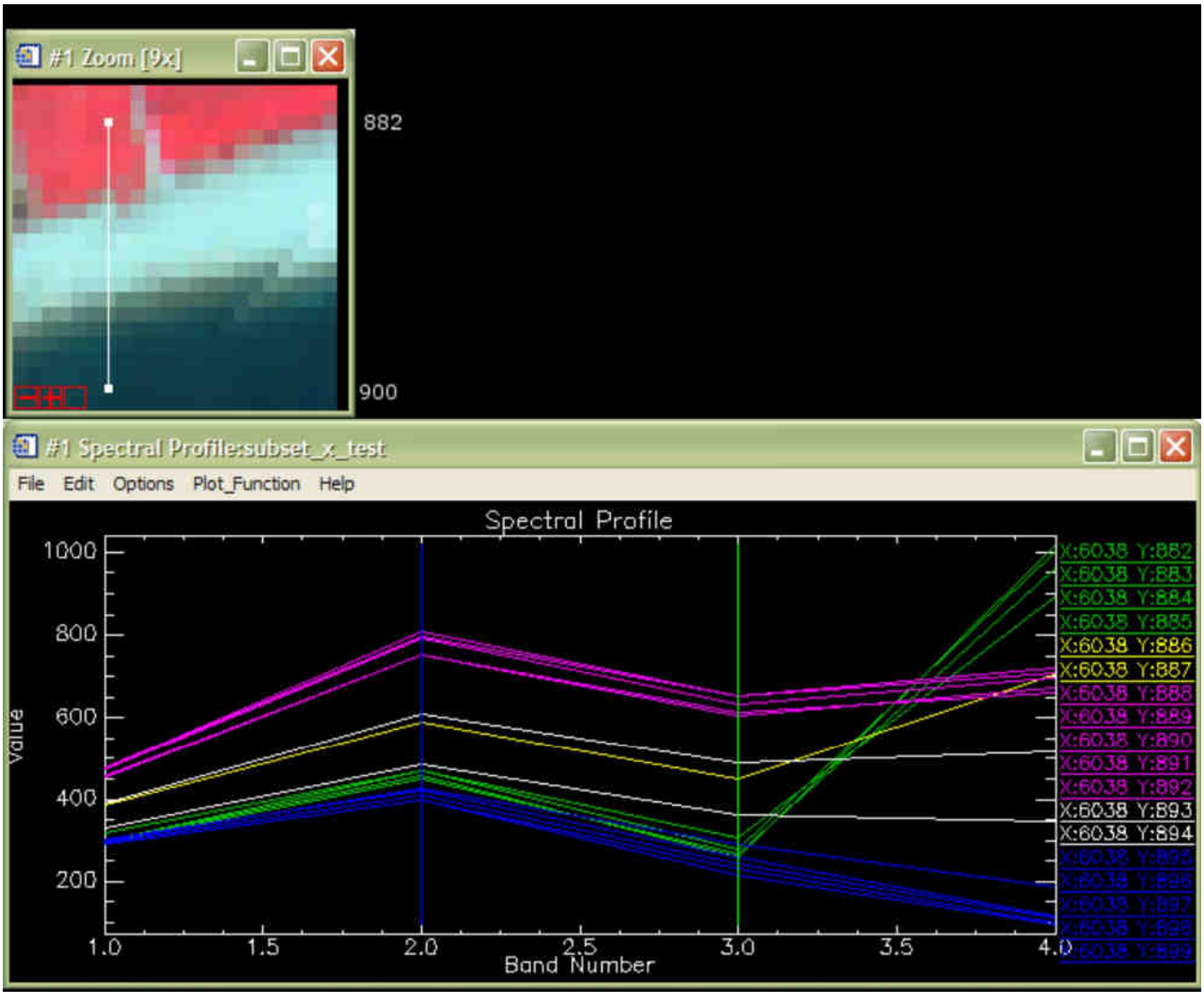

Figure 29: Spectral profiles

Some markers (1 roughly every 10 pixels) were entered on a band 4 image and an NDVI image within the test area, along the shoreline. This was identified using spatial profile analysis, with the help of spectral signatures and then compared with the shoreline identified using photo interpretation (Fig. 30). The maximum deviation is 2 pixels (about 5 m).

Figure 30: Comparison between shoreline data identified using transepts on NDVI images (red points) on NIR images (green points) and a shoreline identified using photo interpretation methods on a pan-sharpened image.

Even though the spatial resolution is higher for the pan-sharpened image it is harder to identify the pixel placed at the water/shore line using spatial profile analysis, while the shoreline is easier to identify using photo interpretation. We are currently working to optimise and improve pan-sharpened data in order to apply the same methods to data with higher resolutions.

Up until now the points have been positioned manually but we are studying a procedure that will enable us to automatically identify these points.

As far as ROI classification techniques are concerned they have all shown fairly good results, but the best ones were given by the maximum likelihood classification algorithm. Even though we do not currently have the land data needed for verifying results, the accuracy of classification obtained using the confusion matrix is stated at 92%. The shoreline, extracted from the corresponding classification using the classification to vector procedure was compared with results obtained using other processes (Fig. 31). A speedy result was also achieved using density slicing on band 4.

Figure 31: Comparison between the shoreline obtained using classification process and the shoreline obtained using photo interpretation.

The analysis of the Principal Components has allowed us to obtain a composite image which shows the difference between water, dry sand and wet sand. We plan to experiment a procedure which will extract the "shoreline" data from this type of image using the creation of ad hoc filters and supervised classification.

Once the shoreline has been obtained from a satellite image using either automatic or semiautomatic methods, it can be compared with data obtained using both photo interpretation techniques (from aerial photos or the actual satellite images) and land data obtained from GPS surveys.

The theoretical potential of frequent repetitions of these steps, considering the brief passages of the satellites over the same area, could, in the medium-long term increase accuracy. However costs of satellite images, especially with planned acquisition of the image, are still fairly high.

Beach nourishment numerical model

This research group aims to experiment a new model that provides volumetric estimates and morphological forecasts in support of artificial beach nourishment interventions. This model is applied for the first time to past nourishment initiatives in order to verify its potential via the use of tests which are mainly based on the comparison between real and predicted data. Three stretches of the Lazio coastline (central Italy) will be considered: Ladispoli, which underwent a nourishment procedure in 2003, as well as Minturno and Fondi where interventions took place more recently (March-April 2007). Agreements are currently underway so that data from another intervention may be included in the experiments.

Phase B activities focused on:

- obtaining topographic and bathymetric data for the three coastlines being analysed;
- improvement of model by extending its use to the post-nourishment phase;
- examination of the effects of the artificial nourishment in Ladispoli;
- application of model to the Ladispoli case;
- sampling of surface sediment (200 samples) from emerged and submarine beaches (up to -10m) from Fondi and Minturno;
- high-resolution grain size analysis (1/4 phi) on 100 samples taken in Fondi.

Improving the model and its characteristics

Part of our role has been to make some changes to the model and extend its use to the coastal monitoring and maintenance (beach re-fill) phases. More specifically we have developed two volume calibration techniques in order to correctly position the shoreline. In addition, the forecasts for spatial sediment distribution, which earlier referred to the entire mass included in the artificial deposit, are now also dedicated to the morphological surface of the nourished area. Finally we created calculus routines which also use real data (monitoring) to implement the accuracy of beach maintenance forecasts. What follow are the features of the updated model, inclusive of changes and an overall rationalization of its tasks.

The Grain-Size Nourishment Model (GNM) finds its main references in the natural progradation process that produces the seaward translation of the beach profile through the deposition of sedimentary bodies juxtaposed in sequence. In particular a single sedimentary body, for its scale dimension and formative processes, is taken to represent the attributes of the nourishment deposit: therefore it is prism in shape and comprised between the natural morphological surface and that following the intervention (Tortora, 1991; Dean, 1991, 1998, 2002). The geometry of this “artificial deposit” is the physical entity taken into consideration and described (3D) using bathymetric and grain size data organized into grid matrices (46 x 60 nodes) covering the coast that is being studied.

The model operates in three ways (module A, B and C): one forecasts results, one manages monitoring data and the other provides forecasts with the addition of real data (monitoring). Each module is applied to specific requirements within the beach recovery project, which generally includes pre-intervention surveys in order to design the nourishment phase (module A), post-intervention surveys to ascertain the performance of the reconstructed beach and plans (module B) for its future maintenance by sand refills (module C).

Module A uses topo-bathimetric and grain size data of pre-intervention surveys to forecast the geometry of artificial deposit based on the type of borrow material and the requested advancement of the shoreline. Processing uses three distinct calculation procedures based on equations that look at links between grain size characteristics, volumes, and geometric elements of the deposit. The first procedure results in a “simple translation” of the pre-intervention surface, with a measure equal to the required advancement of the shoreline. The second one changes the translated surface based on the characteristics of borrow material (Fig. 32). The third one varies it further by increasing or decreasing volumes in order to re-establish the correct position of the shoreline. The forecasts can end with the first process if borrow (B) and the local (L) sediments have the same grain size distribution (rare cases) or with the second process if B is different from L and the predicted shoreline satisfies project requirements, or the third process if it does not. Forecast elements are: topography of emerged and submarine beach, geometry of artificial deposit (thickness), its volume (i.e. quantity of material required), position of shoreline, and geographic sediment distribution through mean size, sorting and sand percentage parameters. Scenarios for more than one preliminary nourishment hypothesis (with different material and volumes) can be compared to choose the best solution for the live project.

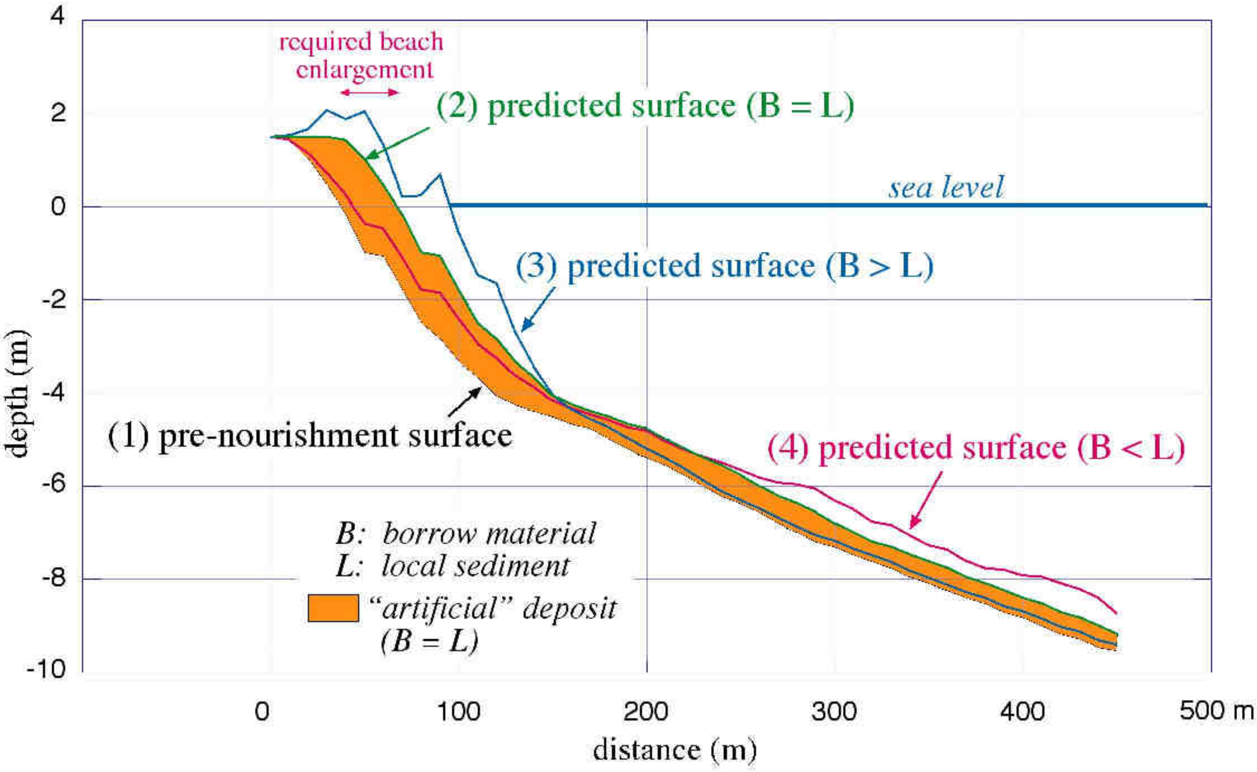

Figure 32: An example of morphological forecast: profile 2 represents the "simple translation" of the pre-nourishment profile 1, assuming local (L) and borrow (B) sediments having same grain size frequency distribution; profile 2 is modified in that 3 or 4 depending on borrow material grain size characteristics.

Module B manages post-intervention monitoring data, which, together with pre-nourishment data give a real picture of the deposit. The result is a morphological and geometrical "photogram" for each monitoring phase. Comparing these pictures, changes in sedimentary balance, morphology and geometry can be rapidly obtained.

Module C, dedicated to beach maintenance by refills, includes the same calculations of Module A but substituting the hypothetical "simple translation surface" with the morphological surface produced by the nourishment, which is further moved seaward and then changed based on the type of available borrow material. Even in this case various hypothetical scenarios can be assessed before choosing the right intervention.

Examination of the effects of the artificial nourishment in Ladispoli

The analysis of this nourishment focused on verifying changes and understanding activity trends, as well as obtaining a series of maps which have been compared with the forecasts provided by the model. The intervention in Ladispoli (March-April 2003) covered a coastal strip measuring about 2000 m whose beach was of limited width (10-30m) and had been retreating for some time: by 3 m/year and 0.8 m/year respectively during years 1950-1977 and 1977-2001. The nourishment action filled the emerged beach and was followed by levelling work which artificially increased it by about 50 m and lifted it by 1-2 m. The added sand had an average diameter of 0.164 mm and came from Lazio's continental shelf.

Data used:

a) 2001 investigation (data from Uniroma): bathymetric surveys (single-beam), sampling (100 samples) and grain size analysis; 2001 research covers the entire coastal compartment up to a depth of 20 m;

b) February 2002 (data from Regione Lazio): detailed bathymetric (multibeam) and topographic (RTK) surveys on the area affected by nourishment, up to -10 m;

c) March 2003 (data from Regione Lazio): detailed bathymetric (single-beam) and topographic (RTK) surveys on nourished area, up to -10 m;

d) April 2003 (data from Regione Lazio): bathymetric (single-beam) and topographic (RTK) surveys on nourished area (up to -7 m);

e) April 2004 (data from Regione Lazio): detailed bathymetric (multibeam) and topographic (RTK) surveys on the area affected by nourishment, up to -10 m;

f) 2005 (data from Uniroma): sampling (60 samples) on the nourished area (up to -10 m) and grain size analysis.

Methods

The data above were processed via automated gridding and contouring techniques obtaining two sets of maps (scale 1:5000), respectively referred to the individual survey periods and the differences between pairings of data from different periods (by subtracting grid matrices).

Five bathymetric maps were produced for the first set (from survey "a" to "e") and 18 sedimentary maps (samples "a", "f"), the latter relating to granulometric parameters: mean size, sorting, skewness, kurtosis, percentage of gravel, sand, mud and types of sediment using ternary classification. For the sampling (a) only, 5 additional maps were produced based on multivariate analysis results (cluster).

The second set of maps covers coastal changes before (surveys "a", "b", "c") and after the nourishment intervention ("d", "e", "f"). Six maps were produced using topo-bathymetric data (from "b" to "e"), allowing us to estimate the quantity of eroded and deposited sediment over the entire area and in single zones. Four maps highlight variations in spatial sediment distribution according to mean size, sorting, skewness and sand percentage.

A general overview of processes in action along the coast was defined by analysing the first set of maps. The sediment sources, routes of sediment transport, external wave action limits (about -6 m) and those parts of the coastline which are more affected by wave impact were identified. The second set of maps show that the artificial deposit, at intervention conclusion, included 367,000 m^3 of sand, 22.950 located on the emerged beach and 137,450 m^3 on the seafloor very close to the shore, which had been brought forward by 40-60 m (Fig. 33a). A year later the deposit decreased to 287,000 m^3 (Fig. 33b) of which 39,000 m^3 were located on the beach (previously 22,950 m^3), 208,000 m^3 within the first 4 m deep, 40.000 m^3 deeper than -4 m while 80.000 m^3 of materials were transported to adjacent coastal zones (lateral spreading). The artificial deposit therefore changed due to erosion of the emerged beach (retreated by about 30 m) and re-distribution on the medium shoreface of eroded material (Fig. 33c). Granulometric map comparisons highlight how, two years after the intervention, there has been a decrease in mean size (mm), a modest improvement in sand sorting and an increase in skewness values. Two years after the intervention the borrow materials could still be found on the emerged beach which leads us to think that the erosion and sediment re-distribution process had not yet completed.

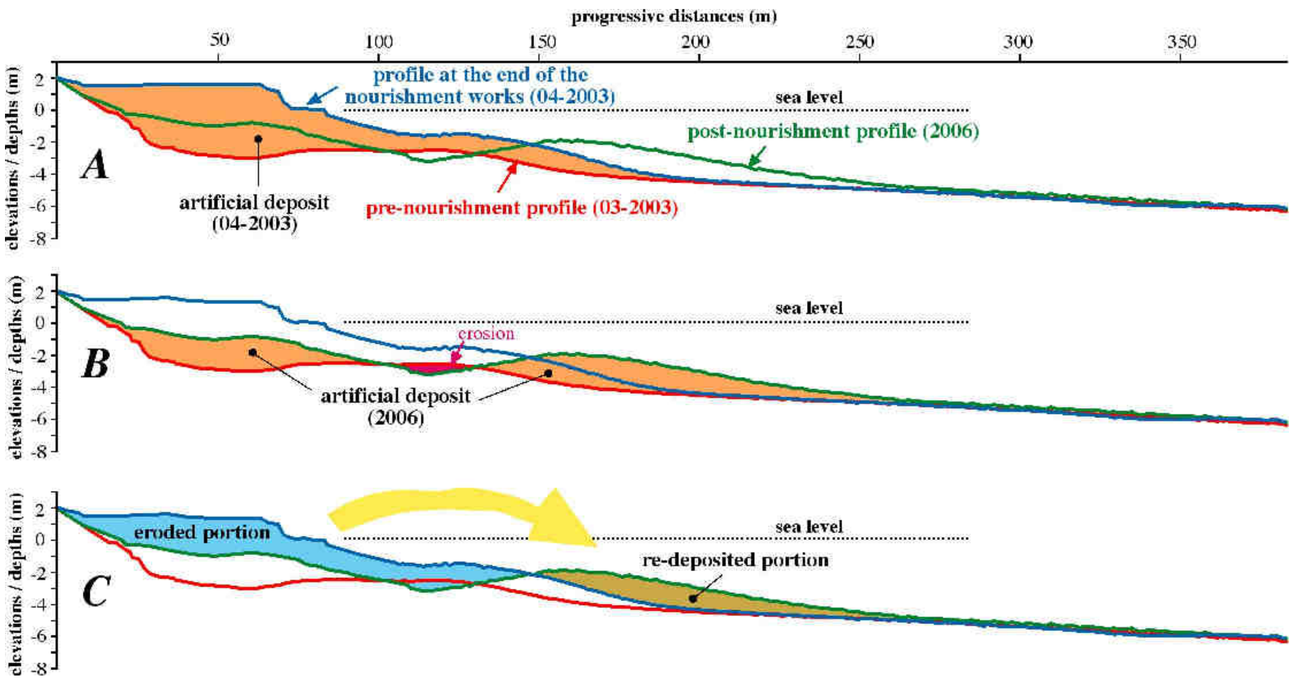

Figure 33: Transept right to the central sector of Ladispoli beach with profiles surveyed in different periods. Reconstructions a and b highlight the shape of the artificial deposit, respectively at the end of nourishment works and three years later. This deposit was re-shaped by waves (c) through erosion (dry beach backshore) and sediment re-deposition (middle shoreface).

Validation tests: Application of model to the Ladispoli case

a) Nourishment forecasts for Ladispoli

This forecasting process used topographic and granulometric data of the emerged and submarine beach (pre-intervention), and the grain size frequency distribution of the borrow material used for the nourishment. A “simple translation” of 33 m was imposed, in order to obtain an artificial deposit which was equal in cubic size to that found a year from the intervention (287.000 m^3). The following maps have been produced (scale 1: 5000) which predict:

- geometry of artificial deposit using thickness variation;
- topography of emerged and submarine beach;
- shoreline position;
- geographical distribution of sediment using mean size, sorting and sand percentage parameters.

These maps were compared with analogous ones based on real post-nourishment data. The matrices for the two thickness maps (respectively with real and forecast results) were also subtracted to verify any forecasting uncertainties, as was done for the two mean size parameter maps. From this comparison we can see that forecasts made are more reliable that expected, even though some uncertainties are present (Figs. 34 and 35).

b) Causes for forecasting uncertainties in (a)

Inverse techniques were applied (Cowell et al, 1995) to “force” the method to reproduce real post-nourishment evidence by acting on optional parameters: closure depth, type and quantity of borrow material. The objective for this operation was to ascertain whether the uncertainties in (a) depended on the parameters used or on the method itself. Many virtual nourishment tests were carried out for different combinations of optional parameters, without however producing any evidence that they were noticeably more correct than those used in the forecast (a). The conclusion is that uncertainties are part of the method and not dependant on how it has been conducted by the operator.

c) Evaluation of model sensitivity with regards to the grain size of borrow material

Eight virtual nourishments were recreated using the same input data but different types of borrow material. By comparing the eight forecasts on the map, significant differences are produced based on the features of the material. As far as shoreline advancement is concerned the best materials are the coarser ones from local sediments. Borrow material which is significantly finer does not advance the shoreline but is deposited on the lower shoreface. Borrow materials which fall in between these two types, will deposit closer to the emerged beach as their size increases. These experiments highlight that GNM is very sensitive to the type of borrow material.

d) Test on the “closure depth” parameter

These are a series of forecasts which are the same in everything except for the values assigned to this parameter, which during simulations affects the external limit of the coast being tested. By comparing the forecasts with each other noticeable differences can be seen, especially with regards to the shoreline, which moves towards the sea as this parameter decreases. The closure depth is a critical element which is to be set with great care before the model is applied.

e) Applying the model to critical cases

A large number of experiments were carried out to verify the predictions of GNM in very complex cases, specifically created altering pre-nourishment data and/or using borrow material of atypical grain size frequency distribution. Three limitations emerge from these experiments. The first is that the model cannot be applied when one or more fractions of the borrow sand are missing in the local sediment (GVN has no grain size references to store them on the coast). The second crops up when the borrow fractions with high percentages are only present in the coast in very restricted areas. In this case GNM concentrates such fractions producing deposits which go beyond the limits of natural aggregation. The third is that this model is sensitive to the along-shore sediment transport as long as bathymetric and grain size data contain the relevant information. On under-supplied coasts (pre-intervention) this information is often lacking which means that any forecast made will underestimate the effects of along-shore sediment transport.

f) Checking GNM calculation routines

In order to correct any programming errors a number of tests have been carried out using various strategies, which vary from isolating the individual calculation routines, to checking the results using inverted calculation routines (starting off from the results to work backwards to the known input data). In some cases specially created control programmes were used. All tests gave negative results and no errors were found.

g) GNM as a research tool

As requested by the Municipality of Ladispoli and in partnership with Regione Lazio, three virtual nourishments were carried out as part of a research project aimed at ascertaining the reasons behind the rapid beach erosion occurred after nourishment. The three forecasts are based on the same sediment amount used in Ladispoli and on a borrow sediment respectively equal, coarser and finer than the sand adopted for this intervention (Fig. 36). By comparing the three forecasts you can gather that the rapid erosion of the beach is due to the sand used, which is too fine and unsuitable for the equilibrium on the emerged beach.

h) Hypothesis for the recovery of the beach of Ladispoli

As requested by the Municipality of Ladispoli two nourishment scenarios were simulated to solve the beach erosion phenomenon which has been taking place since the 2003 intervention. The two hypotheses have both looked at volumes of 150,000 m^3, using two borrow materials with different characteristics, sourced respectively from the shelf areas of Tuscany and Lazio. Their average size is 0.25 mm and 0.17 mm compared with 0.19 mm for local sand. The forecasts were carried out using Module C of the GNM, whose forecasting calculations also use some of the data taken from post-intervention surveys. The model outputs (Fig. 37) show that material measuring 0.25 mm furnishes much better results, providing a shoreline advancing between 10 to 20 m. This material is eight times more stable than that used in 2003 (James, 1975).

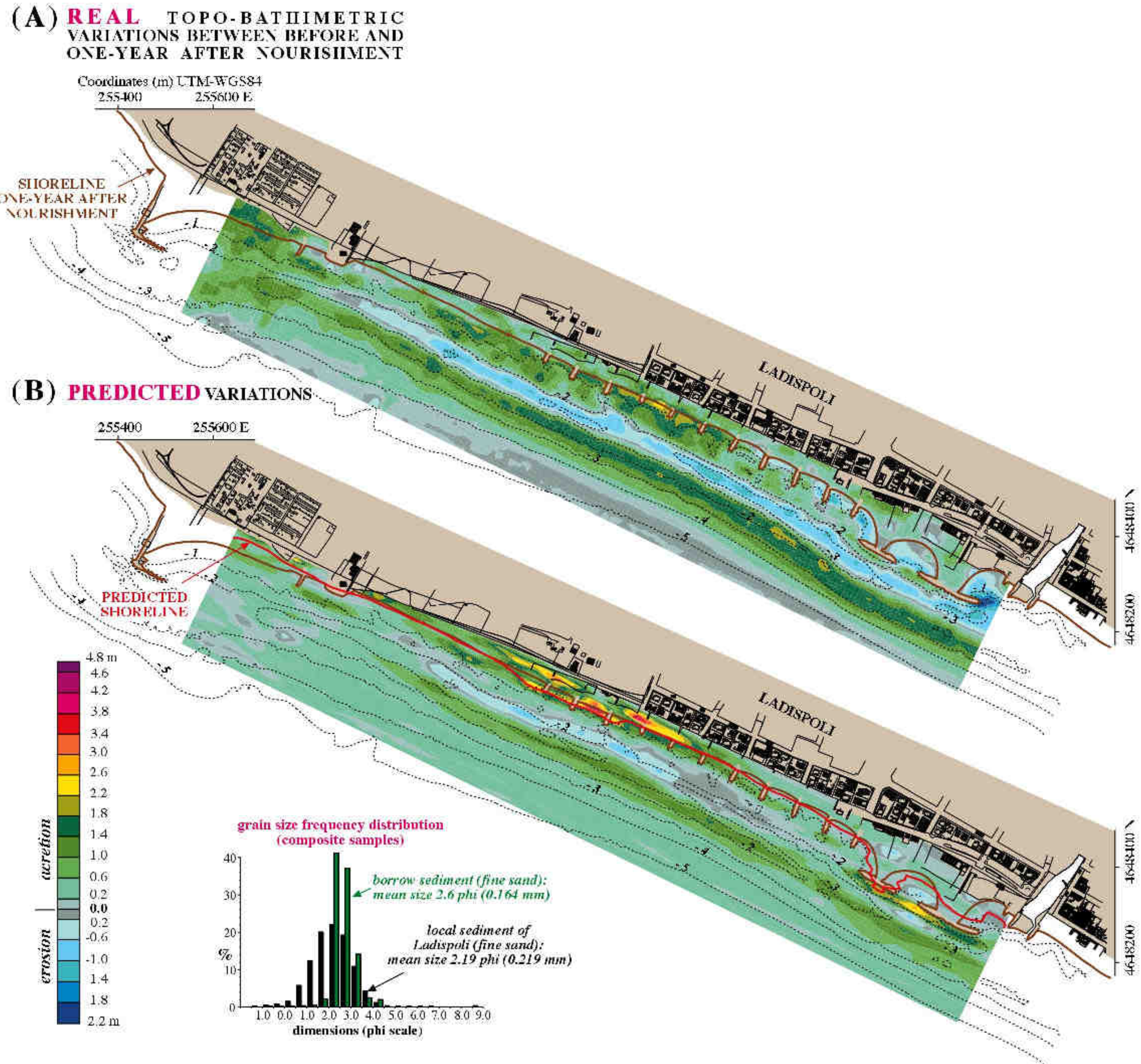

Figure 34: Comparison between the actual (a) and predicted (b) geometry of the artificial deposit. Input data for forecasting are: 287.000 m^3 of borrow sand having the same grain size characteristics of the one used for the Ladispoli nourishment; pre-nourishment topographic and grain size data (beach and shoreface) collected at Ladispoli coast. Deposits a and b have approximately the same volume.

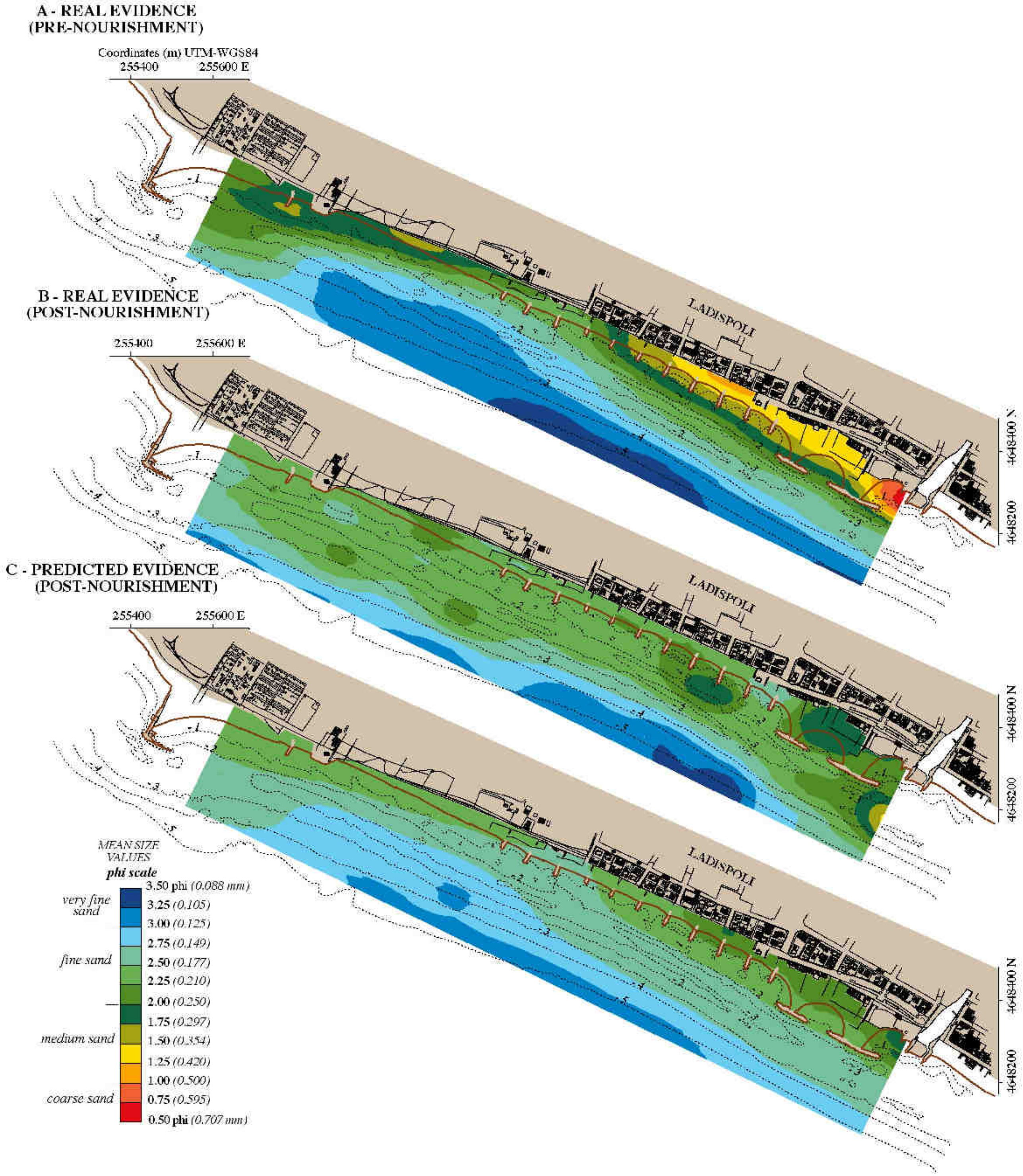

Figure 35: Distribution along the coast of the sand mean size before (a) and two year after (b) the nourishment. In (c), the model output using data as defined in the previous caption.

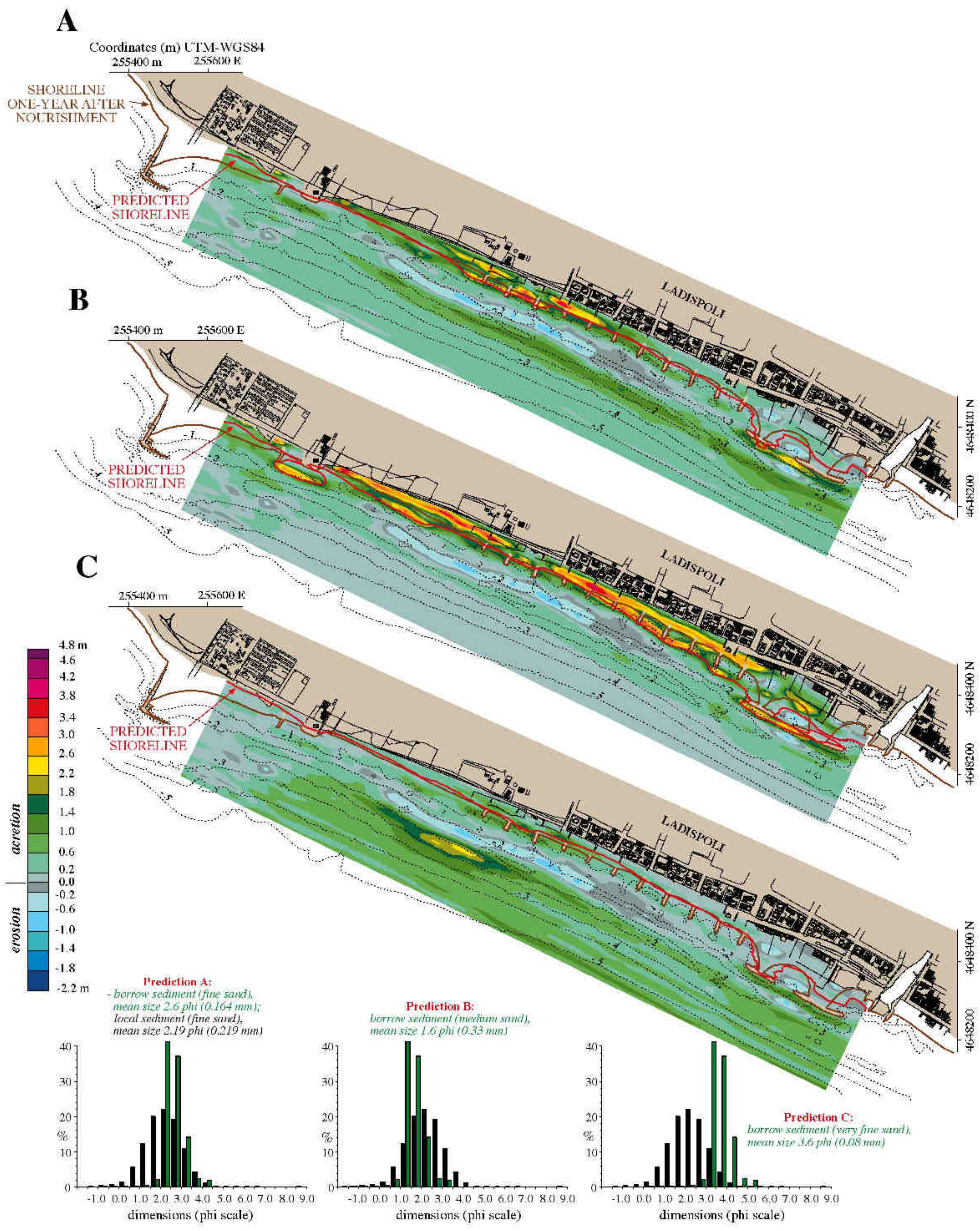

Figure 36: Use of the model in order to explain the very fast shoreline retreat after nourishment. Model outputs A, B and C forecast the geometry of the artificial deposit as it is shaped by a borrow sediment equal (A), coarser (B) and finer (C) than the sand really used for the intervention. These simulations suggest that beach erosion was due to the grain size of the sands, which was too much fine (A). In terms of shoreline advancing and stability a better result would have been obtained with sand of prediction B, a worse result with sand of prediction C.

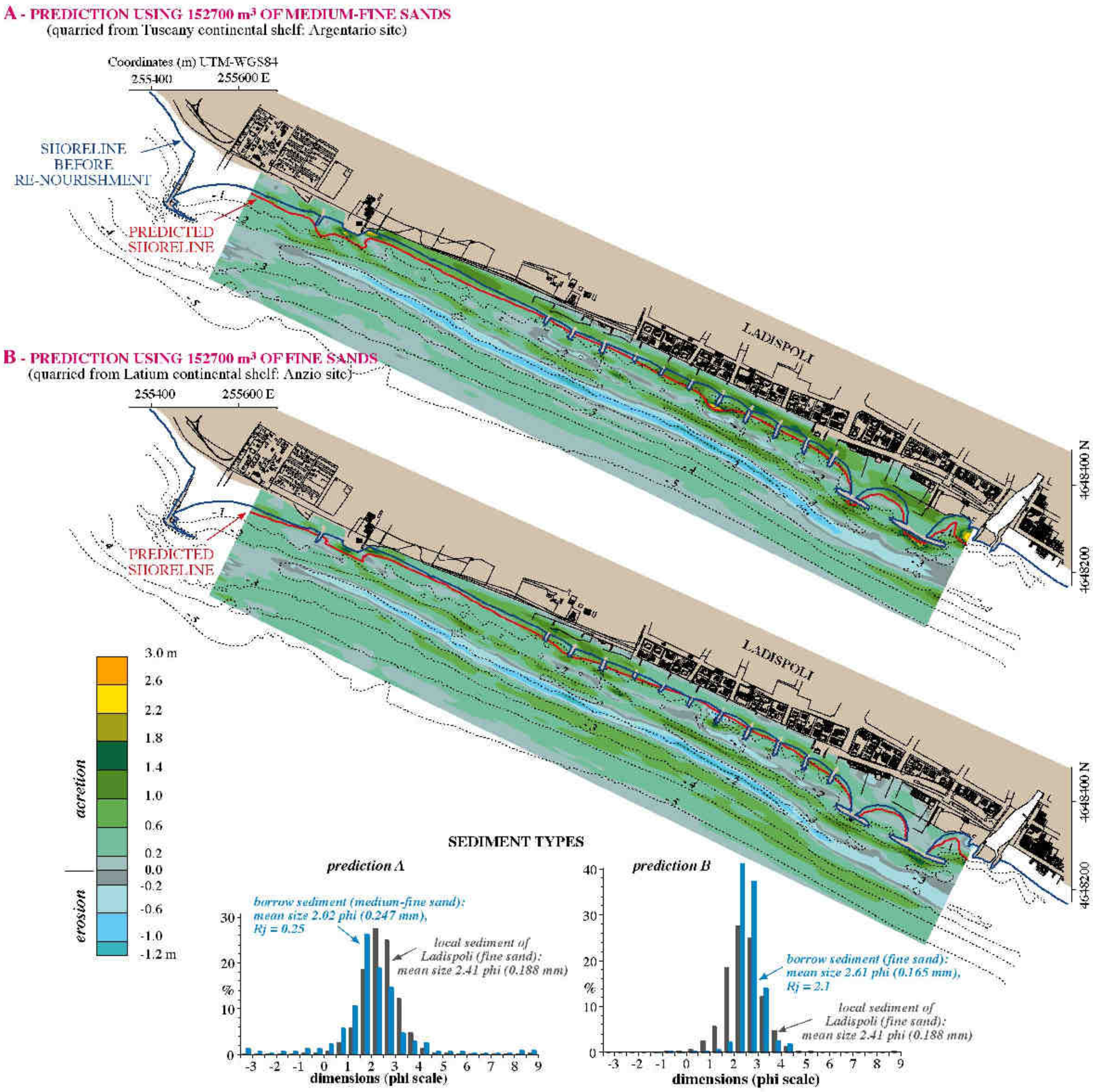

Figure 37: Use of the model for decision making to choose the borrow sediment for the Ladispoli beach re-nourishment. Maps A and B predict the geometry of the artificial deposit and the shoreline position if the same amount of different borrow sands is used. Comparing these maps, the hypothesis A appears better than B. Forecasting results have been obtained calibrating the model with data collected after the first nourishment

P5 - ARPA, Ingegneria Ambientale

Mentino Preti (mpreti@ia.arpa.emr.it); Nunzio De Nigris (ndenigris@arpa.emr.it); Matteo Monti (mmonti@arpa.emr.it)

In 1983 the Emilia-Romagna Region set up three regional monitoring networks to control the evolution of a coastal area measuring 130 km. The three networks measure extent of subsidence and the shoreline as well as topography and bathymetry of active beach, from the foot of the dune to closure depth. Over the years the three networks were measured every 5-8 years. Improvements were made each time to the technology used and the methodologies applied in order to obtain measurements which would increasingly represent real life scenarios. Over time the topo-bathymetric network has become increasingly important as it enables, in addition to examining the morphological changes to the seabed, to calculate volumes accumulated or eroded for each individual strip of coast.

In the last 10 years, in addition to the periodical surveys carried out of the regional networks, detailed surveys have also gradually increased. The latter surveys are used to monitor single strips which are in a critical state and are undergoing nourishment project, as well as assess the effects on the coast of tourist harbour and, more generally, of hard structures.

Detailed bathymetric data is obtained reducing space of the surveyed points grid. A large number of points per surface unit can be obtained either by increasing the number of profiles carried out using the single-beam method or by using multibeam. This latter survey system however is not easy to use in shallow waters such as those located along the Emilia-Romagna coast.

Issues related to the increase in costs due to the compressing of profiles and the long lengths of time required to carry out the survey have led to the decision to experiment in the Adriatic Sea with new surveying methods, more specifically the marine LIDAR. This system would enable a very detailed survey to be carried out in a short space of time even covering areas where seabed characteristics vary greatly, which is typical of areas where there are hard structures such as breakwaters, groins and harbour piers.

The main practical limitation found so far for the marine LIDAR in the Northern Adriatic is the lack of transparency of coastal waters for most of the year, especially those in front of the Emilia-Romagna coast. The coast is shallow and sandy and many rivers, streams and canals flow into it, which, as well as muddying the coastal waters with their clayey deposits, also bring many nutrients out to sea which favour the development of diatoms and other type of unicellular algae. Any surveys carried out with the LIDAR system therefore needs to be carried out in May and June if it is to be successful. This is because, as seen in the last few years, this is when the water is reasonably clear.

As well as problems due to water transparency, the marine LIDAR system still has two limitations which prevent it from being more widely used: the accuracy of data and the costs which are still too high.

Research carried out during Phase A using bibliography and websites and numerous exchanges with various technicians working in the sector, have highlighted the main features of the LIDAR surveying systems. There are three main suppliers in the international market: Canadian company Optech which builds the SHOALS system (www.optech.ca), Australian company Tenix with its LADS system (www.tenix.com) and Swedish company AHAB which supplies Hawk Eye II (www.airbornehydro.com). The three systems all work along the same basic principle and use the same techniques and technologies, even though each one has its own specific features (see report for phase A). At the heart of the system is a scanner which sends two laser beams, one of which can penetrate water. The depth of the seabed can be obtained by combining the results of the two beams when they return to base. This data, together with the positioning survey obtained using the GPS satellite system enables the seabed depth to be worked out.

The three companies guarantee the horizontal and depth accuracy to hydrographic IHO Order 1. Some case studies have shown that depth accuracies of 15 cm can be achieved, even though, due to the many variables found in a survey, the results can be affected by much more significant errors (Beachmed 2005; Milli and Surace, 2006). The maximum depth which can be surveyed depends on the transparency of the water and is equal to about 2-3 times the depth of the Secchi Disk. The density of detectable points is very high, as you can actually survey square grids with sides measuring 2-5 m. Together with the high number of measurable points there is also the speed with which measurements can be made, as areas measuring many tens of km^2 can be surveyed a day.

The costs per km^2 for area surveyed can oscillate between € 1000 - 2000 if the surveyed areas are at least 50-100 km^2. The highest costs incurred are for the aircraft and equipment hire as well as salaries for pilots and specialised technicians. Mobilisation and demobilisation (mob/demob) costs are around €100,000.

Objectives

As tests in the Adriatic Sea using the marine LIDAR system have not so far achieved satisfactory results, ARPA-IA aims to:

- Implement a bathymetric survey using the LIDAR system along the Emilia-Romagna coast during intervals when the water is as clear as possible;
- Carry out comparisons with traditional surveys carried out in the same area and during a time interval which is as close as possible to the LIDAR survey.

Project

Due to the high costs of Lidar surveys and the very modest budget available to ARPA-IA, we would only be able to achieve the first objective mentioned above if a Company which has already or plans to carry out a bathymetric survey using this system along the Emilia-Romagna coast agrees to share the data it has acquired with us.

Back in 2006 we contacted various companies to encourage them to carry out a survey of this type and then make it available to ARPA Ingegneria-Ambientale as part of the Beachmed-e project. We turned to many third parties for the implementation of a LIDAR bathymetric survey along the Emilia-Romagna coast. We found that ENI (Ente Nazionale Idrocarburi) was not only interested but had also implemented a survey of this type in this area, measuring about 50 km, which goes from the piers of the port of Rimini to those of the port of Ravenna. The survey looked at the emerged beach and the seabed up to a bathymetry of 10 m. In some areas the survey reached out to sea up to a bathymetry of 16 m. The work was carried out between the end of May and beginning of June 2006 by Tenix Lads Corporation which used the LIDAR LADS MK II system (Fig. 38). We have already contacted ENIS's technicians so we can acquire the data that was obtained and the survey reports.

As far as the second objective is concerned, which compares the LIDAR survey with ground surveys using traditional methods, we are considering using the surveys carried out in the same area by ARPA – Ingegneria Ambientale during the same period or one as close to it as we can get. In spring 2006, ARPA Ingegneria-Ambientale actually carried out the topo-bathymetric survey of the regional network. This is made up of 251 sections which are perpendicular to the coast and are all 350-500m in distance from one another. In some localities, including Igea Marina, a compressing procedure was also carried out using sections which were perpendicular to the coast, 100 m in distance from one another and formed several parallel crosses to the coast (Fig. 39). The bathymetric survey was carried out using the GPS and single-beam systems together, along the strip of shallow coastline (from a depth of 60 cm up to 2-2.5 m), while multibeam was used in the remaining part out to sea. This detailed campaign was carried out in March, which is therefore just a few weeks from the LIDAR survey.

In order to assess the clearness of the water during the time when the LIDAR survey was carried out, the sea transparency data measured periodically by ARPA Daphne (Fig. 40) will also be acquired. The measurement is carried out using the Secchi Disk. Once all necessary data has been obtained it will be analysed and comparisons will be made between topo-bathymetric surveys carried out using the LIDAR system and those using single-beam and multibeam in order to ascertain any differences and errors.

Figure 38: Aircraft used for Lidar survey.

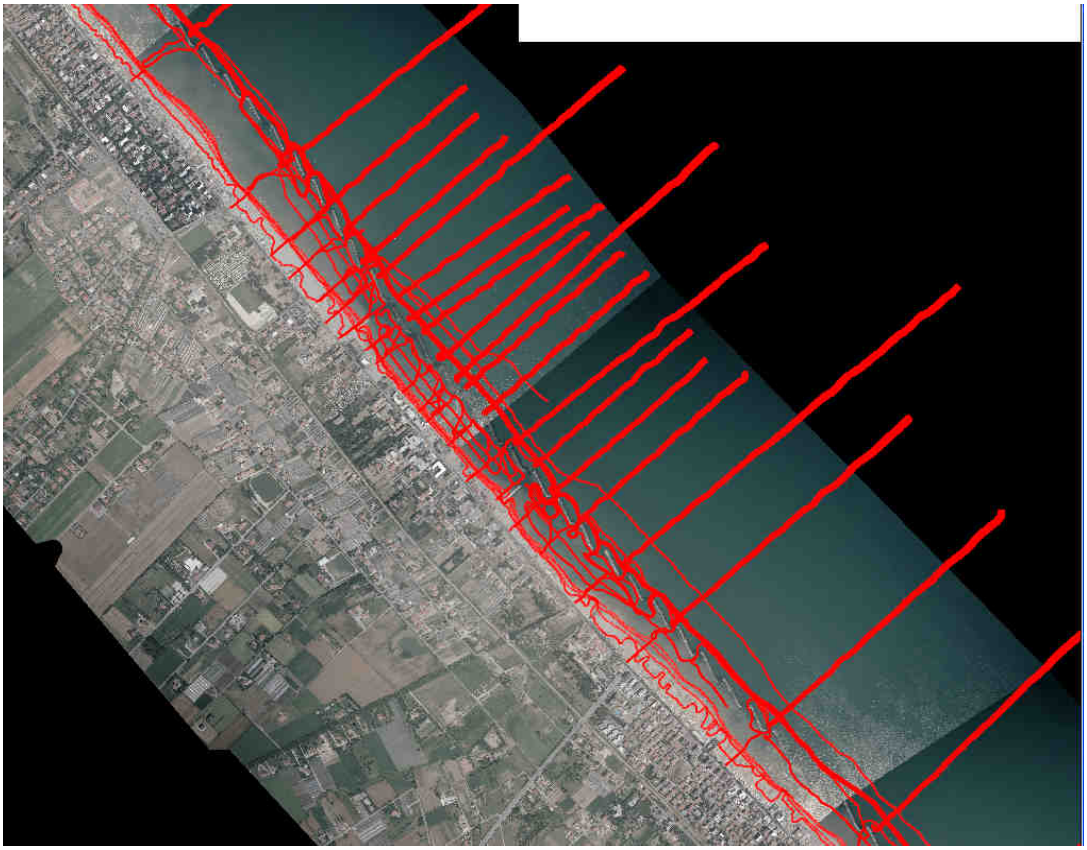

Figure 39: Details of bathymetric survey carried out using single and multibeam in the Igea Marina locality

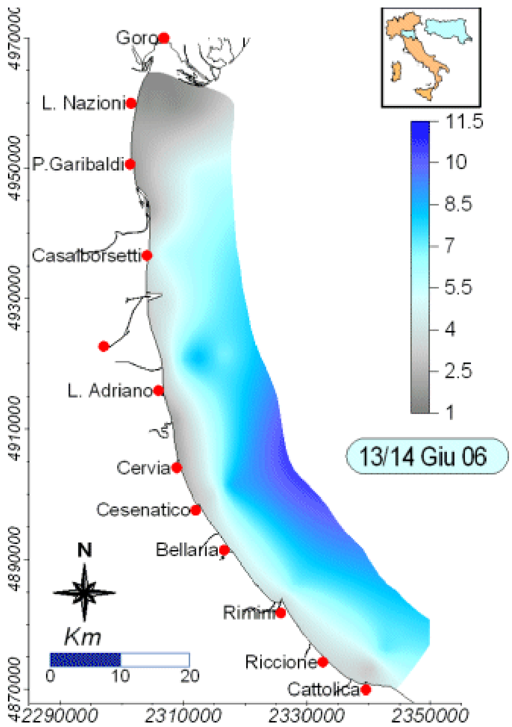

Figure 40: Example of a transparency map, created by ARPA Daphne.

P6 – EID

Hugues Heurtefeux (hheurtefeux@eid-med.org); Audrey Lesaignoux (alesaignoux@eid-med.org); Eric Sire (esire@eid-med.org)

Within Programme OCR Interreg III C Beachmed-e, which is a research schedule centred on new technologies to realize a precise and regular monitoring of the shoreline, EID-MED is testing LIDAR as a monitoring tool. "Conseil général de l'Hérault" and the "Direction Régionale de l'équipement Languedoc Roussillon" are the financial partner of this ambitious project.

This report is at the semi-course of the program, which in terms of administrative times coincides with the phase B. This report presents the analysis of the results of the flight pre-test (presented in the report of the phase A) carried out in Mars 2006, on a zone of 12 km of length and 500 m broad on the Gulf of "Baie d'Aigues Mortes", and also the description of the preliminary phase of the flight test of April 2007. Finally, the technical schedule of conditions of this mission of flight test on "Baie d'Aigues Mortes" is described.

Pre-test flying campaign

In the purpose of testing technical and economical relevance of LIDAR acquisition, an evaluation test was made out on "Baie d'Aigues Mortes" in spring 2006. First results were produced in the phase A report.

Pre-test flying was realised by Admiralty Coastal Surveys AB with Hawk Eye II system to obtain topographic and bathymetric data. In bathymetric mode, LIDAR emits a green laser at 532 nm with a frequency to 4 kHz. It is projected by rotary mirror which sweeps water surface with swath width of 120 m and flight altitude of 300 m. Associated with the LIDAR system, navigation and position are provided by an integrated GPS and inertial reference system which delivers accurate co-ordinates in all three dimensions. Detection system gives point density of 0.45 pts/m^2 (1 point every 1.5 m) in bathymetric mode, and a value superior to 6 pts/m^2 (1 point every 0.4 m) in topographic mode.

Survey's results were: 1) Raw data on disc ASCII format with x, y and z coordinates; 2) Interpolated grids with the step of 8 m. Final positions and heights / depths were referenced on WGS 84 UTM projection system and local French Lambert South III system.

The first stage is to reduce dataset for needed accuracy and means of put calculations. In this study, grid size 2 m, 5 m and 10 m were produced. The interpolation method chosen is Kriging which uses in the same time a weighting by the distance and the variogramme (Swales, 2002). Kriging is an exact interpolator due to estimated value of a point of measurement being equal to the value of it. More, kriging is an optimal interpolator since it minimizes the variance on the error estimation. The main constraint is computing time. Three softwares were used to produce numeric models: Golden Software® Surfer 8, MapInfo® Vertical MapperTM, and ESRI ® ArcGis.

Digital surface models (DSM) were built from data provided. These digital models allowed detection of tiny morphology and exact shape of underwater bars (considered rectilinear hitherto). In Figure 41, DSM provided by LIDAR survey presents pluri-metric morphologies which could never have been observed by the surveys methods known as traditional.

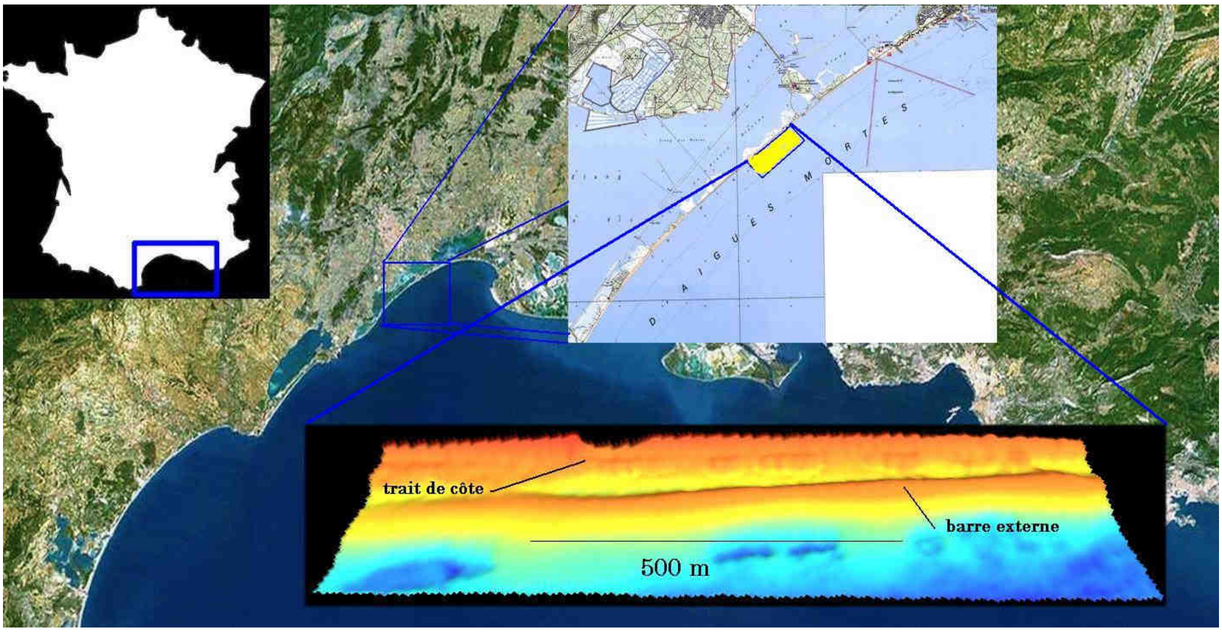

Figure 41: Location of pre-test flying place and Digital Surface Model provided by LIDAR

Figure 42 shows a comparison of Digital Surface Model, one in the Gulf of Aigues Mortes realised from LIDAR data in March 2006 (grid size 5 m), and another provided by echo sounder data in June 2006 (grid size 10 m).

"New" morphologies are put into evidence despite problems of representation related to a more important interpolation on data provided by traditional methods. The infracoast beachrock known as sandstone of Carnon are quite visible on the LIDAR survey: they are presented in the form of chaotic reliefs levelling in the seafloor from 8 to 10 m. However, on the external bar, harmony is acceptable between the surveys methods: if the external bar seems festooned on March 2006 (LIDAR survey) and linear on June 2006 (echo-sounder survey) then it results from a morphological evolution due to marine forcing. In this instance, it is necessary to have a field wake approach in order not to confuse normal evolution and data error.

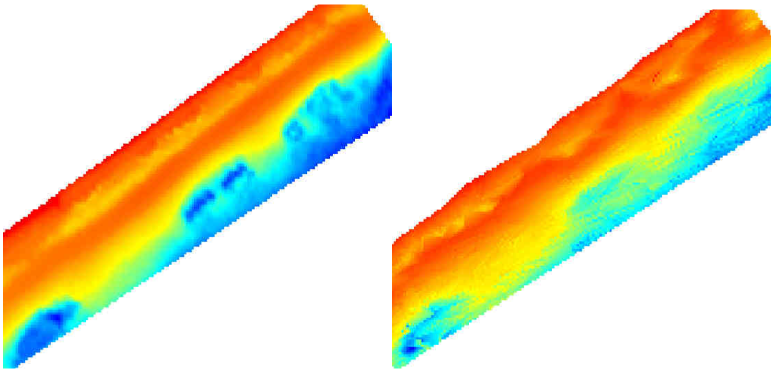

Figure 42: Comparison of digital model provided by "traditional" survey (EID data, June 2006, on the left) and provided by LIDAR survey (data Admiralty Coastal Surveys AB, March 2006, on the right)

The high density of data also makes it possible to identify accurately morphologies of small sizes (sand dunes, mega ridges) created by hydrodynamics of swell and currents. In the nearshore, these morphologies (Fig. 43) are usually mapped by traditional techniques. Indeed, it is almost impossible to obtain sufficient density points with echo-sounder single-beam, and the water in the bar area is too shallow for using multibeam sounder.

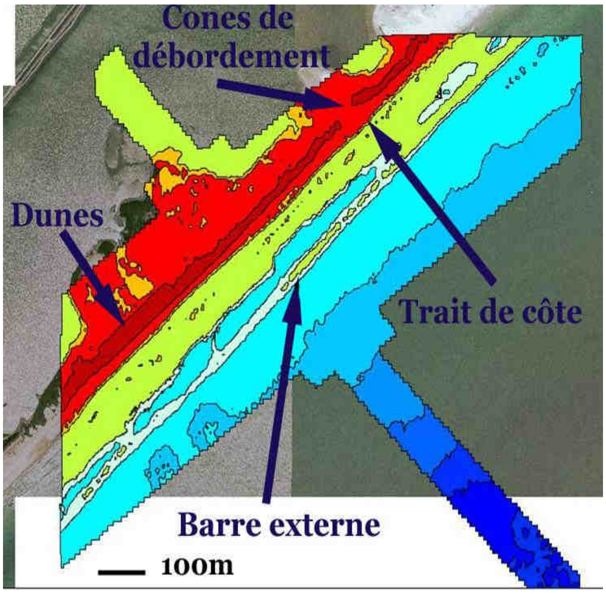

Figure 43: Morphologies highlighted on DSM LIDAR: sand dunes, nebkas bush, contours of the cones of overflows (overwash) in contact with the pond.

Survey evaluation: density

Random samplings were carried out in four sectors of 100 m^2 on the study zone to check real density acquired at the moment of survey. The mean density is about 0.6 pts/m^2 but this one is not regular. We obtain a density of 0.4 pts/m^2 in the sectors not covered, and 0.8 pts/m^2 in the coverage of two flight lines sectors. So, it is necessary to execute coverage of at least 40% between two successive lines to get significant and homogeneous density.

Limits on shallow water and/or with turbidity

It's impossible to characterize the bottom in the shallow water depths with bathymetric LIDAR return due to superposition of the signals corresponding to the water surface and bottom. The "white" in the data is variable and can depend on agitation on the water surface, turbidity, etc. For example, in the areas of mouths which presented more important turbidity, the results are not satisfying. On the other hand, on the Lido of Maguelone, the great diversity of the funds (beach-rock, pebbles, sand) does not seem to have influence on the data of altitude.

Vegetation and framework fitting-out impacts

For example, a survey was also made by the BRGM with Admiralty Coastal Surveys on the Corsica coastal zone. The detailed study of the results obtained made it possible to highlight some features, resulting from broken reliefs (structures of littoral installation), or from the presence of sea grass (*Posidonia oceanica*). Herbarium localisation is relatively easy due to a very chaotic signature on the digital model (Fig. 44). On the other hand, as already studied by many authors, the identification of the bottom and height of the herbarium is much more complex. Indeed, the return can correspond to the top of the herbarium, the bottom, or an intermediate position as function of the penetration of the laser in the sheets.

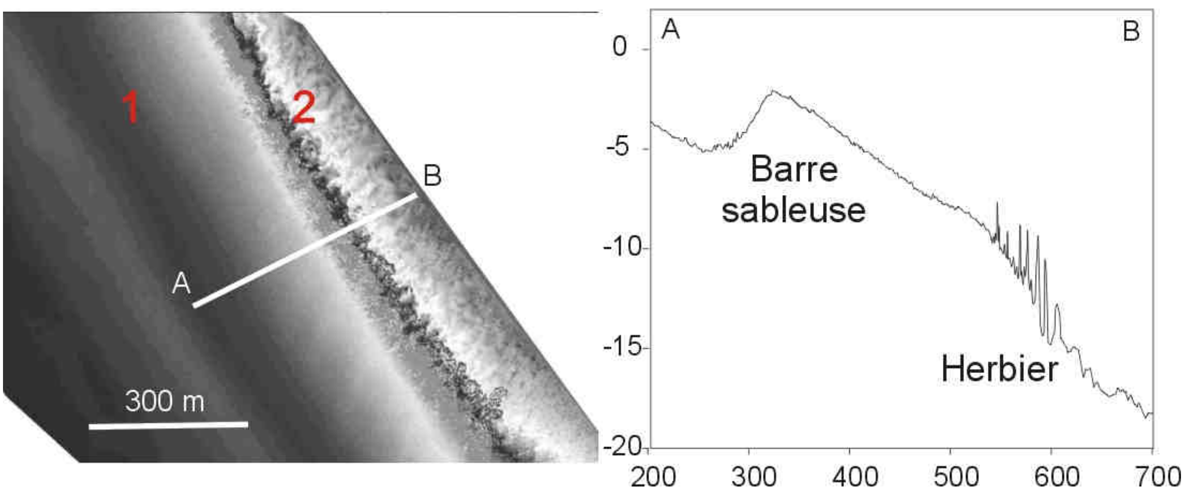

Figure 44: Characterisation of an herbarium of *Posidonia* on the LIDAR data. Morphologies observed on the digital model (on the left): 1) smooth features on the sandy bars and 2) chaotic features on the herbarium. Profile (on the right) showing the strong variation of amplitude on the herbarium.

Conclusion on analysis data of pre-test flying

The results of the campaign executed on the Lido of Villeneuve-les-Maguelone, highlighted a precision of altimetry of LIDAR data in the coastal zone which is comparable to that from technologies known as traditional (bathymetry mono, multiple beam). However, dataset density is more significant and homogeneous. LIDAR technology makes it possible to build digital terrain models (DTM) that are much more realistic and allow to observe low-size morphologies. In addition, the technique makes it possible to obtain a simultaneous survey of topography and bathymetry, with a gap of data close to the shoreline (in shallow water) which remains very limited if the conditions of agitation are weak. Fast operation of LIDAR (about 25 km^2/h) is also a strong asset in comparison to the other techniques in these environments where morphology can evolve very quickly.

Although sensitive to the weather conditions (cloudy cover in particular), it is possible to carry out a post-storm survey as soon as a window of good weather is presented, whereas a ship cannot have such a reactivity, and remains completely dependent on the conditions of marine weather, residual swells, etc. However, if this system can be quickly used, to ensure a post-storm survey, the quality of the results obtained degrades very quickly if the conditions of sea are bad (agitation, broad zone of surfing at the coast, etc.) or in the zones of mouth where turbidity increases following a strong gale wind.

Provision of LIDAR mission

Secchi measures

Measurements of turbidity carried out with Secchi's disc (demonstration below with: a) wager on the sea of the disc b) visibility at -1 m c) visibility at -3 m and d) retrieval data) on three coastal areas of Baie d'Aigues Mortes: Frontignan, Palavas-les-Flots and la Grande Motte (Fig. 45).

On the whole of these three zones, the maximum measured value of the turbidity index (depth ratio on the limit of visibility of the disc of Secchi) amounts to 2,2 (Fig. 46 and 47). Thus, knowing that the depth of acquisition which LIDAR can reach is estimated in the literature between 2,5 and 3 times the Secchi's depth, we can establish that for the zones where the index is equal or lower than 2, turbidity will not have influences on the LIDAR measure.

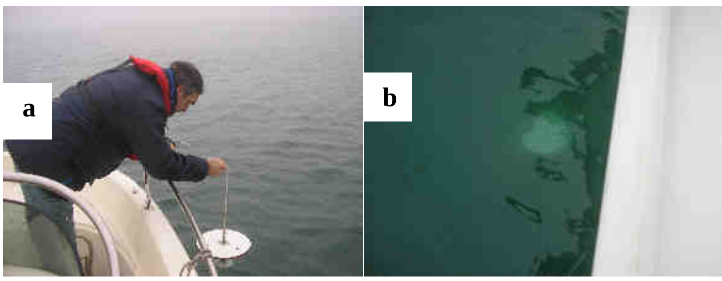

c d

Figure 45: Measurements of turbidity carried out with Secchi's disc (demonstration below with: a) wager on the sea of the disc b) visibility at -1 m c) visibility at -3 m and d) retrieval data) on three coastal areas of Baie d'Aigues Mortes: Frontignan, Palavas-les-Flots and la Grande Motte. The climatic conditions at the time of these measurements of turbidity are presented in Table 3, according to the wavegraph coming from the buoy of Sète.

Table 3: Climatic conditions at the time of turbidity measurements (wavegraph from the buoy of Sète):

Date	**Significant height of the waves (m)**	**Temperature of the sea (°C)**	**Mean velocity of the wind (knots)**	**Wind direction**
15/03/07	0.2	13.5	8	South East

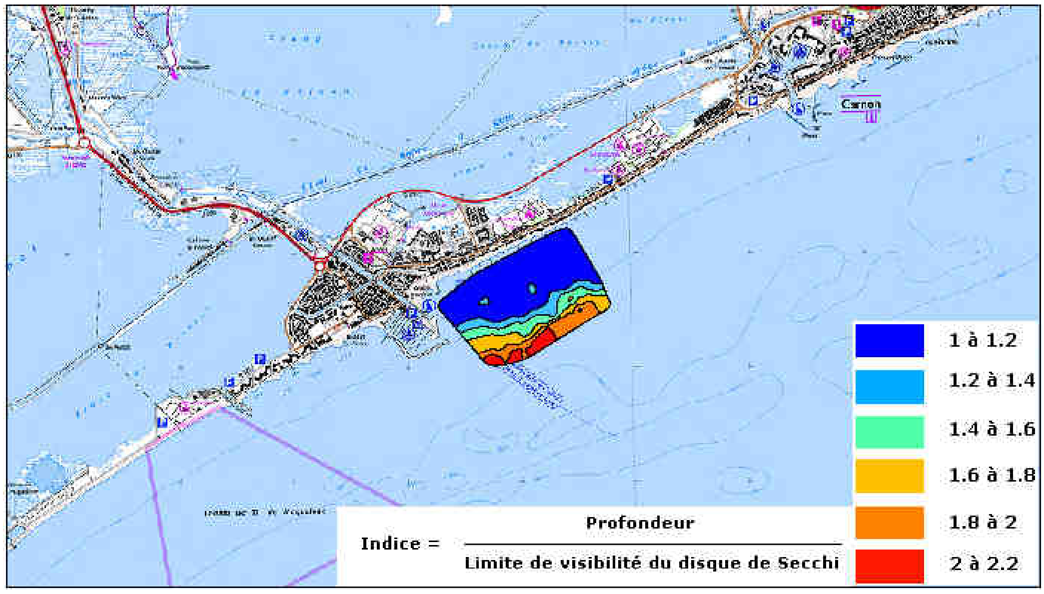

Figure 46: Representation of the interpolation of measurements of the index of Secchi on the zone of Palavas-les-Flots in March 2007 (index is the depth ratio on the visibility limit of Secchi's disc)

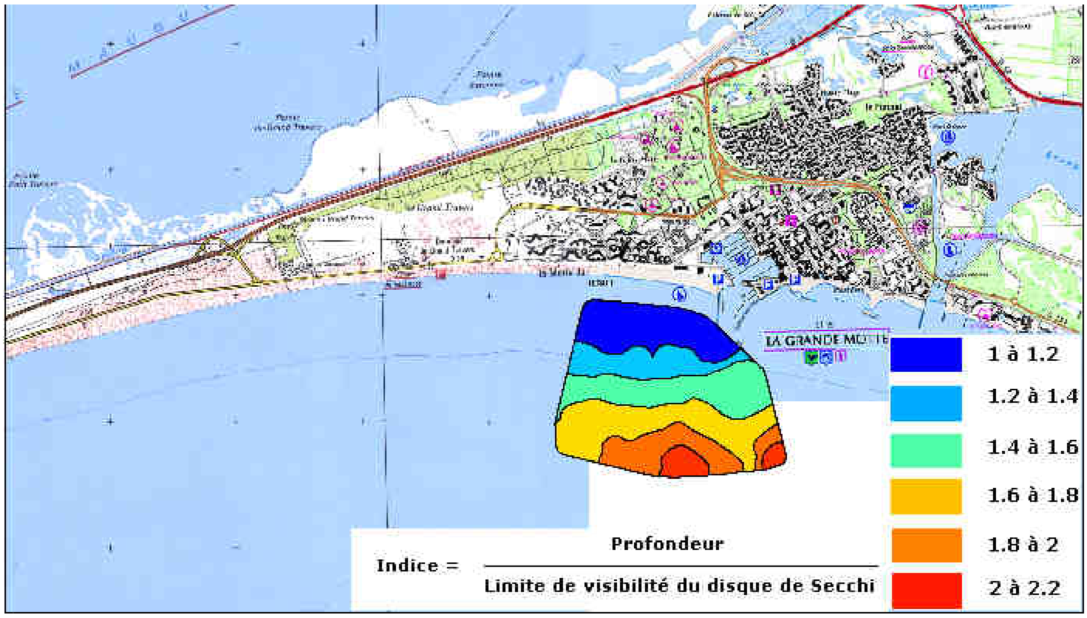

Figure 47: Representation of the interpolation of measurements of the index of Secchi on the zone of the Grande-Motte in March 2007 (index is the ratio of depth on the visibility limit of Secchi disc)

Bathymetric LIDAR systems

Currently, there are three great systems of Bathymetric LIDAR, whose main specifications are gathered in Table 4.

Table 4: main specifications of major bathymetric LIDAR systems

	SHOALS 1000T	**EAARL**	**HAWK EYE II**
Builder	Optech	NASA	Saab Dynamics
Flight altitude	200-400 m	300 m	400 m
Swath width		240 m	140 m
Beam off-nadir angle	0-40°	0-40°	0-40°
Diameter size of laser spot on surface	240 cm	15 cm	40 cm
Vertical accuracy	15 cm	15 cm	25 cm
Horizontal accuracy	-	1 m	5 m
minimum measurable water depth	20 cm	30 cm	30 cm
maximum measurable water depth	60 m	25 m	40-70 m
Type of Laser	Classe IV Nd :Yag	Classe IV Nd :Yag	Classe IV Nd :Yag
Energy green laser	5mJ	70 microJ	5mJ

In all cases, the general principle of bathymetric LIDAR operation (Fig. 48) is the same: send-receive of intense laser impulses (several megawatts), at regular frequency, of which the duration of advance is transformed into distance (laser Telemetry). Its characteristic is the use of impulses in two wavelengths: an impulse in infrared (1064 nm) reflected by the surface of water, and an impulse in the green (532 nm) which penetrates the surface of water and then is reflected by the bottom of water.

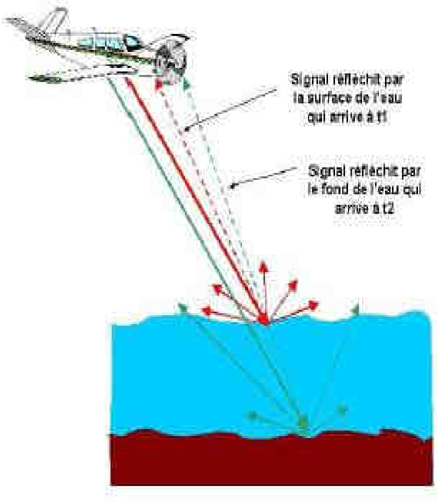

Figure 48: Principle of operation of bathymetric LIDAR (Lesaignoux, 2006)

Technical schedule of conditions

The OPTIMAL project aims at the topographic and bathymetric data acquisition of the emerged and submerged beaches in the littoral of "Baie d'Aigues Mortes" using an airborne bathymetric LIDAR sensor.

The test area to be explored by the LIDAR technique covers a total surface of a little less than 50 km^2: it is a succession of urban beaches (city of Palavas-les-Flots) and more natural sectors, virgin of all anthropisation (Lido of Villeneuve-les-Maguelone). Since these beaches are highly visited in summer, the period of data acquisition was the end of April 2007.

Campaign objectives

The objective of this campaign is to collect, by means of an airborne laser, altimetric information on the coastal zone, which could constitute an indicator which can allow us to generalise thereafter this type of statement on the whole of Golfe du Lion. The density of points, which will determine the smoothness of the survey, will be compatible with the applications and the surroundings and need to allow:

- The study of morphology of field dunes;
- The identification of foredunes;
- The study of possible zones of immersion to the backshore;
- The study of morphology of inner and outer bars (seafloor forms).

This type of LIDAR measurements will have to make it possible to mitigate the lack of data on:

- The feature of coast;
- The space influence of the tricks (ears, mole) and their effects on the surroundings;
- The space influence of the dwellings at sea front when they exist;

- Micro-topography necessary to the hydrodynamic models with fine meshs applied to local problems (such as sedimentary transport).

This topographic and bathymetric survey will make it possible to evaluate the width of phenomena such as erosion and sedimentation on the scale of the beach ensemble. During the course of the mission, the EID Méditerranée executed in parallel control surveys on the ground and at the sea.

Surveys area description

The map (Fig. 49) delimits accurately the areas covered by the bathymetric LIDAR: each green rectangle was digitalised under the software MapInfo®. As this figure shows it rather schematically, the LIDAR area covered is marked by three zones which correspond to indicative tracks of the aircraft way. The reference marks (yellow stars) for the depth were extracted from the database of bathymetric profiles acquired annually by the EID service of littoral monitoring within the framework of the departmental observatory of the littoral. The surface presented covers a totality of 47 km^2.

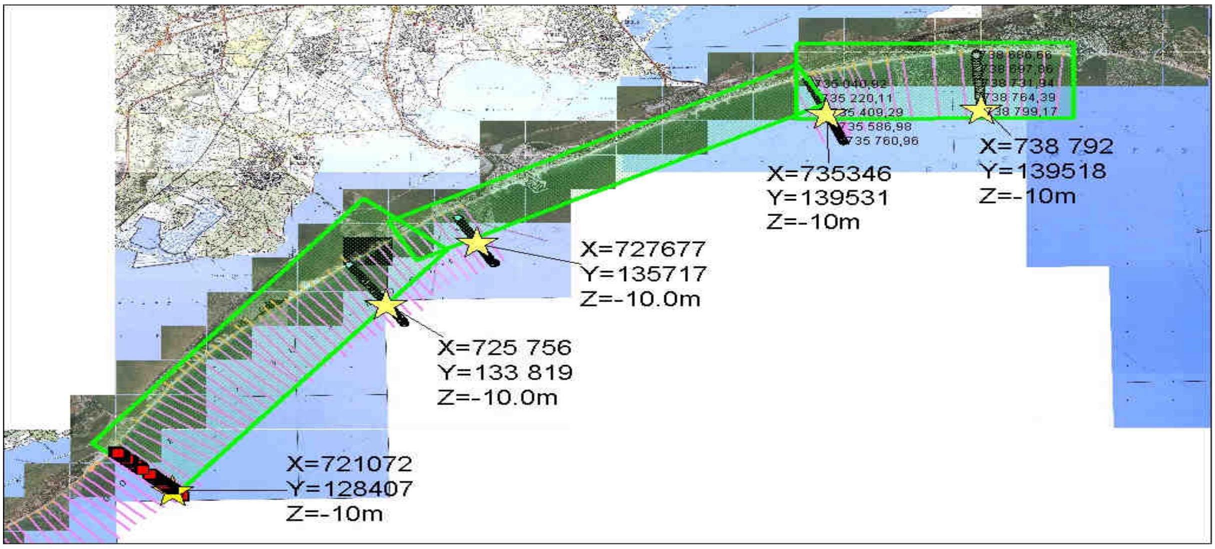

Figure 49: Area covered by bathymetric LIDAR in the Gulf of "Baie d'Aigues Mortes". Co-ordinates given in Lambert III South.

Co-ordinates X and Y of the tops of the zones 1 and 3 (in the direction of the needles of a watch), given in Lambert III South, as well as the co-ordinates of the tops of the rectangle of zone 2, to be covered by the LIDAR flight are presented in Table 5:

Table 5: Co-ordinates X and Y of the tops of the zones 1 and 3 (in the direction of the needles of a watch), given in Lambert III South, as well as the co-ordinates of the tops of the rectangle of zone 2, to be covered by the LIDAR flight

Zone 1 : Frontignan – Villeneuve les Maguelone		**Zone 2 : Villeneuve les Maguelone – Petit travers**		**Zone 3 : Petit travers – La grande Motte**	
Surface : 22 km²		**Surface : 13 km²**		**Surface : 12 km²**	
X	Y	X	Y	X	Y
720500	127700	726400	135200	734700	139300
718800	129300	725800	136200	734700	140900
722500	133700	734800	140800	735600	140900
722800	133500	735400	139700	735600	141100
723300	134100			737000	141100
723400	134000			737000	141300
724000	134700			748000	141300
724100	134600			748000	139300
725500	136700				
727100	135400				

The provider has a duty regarding results, however an absence of data corresponding to a maximum of 5% (that is to say approximately 2,5 km^2) of total required surface (above) will be tolerated.

The LIDAR provider: Admiralty Coastal Surveys AB

The provider who answered our request is the Sweden Company Admiralty Coastal Surveys AB, which had also accomplished the pre-test flight. They use the LIDAR system Hawk Eye II. The technical specifications of this system are presented in Table 6.

Table 6: Technical specifications of LIDAR system Hawk Eye II

PARAMETERS	VALUES
Flight altitude in m	300
Swath width in m	120
Bathymetry sounding density	1 point every 2 m
Topography sounding density	1 point every 1 m
Overlap in m	40
Sounding rate in kHz	3.6
Speed in miles/h (1 miles = 1.852 km/h)	150
Energy of green laser in mJ	3
Beam off-nadir angle in degrés	20
Full Width at Half Maximum in s	7.10^{-9}
Field of view in milliradian	10-50
Diameter size of laser spot on water surface in m	3.3
Diameter size of laser spot on ground surface in m x m	0.33 x 0.66

Data acquisition

Data acquired is altimetry data by LIDAR and vertical airborne pictures. Data acquisition was performed with a twin engine turbo-prop aircraft, a Twin Commander 690 B, of the Swedish "Wermlandsflyg" society. The duration of the data acquisition and preliminary processing assuming the foregoing has been of 3 days.

The bathymetric LIDAR accuracy is:

- Vertical accuracy : ± 25 cm (1σ)
- Horizontal accuracy : ± 3 m (2 σ)
- Topographic height : 25 cm (2 σ)

LIDAR data acquisition was successive flight lines and parallel to the shore line, with an overlap of 40% to cover fully area. Aircraft positioning was done by GPS during data collection. 2x geodetic GPS (dual frequency) base stations with logging were established at precise surveyed marks (centimetric accuracy) and were referenced to WGS84 and transformed to Lambert III South using the process provided by IGN. Data obtained from these geodetic stations were used in post-processing carrier phase. Final positions and heights/depths were referenced:

- X – Y : WGS 84 :(UTM 31 projection system) AND Z : ellipsoid height
- X – Y : Lambert III South AND Z : N.G.F. - IGN 69

The distance to the fixed GPS stations used on land did not exceed 15km. The two stations used are Villeneuve-les-Maguelone and Montpellier (RGP), see the Appendix A (page 15) for the coordinates. Furthermore, during the survey, a minimum of 5 visible GPS satellites having elevations > 10° was avai lable and the PDOP was < 3.5. During the survey, an image was stored every second. The overlap between the images on the water surface is of approximately 50%. The images are of the size 1600 x1200 pixels. The pixel size on the water surface corresponds to approximately 15x15 cm.

Deliverables

Raw data was provided to the EID after the survey in X, Y, Z ASCII (PC, ANSI formats). Final processing will be performed by ACSAB personnel at the ACSAB offices in Sweden and UK, for:

- Data cleaning will be according to coastal zone monitoring standard;
- The data to be filtered according to the following rule: in a radius of 5 m around each point measured, elimination of all the points where the difference in altitude is lower than 30 cm.

In two cases, data will be restored in the form of files X, Y, Z ASCII. For each flight line, an un-interpolated cleaned ASCII XYZ file will be delivered. This file will contain: Surface elevation, bottom elevation, seabed depth and flag for bathymetry and topography. Moreover, data interpolation will be used (geostatistic method) to obtain gridded digital elevation model (DEM), digital slope model (DSM), digital terrain model (DTM) with grid size 2 m, 5 m and 10 m, ASCII format. These digital models will be also returned in the form of GeoTIFF image with colouring representing the variation of altitude. Technical exchange with the provider will allow a better comprehension of data cleaned.

The products and the whole documentation will be provided on DVD-ROM. However, a preliminary report has been delivered at the end of the mission giving confirmation of survey completion and diary of events. A final report (pdf format and hard copy) will be provided with the cleaned data set and associated products:

- Description of the operations , description of the processing of LIDAR data including editing and quality controls, description of the sensor calibration procedures;
- Quality Control values;
- Positioning project report;
- Flight lines map and project coverage area;
- Discussion on data quality including quality assurance (QA) and quality control (QC) procedures;
- Ground control reports;
- Aircraft navigation.

P7 – OANAK

Michalis Lipakis (m.lipakis@oanak.gr)

The IKONOS satellite provides global, accurate, high-resolution imagery for mapping, monitoring, and development. The panchromatic sensor with 82 cm resolution and an 11.3 km wide swath at nadir provides high resolution, intelligence-quality imagery. The multispectral sensor, simultaneously collecting blue, green, red, and near infrared bands with 3.28 m resolution at nadir, provides natural-color imagery for visual interpretation and color-infrared imagery for remote sensing applications. Combining the multispectral imagery with the high resolution panchromatic results in 1-meter color images (pan-sharpen product), which can be afterwards orthorectified. The orthorectification is needed to eliminate the geometric distortions, which will be explained below, so that image features have correct planimetric coordinates. Quantitative estimations such as shoreline detection are performed using orthorectified images.

Apart from the different techniques that can be applied for shoreline extraction and monitoring from high resolution satellite images, the processing chain consists of the following basic steps:

- acquisition of images and pre-processing;
- acquisition of the GCP's with image coordinates and map coordinates;
- computation of the unknown parameters of the mathematical functions used for the geometric correction model;
- image orthorectification using an appropriate DEM;
- automatic, semi-automatic or manual shoreline extraction from the orthorectified imagery;
- monitor the shoreline changes by repeating the above steps at predefined time periods and compare the relative positions of the extracted shorelines.

Thus, before the application of any algorithm for automatic extraction of shoreline from multispectral satellite images, these images should be othorectified to take into account the geometric distortions during the image acquisition, as well as the effect of topography. Each image acquisition system produces unique geometric distortions in its raw images and consequently the geometry of these images does not correspond to the terrain or of course to a specific map projection. Obviously, the geometric distortions vary considerably with different factors such as the platform, the sensor and also the total field of view. However, as it has been described by Toutin (2004), it is possible to make general categorizations of these distortions. The sources of distortion can be grouped into two broad categories: the observer or the acquisition system (platform, imaging sensor and other measuring instruments, such as gyroscope, stellar sensors, etc) and the observed (atmosphere and Earth). In addition to these distortions, the deformations related to the map projection have to be taken into account because the terrain and most GIS end-user applications are generally represented and performed respectively in a topographic space and not in the geoid or a referenced ellipsoid. Most of these geometric distortions are predictable or systematic and generally well understood. Some of these distortions, especially those related to the instrumentation, are generally corrected at ground receiving stations or by image vendors. Others, for example those related to the atmosphere, are not taken into account and corrected because they are specific to each acquisition time and location and information on the atmosphere is rarely available. The remaining geometric distortions require models and mathematical functions to perform geometric corrections of imagery: either through 2D/3D empirical models (such as 2D/3D polynomial or 3D RF) or with rigorous 2D/3D physical and deterministic models. With 2D/3D physical models, which reflect the physical reality of the viewing geometry (platform, sensor, Earth and sometimes map projection), geometric correction can be performed step-by-step with a mathematical function for each distortion/deformation, or simultaneously with a combined mathematical function.

2D/3D physical functions used to perform the geometric correction differ, depending on the sensor, the platform and its image acquisition geometry (Toutin, 2004):

- instantaneous acquisition systems, such as photogrammetric cameras, Metric Camera or Large Format Camera;
- rotating or oscillating scanning mirrors, such as Landsat-MSS, TM and ETM+;
- push-broom scanners, such as SPOT-HRV, IRS-1C/D, IKONOS and Quickbird; and
- SAR sensors, such as JERS, ERS-1/2, RADARSAT-1/2 and Envisat.

Whatever the geometric model used, even with the RF some GCPs have to be acquired to compute/refine the parameters of the mathematical functions in order to obtain a cartographic standard accuracy. Generally, an iterative least-square adjustment process is applied when more GCPs than the minimum number required by the model (as a function of unknown parameters) are used. The number of GCPs is a function of different conditions: the method of collection, sensor type and resolution, image spacing, geometric model, study site, physical environment, GCP definition and accuracy and the final expected accuracy. The aerial triangulation method has been developed and applied with different optical and radar satellite data using 3D physical models (Toutin 2003a, b), as well as with IKONOS data using 3D RF models (Fraser et al. 2002a, b). All model parameters of each image/strip are determined by a common least-squares adjustment so that the individual models are properly tied in and an entire block is optimally oriented in relation to the GCPs.

As it has been already motioned, shoreline extraction needs orthorectified images. To rectify the original image into a map image, there are two processing operations:

- a geometric operation to compute the cell coordinates in the original image for each map image cell, eliminating the geometric distortions as previously explained; and
- a radiometric operation to compute the intensity value or DN of the map image cell as a function of the intensity values of original image cells that surround the previously-computed position of the map image cell.

The geometric operation requires the observation equations of the geometric model with the previously computed unknowns, and sometimes elevation information. 3D models take into account elevation distortion DEM is thus needed to create precise orthorectified images. DEM impact on the orthorectification process, both in terms of elevation accuracy for the positioning accuracy and of grid spacing for the level of details. This last aspect is more important with high-resolution images because a poor grid spacing when compared to the image spacing could generate artefacts for linear features such as shorelines. For any map coordinates (x, y), with the z elevation extracted from a DEM when 3D models are used, the original image coordinates (column and line) is computed from the two resolved equations of the model. However, the computed image coordinates of the map image coordinates will not directly overlay in the original image; in other words, the column and line computed values will rarely, if ever, be integer values. Since the computed coordinate values in the original image are not integers, one must compute the DN to be assigned to the map image cell. In order to do this, the radiometric operation uses a resampling kernel applied to original image cells: either the DN of the closest cell (called nearest neighbor resampling) or a specific interpolation or deconvolution algorithm using the DNs of surrounding cells (Toutin, 2004).

In order to accurately create or extract geographic information from raw IKONOS imagery, the Image Geometry Model (IGM) must accompany the imagery. The IGM consists of several metadata files which contain RPCs (rational polynomial coefficients). The RPCs are a series of coefficients that describe the relationship between the image as it existed when captured and the Earth's surface. Although they do not describe sensor parameters explicitly, RF are simple to implement and perform transformations very rapidly. With the availability of RPCs, the IKONOS interior and exterior orientation are very accurate. Therefore IKONOS imagery can be orthorectified if the IGM, an accurate DEM and some GCPs are available by employing any photogrametric software such as Orthoengine (PCI, 2003) or Leica Photogrammetry Suite (Leica, 2005).

The next step for shoreline extraction is the water-land separation; therefore the orthorectified image should be classified or a polygon corresponding to water (or land) area should be extracted. Taking into account the aforementioned land cover mapping constraints for very high spatial resolution satellite data, a machine learning classifier approach seems the best solution for IKONOS multispectral image classification. This type of classifier uses an inductive learning algorithm to generate production rules from training data. As with a neural network, there are several advantages to using a machine-learning approach. Since ancillary data layers may be used to help improve discrimination between classes, fewer field samples are generally required for training. This machine learning model is non-parametric and does not require normally-distributed data or independence of attributes. It can also recognize nonlinear patterns in the input data that are too complex for conventional statistical analyses or too subtle to be noticed by an analyst. Feature Analyst software (VLS, 2007) was selected for shoreline extraction from IKONOS imagery, since it employs machine-learning techniques which have the potential to exploit both the spectral and spatial information of the image. It provides a paradigm shift to automated feature extraction since it: (a) utilizes spectral, spatial, temporal, and ancillary information to model the feature extraction process, (b) provides the ability to remove clutter, (c) incorporates advanced machine learning techniques to provide unparalleled levels of accuracy, and (d) provides an exceedingly simple interface for feature extraction. It works by taking a small and simple set of training examples, learns from the examples, and classifies the remainder of the image. When classifying the contents of imagery, there are only a few attributes accessible to human interpreters. For any single set of imagery these are: Shape, Size, Color, Texture, Pattern, Shadow, and Association. Traditional image processing techniques incorporate only color (spectral signature) and perhaps texture or pattern into an involved expert workflow process. The shoreline extraction steps using Feature Analyst are shown in Figure 50.

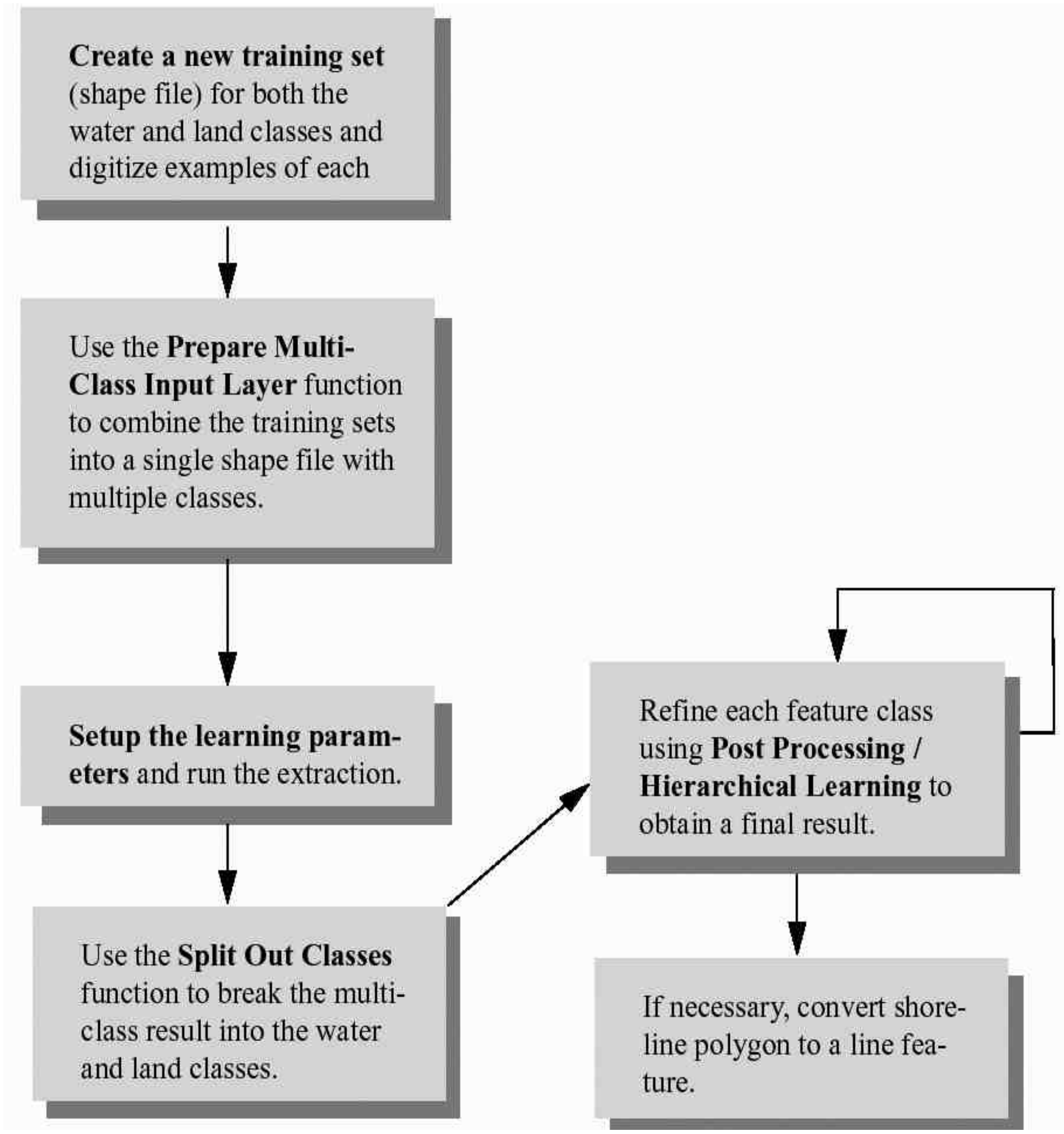

Figure 50: Shoreline extraction work flow (adapted from VLS, 2007).

P8 - IACM, FORTH

E. V. Koutandos (ekoutant@iacm.forth.gr); N. A. Kampanis. (kampanis@iacm.forth.gr); Th. V. Karambas (karambas@marine.aegean.gr)

Shoreline change models are used to predict shoreline changes associated with coastal structures or storm effects over the long term. These models are based on the single line or multiple line theories, where the potential long shore and cross shore sediment transport components are calculated empirically for the open shore case. These models have the advantage of being very fast, and they can predict long-term shoreline changes very well after suitable calibration. However, they cannot accurately predict the impact of morphological changes in the vicinity of coastal structures that are due to short-term storms. An alternative approach involves the modelling of the whole suite of elementary processes responsible for the local morphological changes in a given area (Leont'yev, 1999). A typical coastal area model consists of several modules describing the wave field, the spatial distribution of wave-induced currents, the associated sediment transport fluxes, and finally the resulting spatial and temporal changes of the bed level. Such an approach is employed in the models developed by Delft Hydraulics (De Vriend et al, 1993; Roelvink et al, 1995), Danish Hydraulic Institute (Broker, 1995; Broker et al, 1995), or HR Wallingford (Price et al, 1995). The attempts to evaluate the short-term morphological impacts of coastal structures using these models are not yet numerous, but the results obtained are encouraging. Although these models can be used to predict medium-term morphological impacts on coastal structures, the long-term morphological impacts are still predicted solely by the shoreline models.

Many models exist for the evaluation of wave deformation in the coastal region but most of them are based on the progressive wave assumption (period averaged refraction wave models) and employ elliptic or parabolic type differential equations which are in general difficult to solve numerically. Besides they are not valid for a compound wave field near coastal structures where the waves are subject to the combined effects of shoaling, refraction, diffraction, reflection and breaking.

The evaluation of the wave field only is not sufficient for the design of coastal structures. The current pattern, the sediment transport and the bottom topography changes also play an important role in the design. Basic to the description of these currents is the incorporation of the wave breaking (into the wave model) and the formulation of the driving forces (radiation stress) from the wave model results.

In the present work the model ALS is presented. The wave submodel WAVE-L, based on the hyperbolic type mild slope equation, valid for a compound wave, after the incorporation of breaking and the evaluation of the radiation stress, drives the depth-averaged circulation and sediment transport submodel CIRC-L for the description of the nearshore currents and beach deformation. A new one-line model, 1L-L, with additional terms, is proposed in order to calculate shoreline position taking into account the cross-shore related seasonal shoreline variation.

Wave submodel - WAVE-L-

The breaking and non breaking wave model is based on the hyperbolic type mild slope equation without using the progressive wave assumption. The model consists of the following pair of equations (Copeland, 1985a):

$$\frac{\partial \zeta_w}{\partial t} + \frac{c}{c_g} \nabla \frac{c_g}{c} \mathbf{Q}_w = 0$$

$$\frac{\partial \mathbf{U}_w}{\partial t} + \frac{c^2}{d} \nabla \zeta_w = 0 \tag{4}$$

where ζ_w is the surface elevation, Uw the mean velocity vector Uw =(U ,V), d the depth, Qw = Uw hw=(Qw, Pw), hw the total depth (hw=d+ ζ_w), c the celerity and cg the group velocity.

The above equations, derived by Copeland (1985a), are able to compute the combination of wave refraction, diffraction and reflection (total or partial).

The numerical model is adapted for engineering applications:

- The input wave is introduced in a line inside the computational domain according to Larsen and Dancy (1983);
- A sponge layer boundary condition is used to absorb the outgoing waves in the four sides of the domain (Larsen and Dancy, 1983);
- Total reflection boundary condition (Uw or Vw=0) is incorporated automatically in the model. The existence of a vertical structure with 100% reflection coefficient is introduced from the depth file (depth d=-1).

Submerged structures are incorporated as in Karambas and Kriezi (1997).

Partial reflection is introduced from an artificial eddy viscosity file. The values of the eddy viscosity coefficient are estimated from the method developed by Karambas and Bowers (1996), using the values of the reflection coefficients proposed by Bruun (1985).

Floating structures are incorporated as in Koutandos et al (2002).

The model is extended in the surf zone in order to include breaking effects providing the equations with a suitable dissipation mechanism by the introduction of a dispersion term in the right-hand side of momentum Equation (4):

$$\nu_h = \nabla^2 \mathbf{U}_w \tag{5}$$

where ν_h is an horizontal eddy viscosity coefficient estimated from Battjes (1995):

$$\nu_h = 2d\left(\frac{D}{\rho}\right)^{1/3} \tag{6}$$

in which ρ is the water density and D is the energy dissipation given by Battjes and Janssen (1978) :

$$D = \frac{1}{4} Q_b f \rho g H_m^2 \tag{7}$$

with f the mean frequency, Hm the maximum possible wave height and Qb the probability that at a given point the wave height is associated with the a breaking or broken wave. For a Rayleigh type probability distribution, we use Battjes and Janssen (1978):

$$\frac{1-Q_b}{\ln Q_b} = \left(\frac{H_{rms}}{H_m}\right)^2 \tag{8}$$

in which Hrms is the mean square wave height: Hrms=2 (<2 ζ_w 2>)1/2 and the brackets <> denote a time mean quantity.

<u>Wave-induced circulation submodel -CIRC-L-</u>

Radiation stress and wave-induced current submodel

Taking the horizontal axes x1 and x2 on the still water surface, and the z axis upward from the surface, the definition of the radiation stress Sij component is:

$$S_{ij} = < \int_{-d}^{\zeta_w} \left(p\delta_{ij} + \rho u_i u_j\right) dz > -0.5\rho g\left(d + < \zeta >\right)^2 \delta_{ij} \tag{9}$$

where δ_{ij} is the Kroneker's delta, ui(z) is the wave horizontal velocity component in direction xi , ζ is the mean sea level, p the pressure and < > denotes a time average.

The total pressure p is obtained from the vertical momentum equation:

$$p = \rho g(\zeta - z) - \rho {u_3}^2 + \frac{\partial}{\partial x_1}\int_z^0 \rho u_1 u_3 dz + \frac{\partial}{\partial x_2}\int_z^0 \rho u_2 u_3 dz + \frac{\partial}{\partial t}\int_z^{\zeta} \rho u_3 dz \tag{10}$$

where u3 is the z-velocity component.

Based on the above Equation (10) and after the substitution of ui and p, from model results (Equation 4) using linear wave theory, Copeland (1985b) derived the expressions for Sij without the assumption of progressive waves. Those expressions are used in the present model.

The radiation stresses are the driving forces of a 2D horizontal wave-induced current model:

$$\frac{\partial \zeta}{\partial t} + \frac{\partial (U h)}{\partial x} + \frac{\partial (Vh)}{\partial y} = 0$$

$$\frac{\partial U}{\partial t} + U\frac{\partial U}{\partial x} + V\frac{\partial U}{\partial y} + g\frac{\partial \zeta}{\partial x} =$$

$$-\frac{1}{\rho h}\left(\frac{\partial S_{xx}}{\partial x} + \frac{\partial S_{xy}}{\partial y}\right) + \frac{1}{h}\frac{\partial}{\partial x}\left(\nu_h h\frac{\partial U}{\partial x}\right) + \frac{1}{h}\frac{\partial}{\partial y}\left(\nu_h h\frac{\partial U}{\partial y}\right) - \frac{\tau_{bx}}{\rho h}$$

$$\frac{\partial V}{\partial t} + U\frac{\partial V}{\partial x} + V\frac{\partial V}{\partial y} + g\frac{\partial \zeta}{\partial y} =$$

$$-\frac{1}{\rho h}\left(\frac{\partial S_{xy}}{\partial x} + \frac{\partial S_{yy}}{\partial y}\right) + \frac{1}{h}\frac{\partial}{\partial x}\left(\nu_h h\frac{\partial V}{\partial x}\right) + \frac{1}{h}\frac{\partial}{\partial y}\left(\nu_h h\frac{\partial V}{\partial y}\right) - \frac{\tau_{by}}{\rho h} \qquad (11)$$

where h is the total depth h=d+ζ, U, V are the current horizontal velocities and τ_{bx} and τ_{by} are the bottom shear stresses.

In the current model the treatment of the bottom stress is critical (all longshore current models employing radiation stress solve for the mean current velocity through its role in the bottom friction term). The general expression for the time-average bottom shear stress in the current model is written:

$$\tau_{bx} = \rho C_f < (U + u_b)\sqrt{(U + u_b)^2 + (V + v_b)^2} >$$

$$\tau_{bx} = \rho C_f < (V + v_b)\sqrt{(U + u_b)^2 + (V + v_b)^2} > \qquad (12)$$

where Cf is the friction coefficient which depends on the bottom roughness and on the orbital amplitude at the bed (Karambas, 1998), and ub and vb are the wave velocities at the bottom.

Inside surf zone the existence of the undertow current that is directed offshore on the bottom cannot be predicted by a depth averaged model. However, representing the cross-shore flow is essential for a realistic description of the sediment transport processes. The present model calculates local vertical distribution of the horizontal velocity using the analytical expression for the cross-shore flow below wave trough level proposed by Stive and Wind (1986):

$$v_u = \frac{1}{2}\left[(\xi-1)^2 - \frac{1}{3}\right]\frac{h-\zeta_t}{\rho\,\nu_\tau}\frac{dR}{dy} + \left(\xi - \frac{1}{2}\right)\frac{(h-\zeta_t)\tau_s}{\tilde{n}\nu_\tau} - \frac{M\cos\Theta}{h-\zeta_t} \quad (13)$$

where vu is the undertow velocity in the y (shore-normal) direction, ξ=z/(h-ζ_t), ζ_t is the wave trough level, dR/dy=0.14ρ gdh/dy, τ_s is the shear stress at the wave trough level, M is the wave mass flux above trough level, Θ is the direction of the wave propagation and ν_τ the eddy viscosity coefficient given by Equation (4). The value of the coefficient in Equation (6) is now taken equal to 0.03 (instead of 2). The direction of the wave propagation Θ is given by:

Θ =arctan [(<Qw2>/<Pw2>)1/2] (14)

Sediment transport model -SED-L-

Sediment transport submodel

Sediment transport in the surf zone

The prediction of the sediment transport is based on the energetics approach, in which the submerged weight transport rates, ixt in the x direction and iyt in the y direction, are given by Karambas (1998):

$$i_{xt} = \left< \left[\frac{\varepsilon_b}{\tan\phi}\left(\frac{u_o}{u_{ot}} + \frac{d_x}{\tan\phi}\right)\omega_b + \varepsilon_s\frac{u_{ot}}{w}\left(\frac{u_o}{u_{ot}} + \varepsilon_s d_x \frac{u_{ot}}{w}\right)\omega_t\right]\right>$$

$$i_{yt} = \left< \left[\frac{\varepsilon_b}{\tan\varphi}\left(\frac{v_o}{u_{ot}} + \frac{d_y}{\tan\phi}\right)\omega_b + \varepsilon_s\frac{u_{ot}}{w}\left(\frac{v_o}{u_{ot}} + \varepsilon_s d_y \frac{u_{ot}}{w}\right)\omega_t\right]\right> \quad (15)$$

where w is the sediment fall velocity, ϕ is the angle of internal friction, ε_b and ε_s are the bed and suspended load efficiency factors respectively (ε_b =0.13, ε_s=0.01), uot=$\sqrt{u_o^2+v_o^2}$ (uo, vo are the total flow velocities at the bottom), dx and dy are the bottom slopes $\omega_b = C_f\rho u_{ot}{}^3$, and ω_t is the total rate of energy dissipation given by Leont'yev (1996, 1997):

$$\omega_t = \omega_b + D e^{3/2(1-h/H)} \quad (16)$$

in which H is the wave height (H=Hrms), D is the mean rate of breaking wave energy dissipation per unit area given by Equation (7).

In Equation (16) the first term express the power expenditures due to bed friction while the second due to excess turbulence penetrating into bottom layer from breaking waves.

The above method had been applied using a non linear dispersive wave model based on the Boussinesq equations (Karambas et al, 1995; Karambas, 1998). A Boussinesq model automatically includes the existence of the mean wave-induced current and consequently there is no need to separate the bottom velocities into a mean and an oscillatory part. However, since the present model is a linear one, the total flow velocity at the bottom is considered as a sum of the steady U, V, vu and the oscillatory ub, vb components which include two harmonics:

$$uo=U+ubm\cos(\omega t) + ub2m\cos(2\omega t)$$

$$vo = V+vu+vbm\cos(\omega t) + vb2m\cos(2\omega t+a) \qquad (17)$$

in which ω is the wave frequency, a is the phase shift and ubm, ub2m , vbm and vb2m are the velocity amplitudes given by Leont'yev (1996; 1997) .

The above sediment transport formula has been derived directly form the Bailard primitive equations without the assumption that the only dissipation mechanism is the bed friction. This is the most important limitation of the Bailard theory and precludes the use of the original formula within the surf zone, where the dissipation of energy associated with the process of wave breaking is largely dominant.

Sediment transport in the swash zone

Adopting the procedure proposed by Leont'yev (1996), the submerged weight transport rates iys near the shoreline, in the y (shore-normal) direction, is given by:

$$i_{ys} = \frac{\varepsilon_b f_R}{2\tan^2\phi}\rho\left|< u_R{}^3 >\right|\left(\tan\beta_{eq} - \tan\beta\right) \qquad (18)$$

where fR is the run-up friction coefficient (of order 10-1-10-3), uR is the flow velocity in the swash zone, tan β is the actual slope gradient and tan β_{eq} is the slope under equilibrium state approximated by Yamamoto et al (1996):

$$\tan\beta_{eq} = \left(\frac{0.0864\, s\, g\, d_{50}\, T^2}{H_b{}^2}\right)^{2/3} \qquad (19)$$

where s is the specific gravity of sediment in water, d50 is the median grain size, Hb is the breaker height and T the wave period.

The flow velocity in the swash zone uR is parameterized in terms of the run-up height R according to Leont'yev (1996): uR=(2g (R-zc)), where zc is the height of water mass above the water level which increases proportionally to the distance from the upper run-up boundary. If the bottom gradient exceeds the equilibrium value then iys<0 (erosion). In the opposite case, iys>0 (accretion).

The longshore (x direction) total swash sediment transport ixs is calculated by the global expression proposed by Briad and Kamphuis (1993).

3D bed evolution and one-line models

The submodel CIRC-L is coupled with a 3D bed evolution model or with an one-line model to provide bathymetry or shoreline changes. The nearshore morphological changes are calculated by solving the conservation of sediment transport equation:

$$\frac{\partial d}{\partial t} = \frac{\partial q_x}{\partial x} + \frac{\partial q_y}{\partial y} \tag{20}$$

where d is the still water depth and qx, qy are the volumetric longshore and cross-shore sediment transport rates, related to the immersed weight sediment transport through:

$$q_{x,y} = \frac{i_{x,y}}{(\rho_s - \rho)gN} \tag{21}$$

in which N is the volume concentration of solids of the sediment (N= 0.6) and ρ_s and ρ are the sediment and fluid densities.

Under certain assumptions Equation (20) can be transformed into an 1D equation (one-line model). The one-line models find wider engineering use as they are much less costly to run. Let us define the total longshore sediment transport Q and the mean (cross-shore) water depth $\bar{d}$ by the equations:

$$Q = \int_0^{y_s} q_x dy \qquad \bar{d} = \frac{1}{y_s}\int_0^{y_s} d\,dy \tag{22}$$

where ys is the width of the nearshore zone.

The integration of Equation (21) over the width of the nearshore zone from its outer boundary (y=0) to the shoreline (y=ys), using the Leibnitz relation, leads to the following equation:

$$\frac{\partial\left(y_s\bar{d}\right)}{\partial t} = \frac{\partial Q}{\partial x} - q_x(y_s)\frac{\partial y_s}{\partial x} + q_y(y_s) \tag{23}$$

where we have supposed that the following conditions are valid: d=0 at shoreline (y=ys) and the transport rates qx(0)=0, qy(0)=0 at the outer boundary (y=0) are zero.

Equation (23) differs from a standard one-line model in the last two terms. The second term of the right hand side of the equation is related to the longshore transport rate near the shoreline while the last term incorporates the cross-shore related seasonal shoreline variation.

The cross-shore transport rate near the shoreline qy(ys) is given Sunamura formula (Yamamoto et al, 1996):

$$q_y(y_s)=K\,U_r^{0.2}\,\Phi\,(\Phi-0.13\,U_r)\,w\,d_{50} \qquad (24)$$

where Ur is the Ursell parameter $U_r=gHT^2/h^2$ (H is the wave height and h is the wave set-up at shoreline), $\Phi=H^2/shd_{50}$ (s is the specific gravity of sediment) and K is a coefficient of sediment transport rate:

$$K=Ae^{-Bt/T} \qquad (25)$$

where the coefficient A and B are given by Yamamoto et al (1996):

$$A=1.61.10^{-10}\,(d_{50}/H_o)^{-1.31}$$

$$B=4.2.\,10^{-3}\,(\tan\beta)^{1.57} \qquad (26)$$

where Ho is the deep water wave height.

The coefficient K of Equation (25) is a function of time since the rate of cross-shore sediment transport decreases with the lapse of time and the beach profile approaches the equilibrium state. Also it can be expected that the mean depth $\bar{d}$ is relatively conservative characteristic in comparison with the local shoreline position ys, and consequently, it can be considered as a constant in Equation (23).

Application of the numerical models in the region of Kokkinos Pirgos

The above methodology is applied in the region of Kokinos Pirgos near Timbaki in South Crete in order to determine the wave climate and the current pattern. The sediment balance of the coast has been significantly influenced by the construction of a small harbour in the west corner of the beach. In Figure 51 a map of the area of Kokinos Pirgos near Timbaki in South Crete is presented. In Figures 52 and 53 satellite images of the coast of are presented where the small harbour is visualised in detail.

Figure 51: Map of the area of Kokinos Pirgos near Timbaki in South Crete.

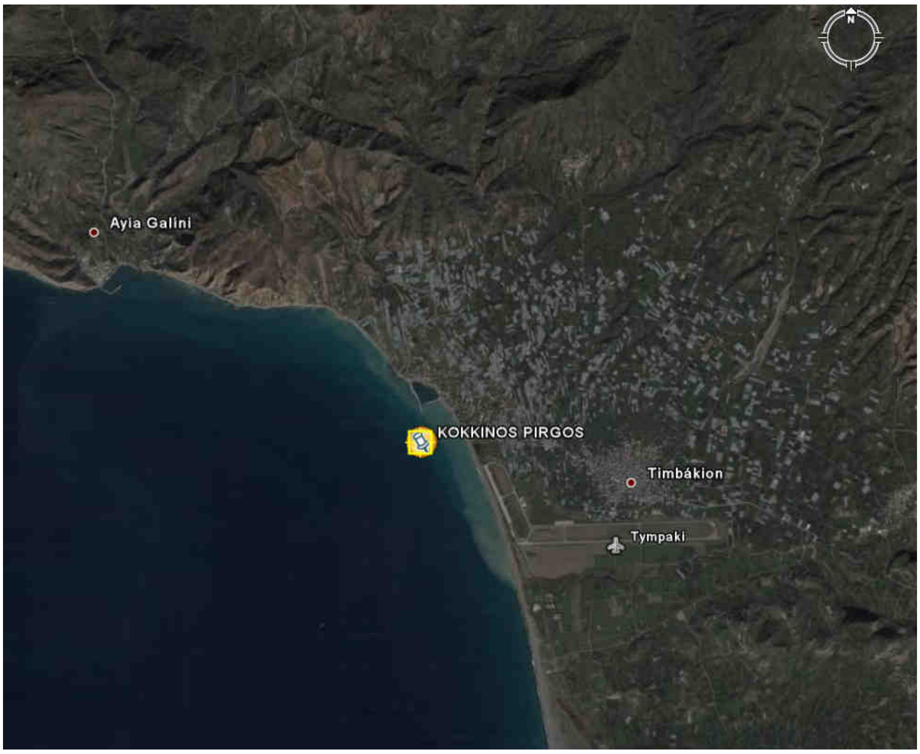

Figure 52: Satellite image of the area of Kokinos Pirgos near Timbaki in South Crete.

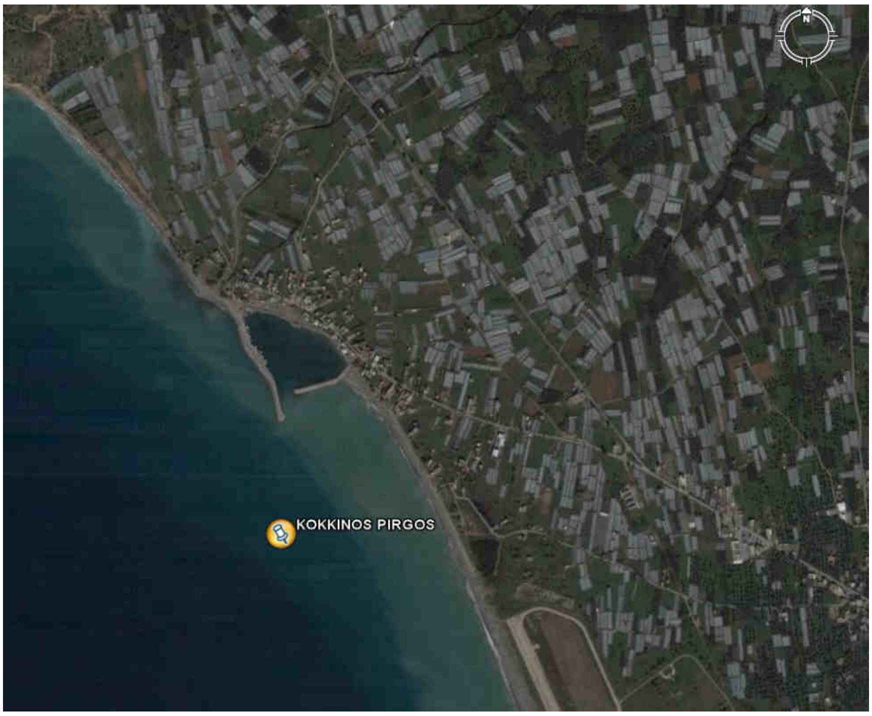

Figure 53: Satellite image of the coast of Kokinos Pirgos near Timbaki in South Crete.

For the calculation of the wave climate in the open sea of the specific region, the estimation of the significant wave height Hs, the peak wave period Tp, the maximum energy density and the mean period Tz are calculated using the JONSWAP approach:

(27)

(28)

(29)

Supposing that F is the fetch, we check the validity of the following relationship:

(30)

where tD is the duration.

If Equation (30) is valid we replace x with F. If Equation (30) is not valid we set the two parts of the equation equal and solve for F in the place of x. Numerical calculations were performed for three directions West, South-West and South sector.

The calculation of the active fetch is performed in a sector ±45o in relation to the main direction, with radius of 10o. Mean velocities for moderate and strong/severe winds are U=10 and 22 m/s accordingly.

Using the wind data from Station 759 of the Greek Meteorological Service we get the results of Tables 7, 8 and 9.

Table 7: Wave parameters for West wind.

	BF	U (m/s)	Duration (hr)	Frequency of Appearance %	Hos (m)	Tp (sec)
Moderate	4-6	10	11	11,4	1,88	6,92
Strong/Severe	>7	22	8	0,8	3,98	8,76
Total				12,2		

Table 8: Wave parameters for South-West wind.

	BF	U (m/s)	Duration (hr)	Frequency of Appearance %	Hos (m)	Tp (sec)
Moderate	4-6	10	11	4,5	1,88	6,92
Strong/Severe	>7	22	8	0,2	3,98	8,76
Total				4,7		

Table 9: Wave parameters for South wind.

	BF	U (m/s)	Duration (hr)	Frequency of Appearance %	Hos (m)	Tp (sec)
Moderate	4-6	10	11	0,7	1,88	6,92
Strong/Severe	>7	22	8	-	3,98	8,76
Total				0,7		

Where Hos is the significant wave height in deep waters and Tp is the peak period of the wave spectrum. The equivalent wave height He on an annual basis are set according to Borah and Balloffet (1985) as following:

$$H_e^2 T = \frac{\sum H_i^2 T_i f_i}{\sum f_i} \qquad (31)$$

where T is the equivalent wave period, Hi, Ti, fi are the height, the period and the frequency of the waves that correspond on the various levels of wind intensity from each incident direction.

The equivalent wave is actually the wave that appears with the frequency $\sum f_i$ and includes the same wave energy with the series of the waves of various intensity of the specific direction. Using the wind data from the specific area from the Greek Metereological Service and applying the JONSWAP wave prediction method the significant wave heights He, the periods T and the frequencies of the equivalent open sea waves were deduced (Tab. 10).

Table 10: Equivalent waves characteristics.

West direction waves				**Equivalent period**	**Equivalent wave height**
	Frequency of Appearance	Hos(m)	Tp(sec)	T(sec)	H (m)
Moderate	11,4	1,88	6,92	7,04	2,13
Strong/Severe	0,8	3,98	8,76		
Total frequency	12,2				
South-West direction waves				***Equivalent period***	***Equivalent wave height***
	Frequency of Appearance	Hos(m)	Tp(sec)	T(sec)	H (m)
Moderate	4,5	1,88	6,92	6,998	2,05
Strong/Severe	0,2	3,98	8,76		
Total frequency	4,7				
South-direction waves				**Equivalent period**	**Equivalent wave height**
	Frequency of Appearance	Hos(m)	Tp(sec)	T(sec)	H (m)
Moderate	0,7	1,88	6,92	6,92	1,88
Strong/Severe	0	3,98	8,76		
Total frequency	0,7				

In the present work the model ALS has been presented for beach erosion monitoring and the methodology followed has been analysed. The wave submodel WAVE-L, based on the hyperbolic type mild slope equation, valid for a compound wave, after the incorporation of breaking and the evaluation of the radiation stress, drives the depth-averaged circulation and sediment transport submodel CIRC-L for the description of the nearshore currents and beach deformation. A new one-line model, 1L-L, with additional terms, is proposed in order to calculate shoreline position taking into account the cross-shore related seasonal shoreline variation. The first two submodels have been applied for the region of Kokinos Pirgos near Timbaki in South Crete in order to determine the wave climate and the current pattern due to the fact that the sediment balance of the coast has been significantly influence by the construction of a small harbuor in the west corner of the beach. Results can be seen in Figures 54 to 59.

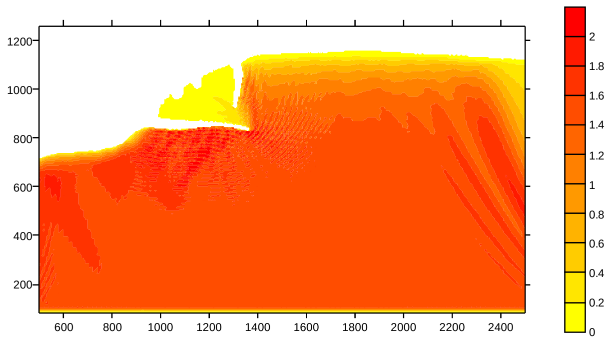

Figure 54: Current status: Hs contours for South direction winds.

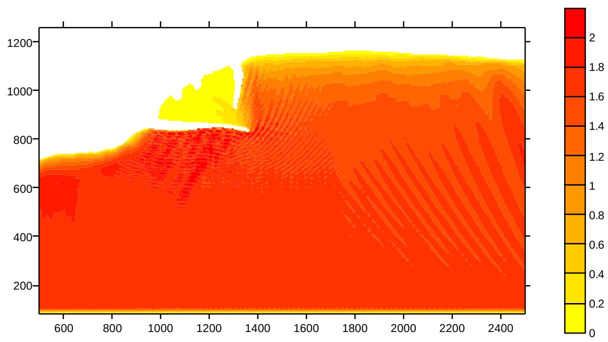

Figure 55: Current status: Hs contours for South-West direction winds.

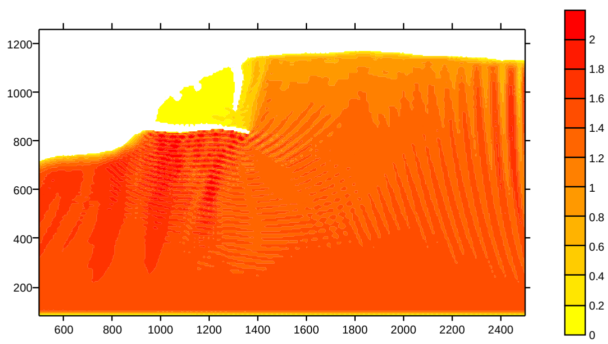

Figure 56:Current status: Hs contours for West direction winds.

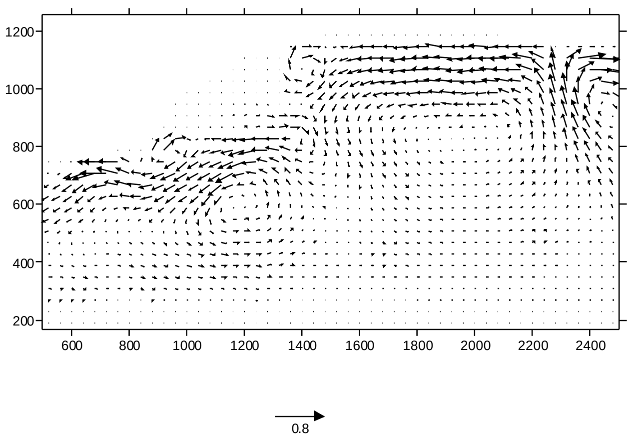

Figure 57: Current status: Wave induced current velocities for South direction winds.

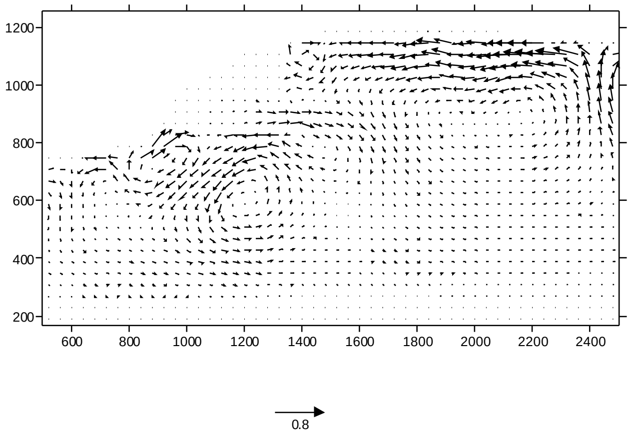

Figure 58: Current status: Wave induced current velocities for South-West direction winds.

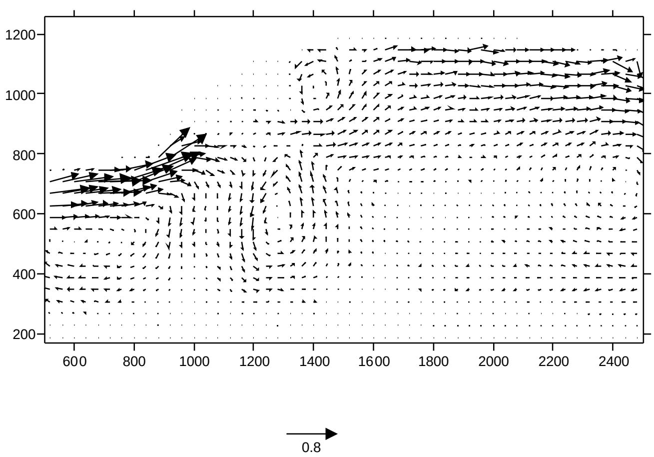

Figure 59: Current status: Wave contours current velocities for West direction winds.

The following conclusions have been derived:

- Hs contours reveal the wave propagation pattern for each wind direction;

- Wave refraction and breaking phenomena due to the existence of the coast and the harbour works are revealed;
- Wave induced currents calculations reveal the existence of a alongshore current in the breaker zone with a mean value of 1 m/s;
- South and South-West winds produce currents of North-West direction while West winds currents of South-East direction.
- For West winds the wave induced current in the leeside of the east seawall changes in direction and reformulates, a phenomenon that will lead to sediment accretion in the region of the breakwater and erosion in the South-East part of the coast.

P9 - School of Engineering, Democritus University of Thrace

Nikolas Kotsovinos (kotsovin@civil.duth.gr); George Xeidakis (xeidakis@civil.duth.gr); Anastasios Georgoulas (ageorg@civil.duth.gr); Dimitris Petridis (dpetrid@tee.gr)

The total length of the coast of the East Macedonia & Thrace Region is about 420 km. The problem of erosion and accretion was monitored sporadically in the past years by the Democritus University of Thrace, using mainly traditional topography. There is a lack of accurate shoreline data from previous years, regarding the coastline of the Region. Only some aerial photographs (taken for other purposes from various authorities) are available for some parts of the region. There are not frequent and systematic measurements available. The existing mapping at scale 1:5000 is not accurate enough for the precise extraction of older shorelines. There is not any detailed database regarding the coastline change in the region apart from some sporadic topographic measurements in some parts of the region in order for the National Land Property Authority, to define public land properties. There is not any previous participation of the Region of East Macedonia and Thrace in any EU or National project regarding the coastline erosion, accretion and change monitoring.

The General Building Regulations of the country do not allow buildings to be constructed close to the shoreline. Hence there are not any safe places where webcams could be installed. Moreover webcams can only monitor coastline segments of approximately 500 to 1000 m length. Hence, in order to achieve an integrated monitoring system for the whole 420 km of coastline in the Region of East Macedonia & Thrace, using webcams would require the installation of hundreds of webcams and stations which would be very difficult and expensive. There is not in the region a beach of high economic value and with high rate of erosion or accretion to justify (in terms of profits or scientific interest) hourly measurements . Therefore webcam monitoring for the whole region is inappropriate comparing to alternative methods such as satellite monitoring and GPS measurements. For the region of East Macedonia & Thrace webcams could only be used in some later stage in some selective spots of the coastline in order to investigate the morphodynamics and the “short-term” evolution of the shoreline “hot spots”, at local scale, under extreme weather conditions.

The chosen methodology for the Region of East Macedonia & Thrace is the use of high resolution satellite images (Quickbird & IKONOS) in combination with high resolution GPS surveying, specifically:

- Comparison of past and present shoreline positions in order to identify coastal areas with high values of rate of erosion or accretion;
- Use of Quickbird (QB) and IKONOS satellite imagery for shoreline extraction once per year for the whole shoreline of the region (420 km);
- Orthorectification of satellites images using the LPS 8.7 Software (Leica Photogrammetry Suite);
- horeline extraction from the orthorectified satellites images, using the Arc Map Software (Arc GIS Desktop 9.0);
- Use of D-GPS or field in situ measurements for monthly or seasonal shoreline extraction at certain selected spots along the pilot study area. The frequency of in situ measurements (monthly or seasonally) depends on the rate of erosion or accretion.

Our research indicates that the accuracy of the absolute shoreline position using orthorectified satellite images is less than one meter, in agreement with the results of other investigators (Kaichang et al, 2003a,b). The accuracy of this methodology is considered very good to evaluate the annual changes of the shoreline position. Field measurements of the shoreline distance from various reference points at certain directions allow to investigate the seasonal evolution and sensitivity of the shoreline at certain selected spots along the pilot study area.

The proposed methodology is tested in a specific part of the selected pilot study area (AKRONERI-KERAMOTI). The procedure followed is described and illustrated bellow:

Coastline extraction from 2002 Quickbird Satellite Imagery

Step 1 - Gathering of Archive QB Satellite images (year 2002) from GEOMET LTD which is one of the authorized resellers for QB images for the Region of East Macedonia and Thrace. The cost of 25 km^2 orthorectified QB image from archives and for academic users is approximately 1200 Euros, while the cost for the same area is about 3000 Euros for ordering a new satellite image for non academic users.

The selected Test Area Shape file Coordinates are shown in the following table (Tab. 11). This area corresponds to 25 km^2.

Table 11: Test Area Shape file Coordinates

POINT	LAT	LON
A	40.853482°	24.619381°
B	40.856613°	24.667729°
C	40.840158°	24.737390°
D	40.865587°	24.738098°
E	40.880040°	24.660290°
F	40.864227°	24.614059°

The selected combination of 2002 QB satellite images regarding the selected Test Area, from the Digital Globe archive are shown in Figure 60.

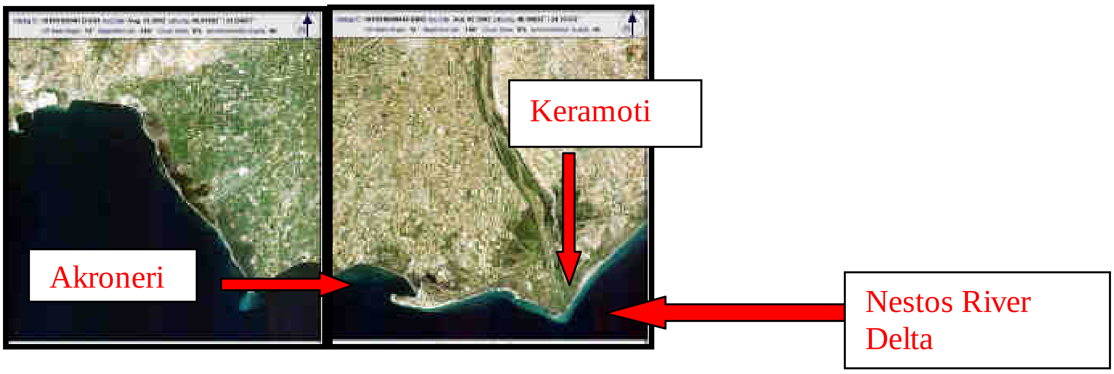

Figure 60: 2002 QB Satellite Images.

The raw QB-Satellite data that comprise the area defined by the ordered shape file are shown in Figures 61 and 62.

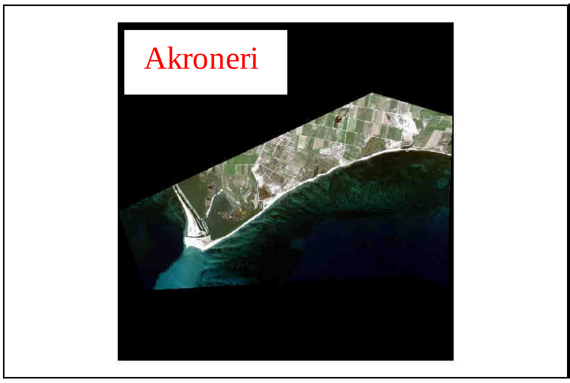

Figure 61: QB image,2002, Akroneri

Figure 62: QB image,2002, Keramoti

Step 2 - Image Orthorectification: the orthorectification procedure of the Quickbird satellite images, using the LPS 8.7 Software (Leica Photogrammetry Suite), can be summarised as follows:

- Creation of a new block file and selection of the satellite parameters;
- Insertion of the satellite image and internal alignment;
- Definition of ground control points – GCP's in the satellite image;
- Use of the appropriate Digital Terrain Model – DTM, in order to define the altitudes of the GCP's;
- Re-sampling of the image at the corrected X,Y,Z, coordinates;
- Checking and evaluation of the orthorectified (corrected) image.

Some steps of the procedure are illustrated in Figures 63 and 64.

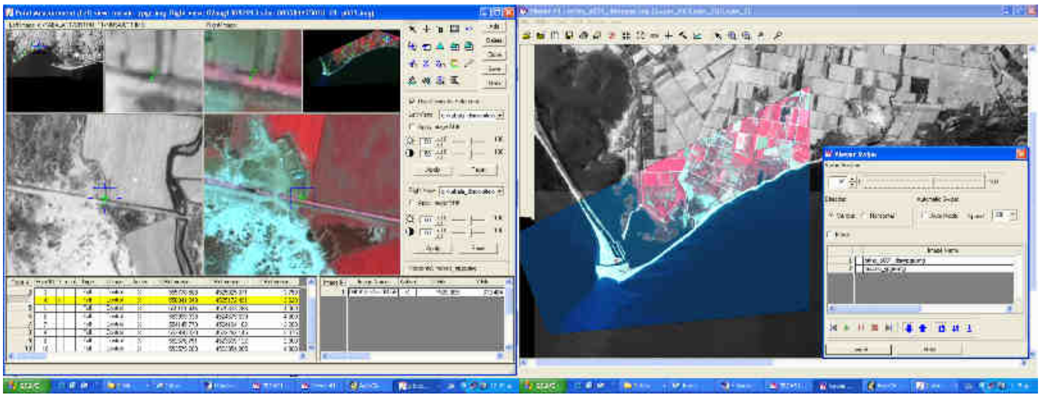

Figure 63: Ground Control Point Selection (GCP's) & Final image (Geometrically Corrected and Orthorectified)

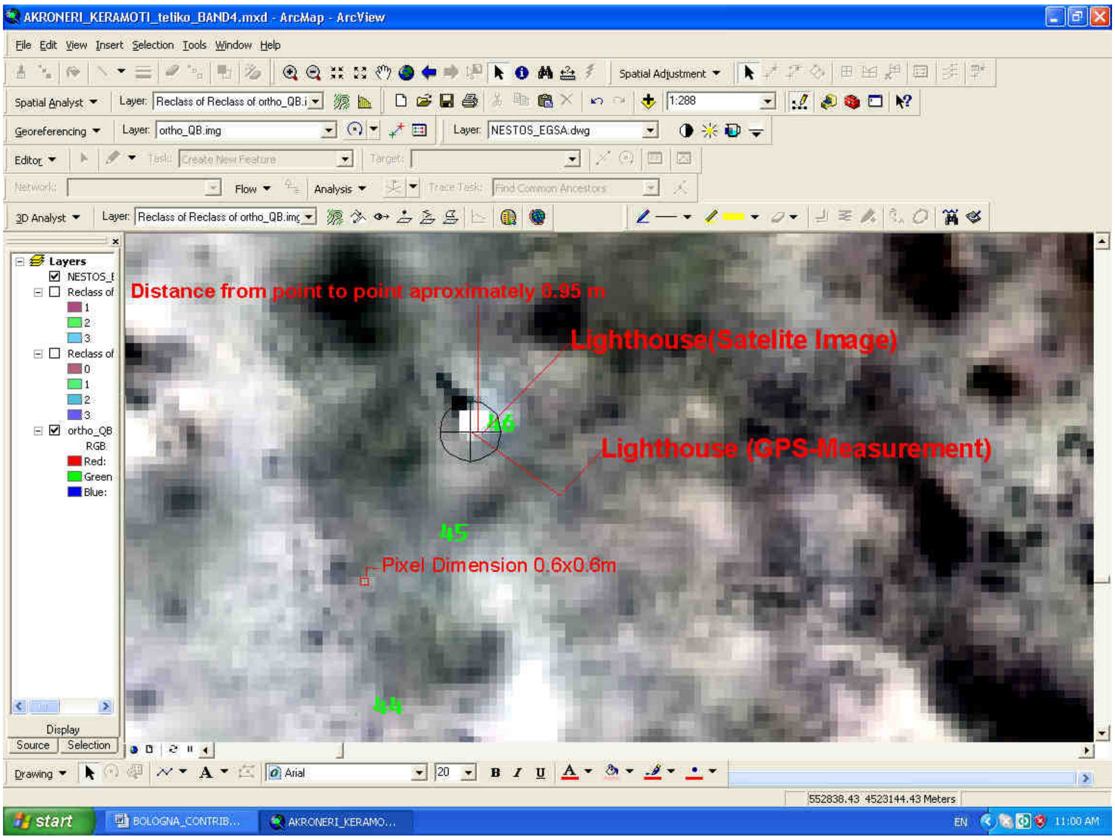

Figure 64: Orthorectification accuracy check (Accuracy less than a 1m)

Step 3 – Shoreline Extraction: After the geometric correction and the orthorectification, the images were combined in one image that represents the entire test area. Then the whole orthorectified image was analysed using the Arc Map Software (Arc GIS Desktop 9.0) and the shoreline was extracted. The main steps of the procedure are illustrated at the following figures. Initially, pixel classification of the image is made (using the infrared band of the image) in order to separate water from land pixels using the Natural Breaks (Jenks) classification method of the spatial analyst tool of the software. The panchromatic, the infrared images and the corresponding classification result are shown in Figures 65, 66 and 67, respectively. Finally a contour is drawn automatically at the classification interface, using the “draw contour” tool of the software, which represents the shoreline (Figures 68, 69, 70, 71 and 72).

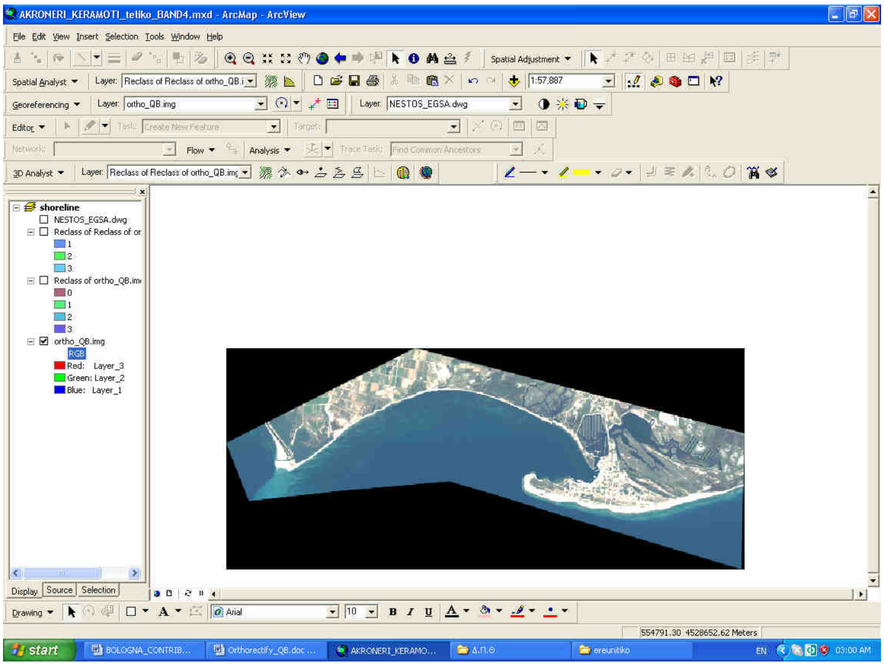

Figure 65: Combined image representing the test area.

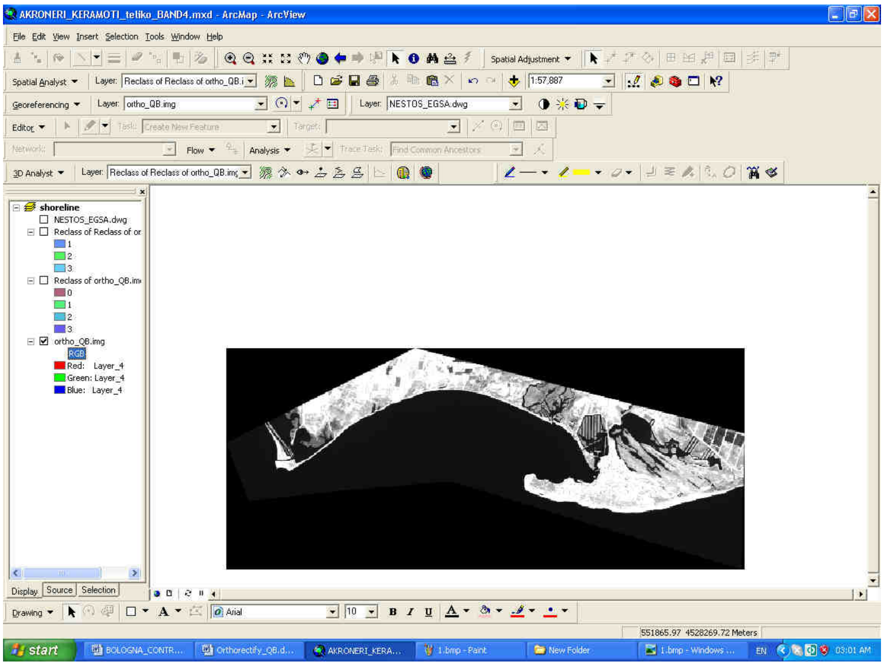

Figure 66: Infrared band from the combined image representing the test area.

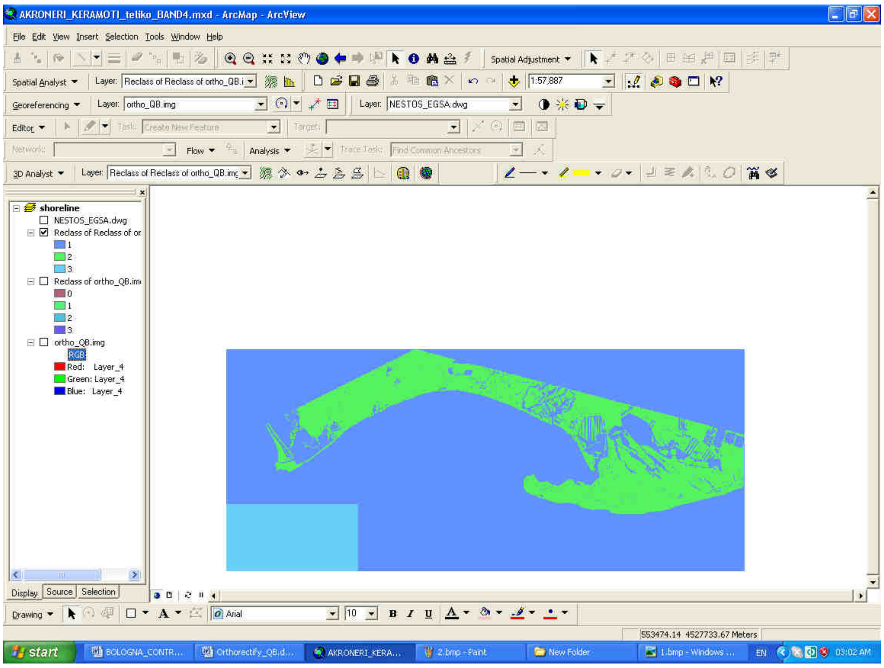

Figure 67: Pixel classification using one of the standard classification schemes in Arc Map software, Natural Breaks (Jenks) Classification.

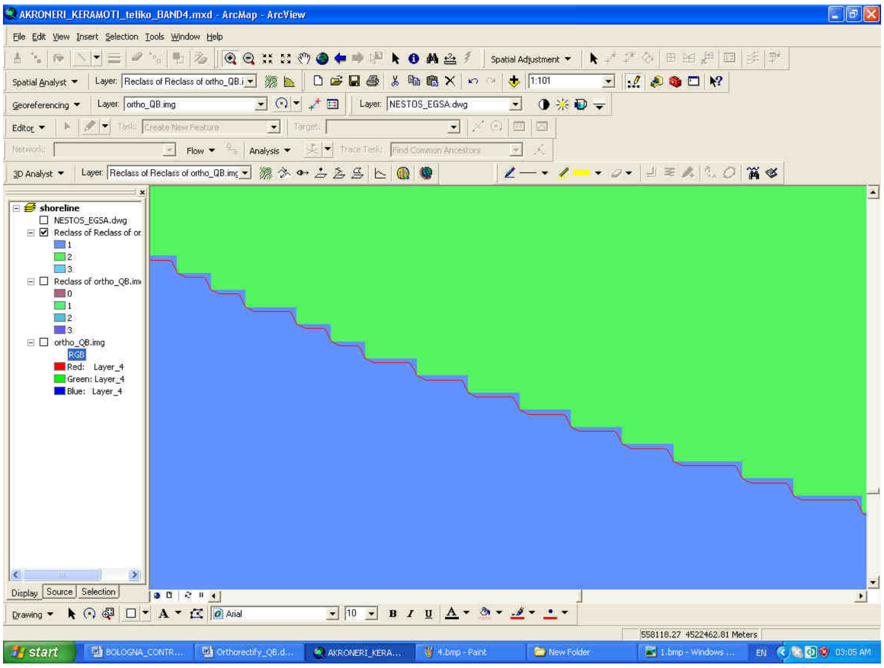

Figure 68: Automatically drawn contour representing shoreline (red line) at the classification interface (Green is land and blue is water).

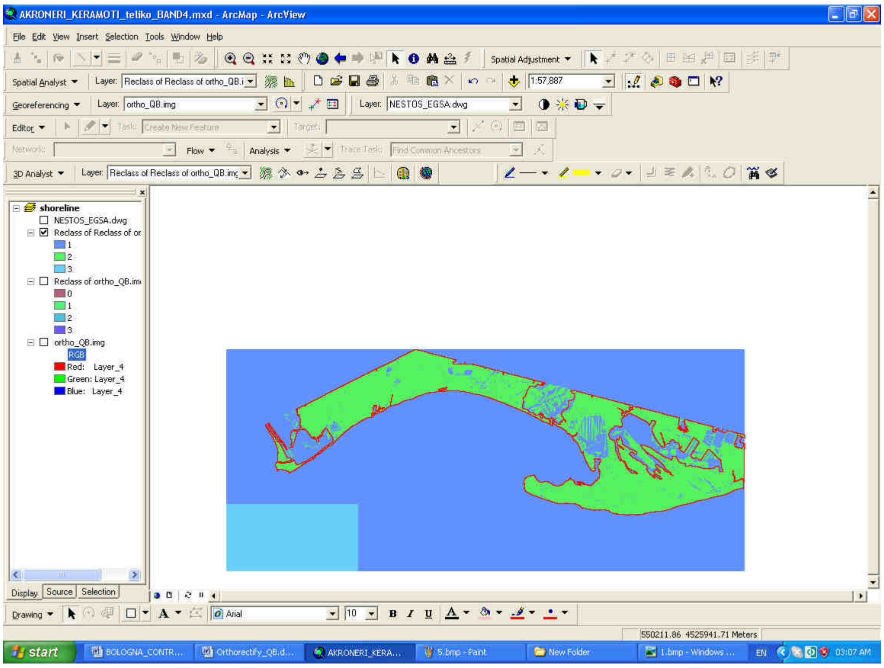

Figure 69: Automatically drawn contour representing shoreline (Entire Image).

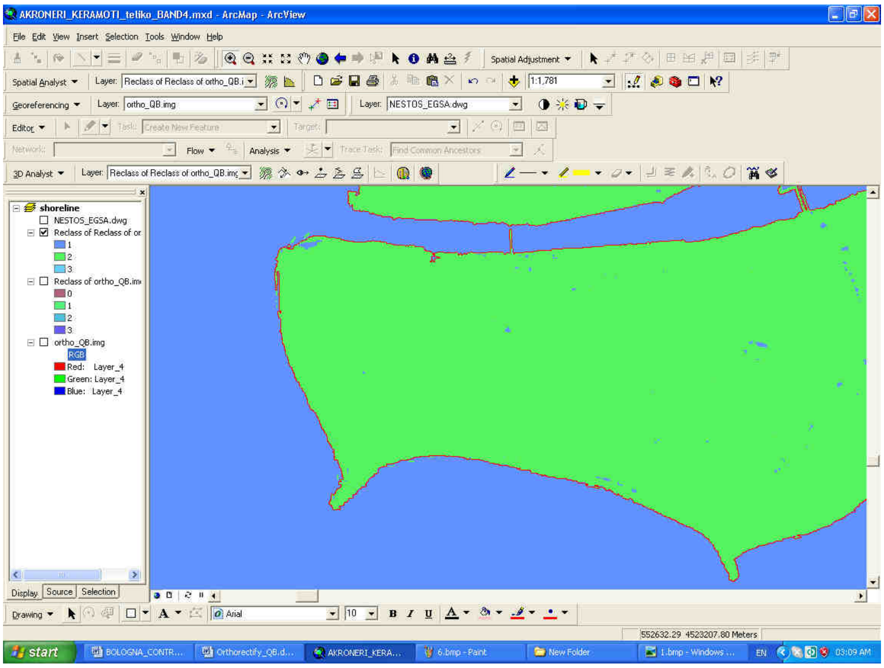

Figure 70: Automatically drawn contour representing shoreline on top of Classification Result.

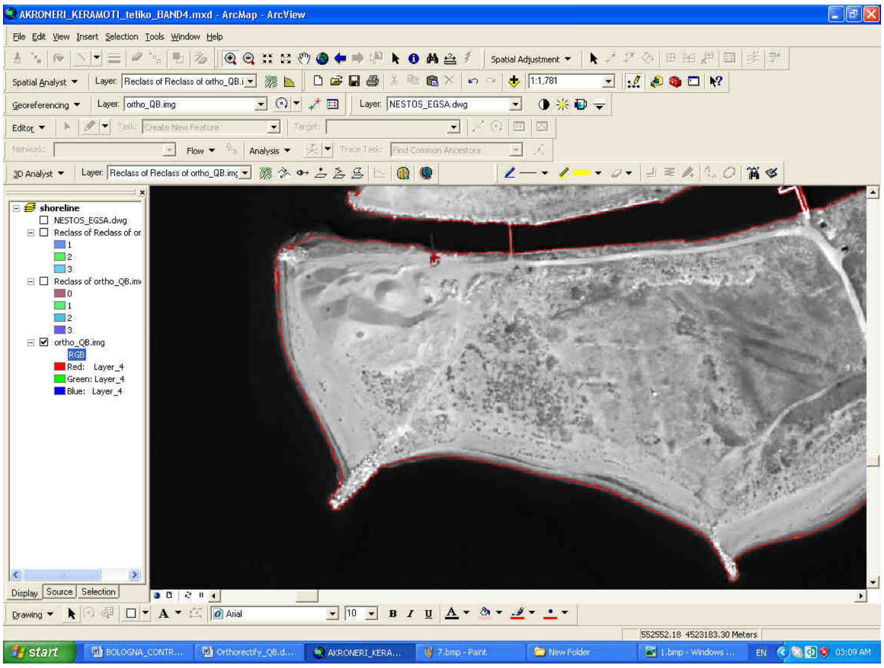

Figure 71: Automatically drawn contour representing shoreline on top of Infrared Band of the image.

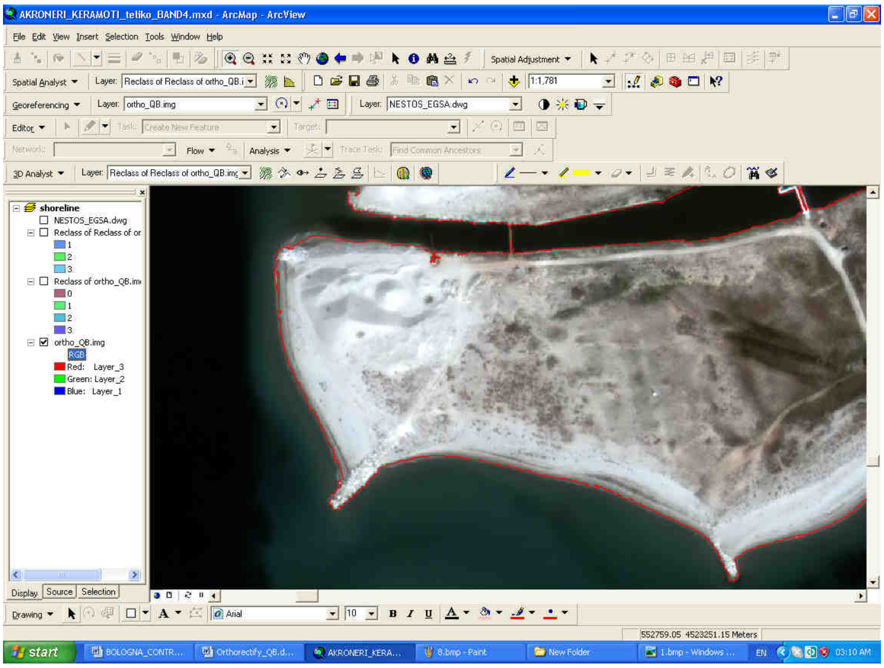

Figure 72: Automatically drawn contour representing shoreline on top of Panchromatic Image (Colour Composite).

The following figures show how the automatically created shoreline is drawn at water-rock interfaces and at water-concrete interfaces (Figures 73 and 74).

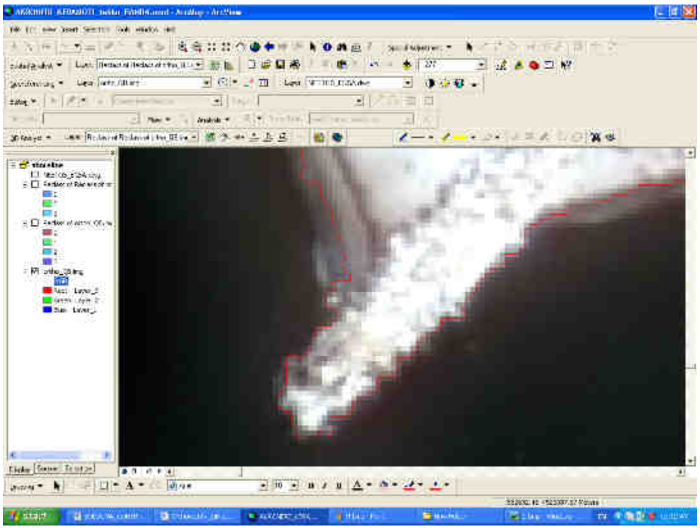

Pixel Dimensions
0.6x0.6m

Figure 73: Automatically drawn contour representing shoreline at a water-rock interface (In a shore protection construction).

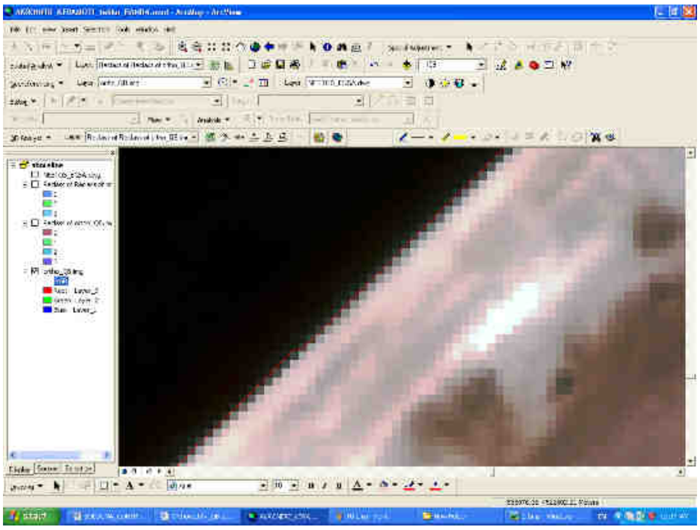

Pixel Dimensions
0.6x0.6m

Figure 74: Automatically drawn contour representing shoreline at a water-concrete interface (In a port area).

Present shoreline Definition (2006 Shoreline Extraction)

Present Shoreline Definition is done using high resolution GPS Surveying. Some main steps are illustrated in the following figures (Figures 75, 76 and 77).

Figure 75: Static GPS receiver placed at a known reference point installed by the Military Geographic Service of Greece (Static receiver).

Figure 76: Movable GPS receiver for shoreline delineation (Rover receiver).

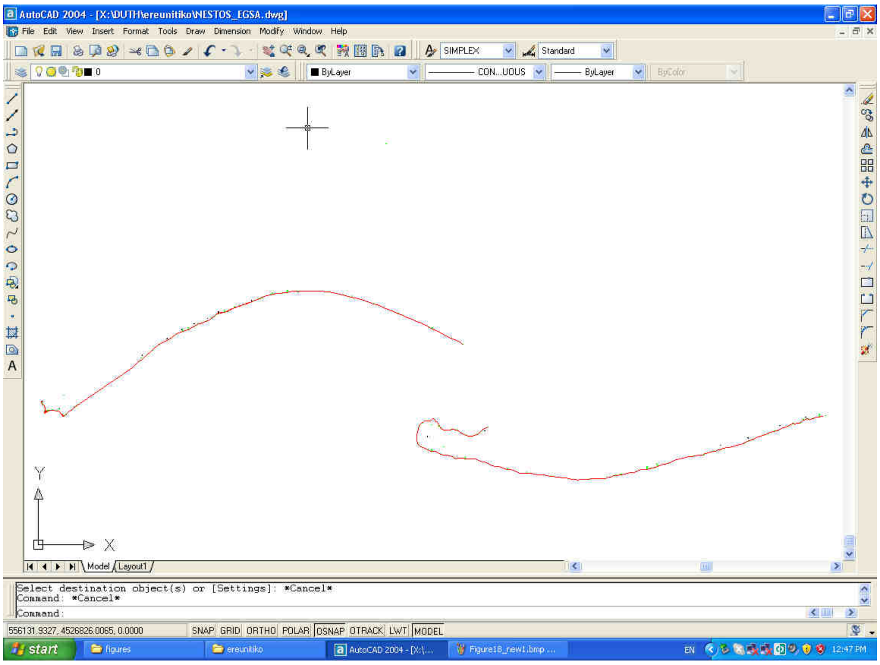

Figure 77: Extracted Shoreline from GPS measurements (2006).

Comparison of 2002 (QB) Shoreline with 2006 (D-GPS) Shoreline

The 2006 extracted shoreline from the D-GPS Measurements can now be placed as a new layer in the GIS database where the 2002 shoreline from the Quickbird images is shown. Hence, comparisons and measurements in order to obtain quantitative and qualitative results can be made. The following figures illustrate two areas where erosion and accretion are dominant (Figures 78 and 79).

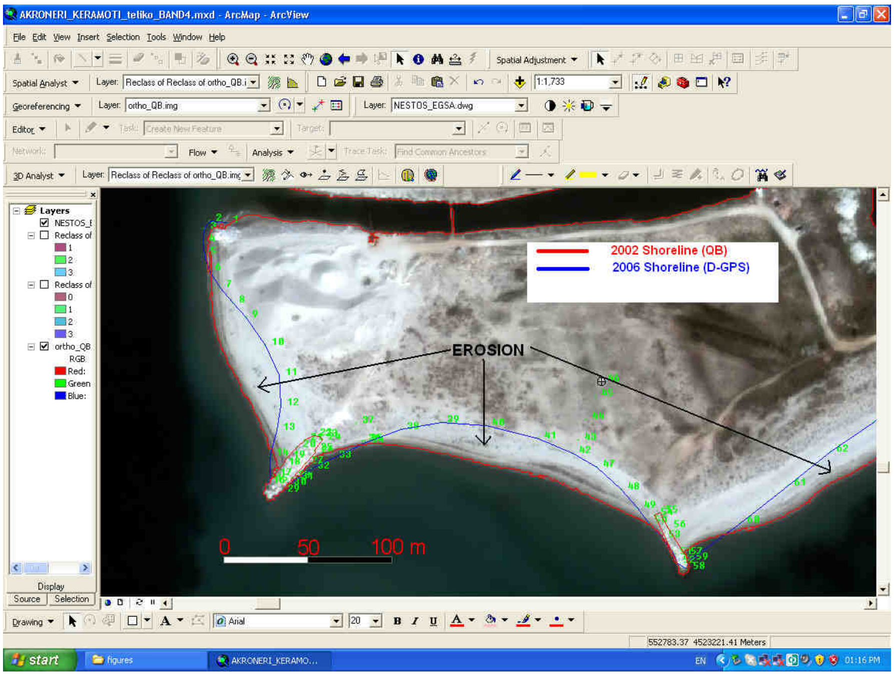

Figure 78: Extracted Shoreline from GPS measurements (Blue Line) on top of the satellite image and automatically drawn shoreline (Red Line).

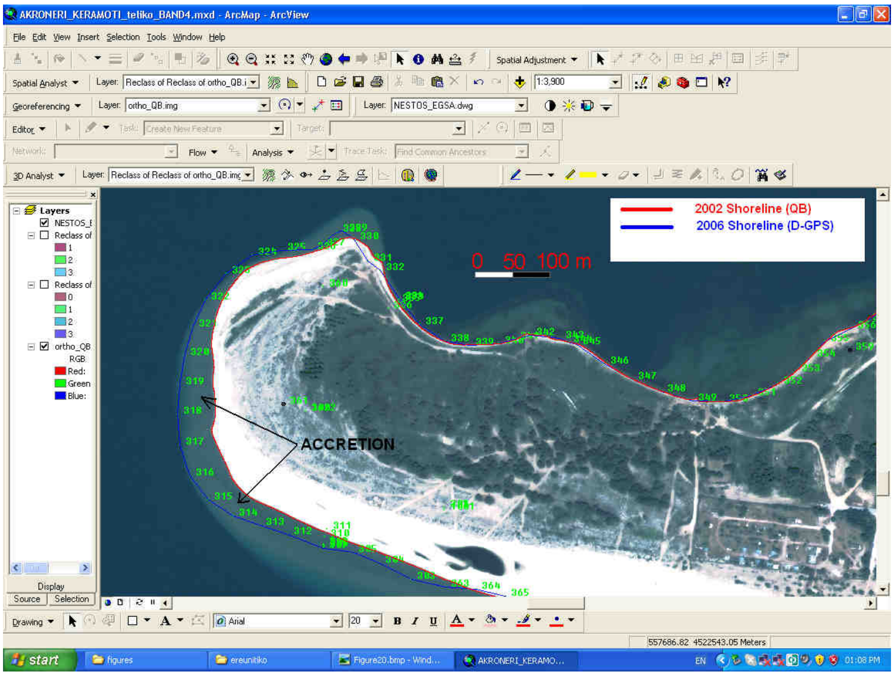

Figure 79: Extracted Shoreline from GPS measurements (Blue Line) on top of the satellite image and automatically drawn shoreline (Red Line).

The cost of the chosen methodology for shoreline evolution monitoring is analysed in Table 12.

Table 12: Cost of adopted methodology

Applications	Shoreline Length (km)	Cost (€) for 5 km/year	Cost (€) for one km /year
Orthorectified Quick Bird Images	5	2500	500
D-GPS Measurements (one working day/season)	5	1500	300
Post Prossesing	5	1000	200
TOTAL	-	5000	1000

Hence, from the table above it is concluded that the average cost of the adopted methodology is 1000 €/km. This includes the cost of obtaining once per year one orthorectified satellite image, and the cost of four *in situ* measurements per year using high precision D-GPS. Clearly the chosen methodology is economical, accurate, and appropriate for this region. Furthermore, the proposed method is fairly easy to apply and gives satisfactory results for the shoreline evolution monitoring of the region of East Macedonia and Thrace in Greece.

P10 - ICM

Ruth Durán (rduran@icm.csic.es), David Casas (davidc@icm.csic.es), Belén Alonso (belen@icm.csic.es), Ana Bernabeu (bernabeu@uvigo.es), Farran Estrada (festrada@icm.csic.es), Gemma Ercilla (gemma@icm.csic.es), Marcel.li Farran (mfarran@icm.csic.es)

During the phase B, the Institute of Marine Sciences of Barcelona (ICM- CSIC) has defined field measures and it has developed the methodological test and evaluation of the two methodologies proposed: (a) the high resolution seismic data for the characterisation of the existing sedimentary bodies such as littoral prisms, their thickness, lateral variability and morphosedimentary evolution; and (b) the application of numerical models for the prediction of morphodynamic evolution of dredge and nourishment areas.

High resolution seismic data

High resolution seismic profiles have been used to characterise the littoral prism (thickness, extension, volume) of the study area, and the GeoPulse Boomer System has been chosen.

The GeoPulse Boomer (Fig. 80) is a widely seismic system used for high resolution, deep penetration profiling in both deep ocean and shallow coastal environments. GeoPulse offers a flexible high resolution solution and it also provides up to three times the acoustic energy of conventional profiling systems while operating in very shallow water and in high noise environments.

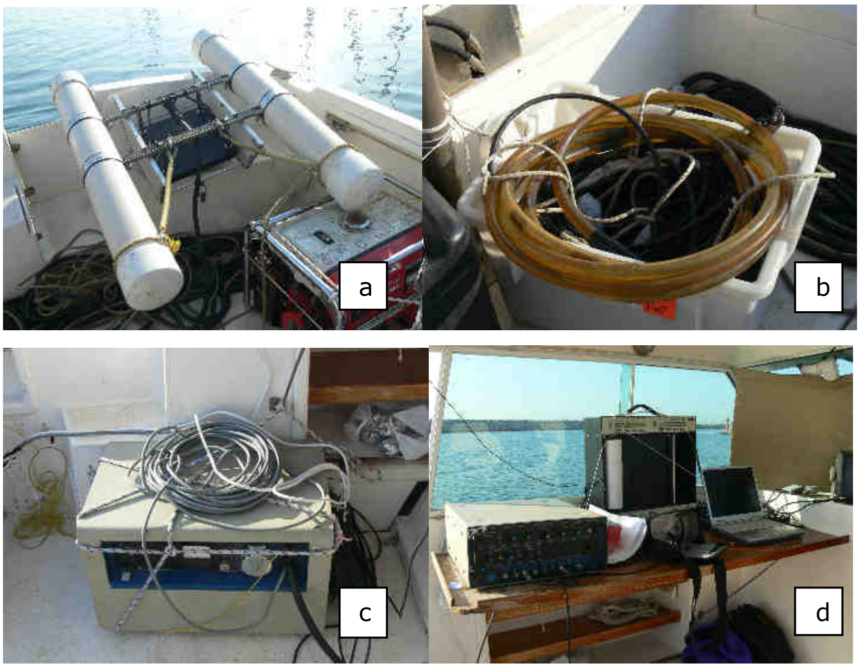

Figure 80: The basic seismic system includes different parts: (a) Boomer plate mounted on a Catamaran; (b) Hydrophone; (c) Power Supply; and (d) Receiver and EPC graphic recorder.

The basic seismic system characteristics are described in the phase B report for Beachmed-e sub-project GESA, but as general features we can underline:

- Deep penetration in wide variety of sub-bottom structures;

- Good shallow water performance;
- Easy to operate and install (it can be deployed by one-two people);
- Rugged and reliable;
- Proven method.

In this way, the field measures has been conduced during phase B in the study area of Masnou (Maresme-Barcelona) and they are described in the GESA phase B report.

Methodological test and evaluation

The main objective getting seismic profiles is the interpretation of seismic units to define the cartography of sand bodies (littoral prisms) and their thickness, lateral variability and morphosedimentary evolution. This is performed by the identification of concordant reflections separated by discontinuity surfaces (Vail, 1977). The definition of geological environment and litho-seismic units (Fig. 81) can be done following some criteria:

- Identification of discontinuity surfaces on the top and the base, which can be correlated between profiles; and
- Identification of the internal reflection characteristics that allow to define the development of the sedimentary units (geometry, continuity, amplitude and frequency). Therefore, to carry out this work it is necessary to get enough spatial resolution and penetration.

Taking into account previous seismic works (Medialdea et al, 1989) with similar geologic settings than the study area (littoral environment, coarse sediment, etc.) the GeoPulse boomer compared with other seismic systems, e.g. 3.5 kHz (Fig. 82), has a better performance in terms of resolution and penetration.

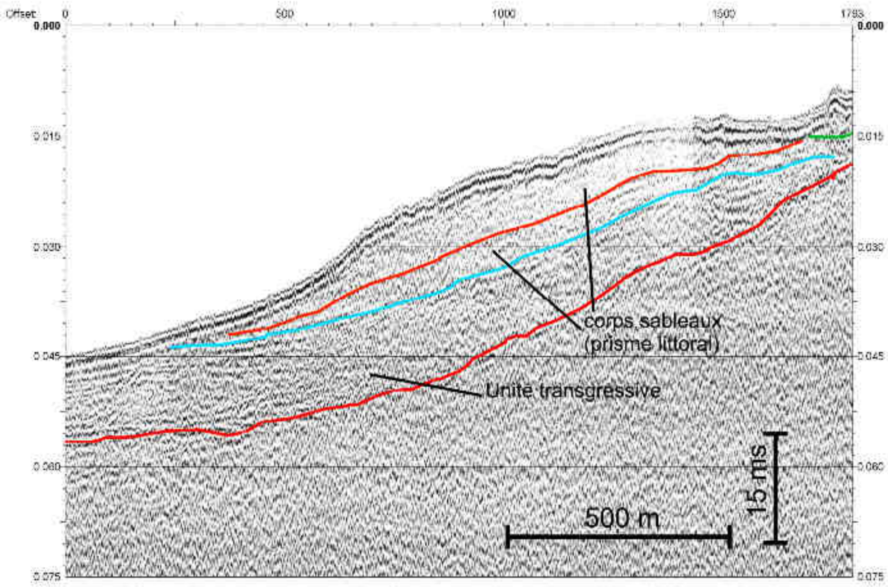

Figure 81: Seismic profile recorded in the Masnou area (Maresme, Catalunya) with the Geopulse Boormer System, where different seismic units can be differentiated.

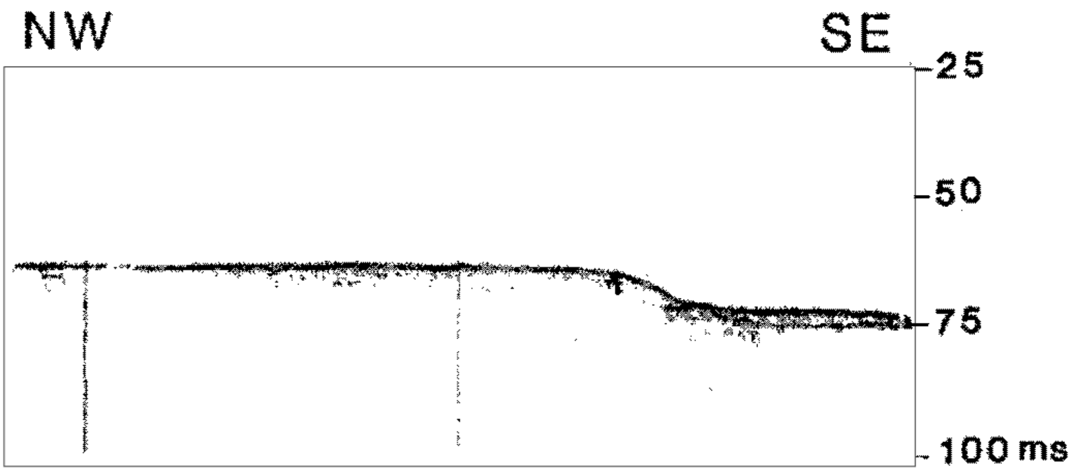

Figure 82: Example of 3.5 kHz profile recorded in a similar geologic setting of the study area.

The spatial resolution and penetration depend of the several variables equilibrium, but maybe the most important are the power of seismic source (Fig. 83) and the shot rate. During the period of the seismic in-situ tests, several settings have been tried, but two configurations showed acceptable results in terms of resolution, penetration and performance:

A power of 350 J and a shot rate of 0.5 s in the first case and 455 J and 0.75 s in the second one were used, although the second showed a better response regarding the intense acoustic noise present in the study area.

With these configurations a resolution between 0.75 m and 1m and a penetration of about 20 m has been obtained. In both cases a recording window of 150 ms was enough to register all acoustic signals available.

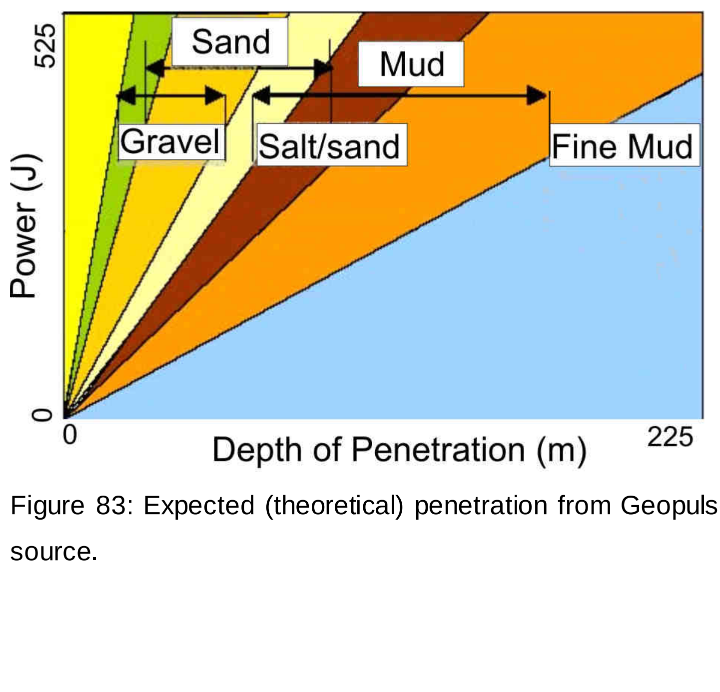

Figure 83: Expected (theoretical) penetration from Geopulse, which is correlated with the power of seismic source.

Coastal Modelling System

In this project, the "Coastal Modelling System" (SMC) is considered to be validated by checking their results with real data. For this propose, the beach nourishment performed on the Masnou (Maresme, Catalunya) during the last year (2006) was monitored. The morphodynamic model included in the SMC is used to predict the nourished beach behaviour during this period. It is proposed for estimating the efficiency and the durability of a nourishment plan on sandy beaches.

In this context, the methodological approach designed for the phase B includes the methodological test of the models and the acquisition of field measures. These field measures constitute the data input of the numerical models and they are used in this phase in the methodological test (Fig. 84).

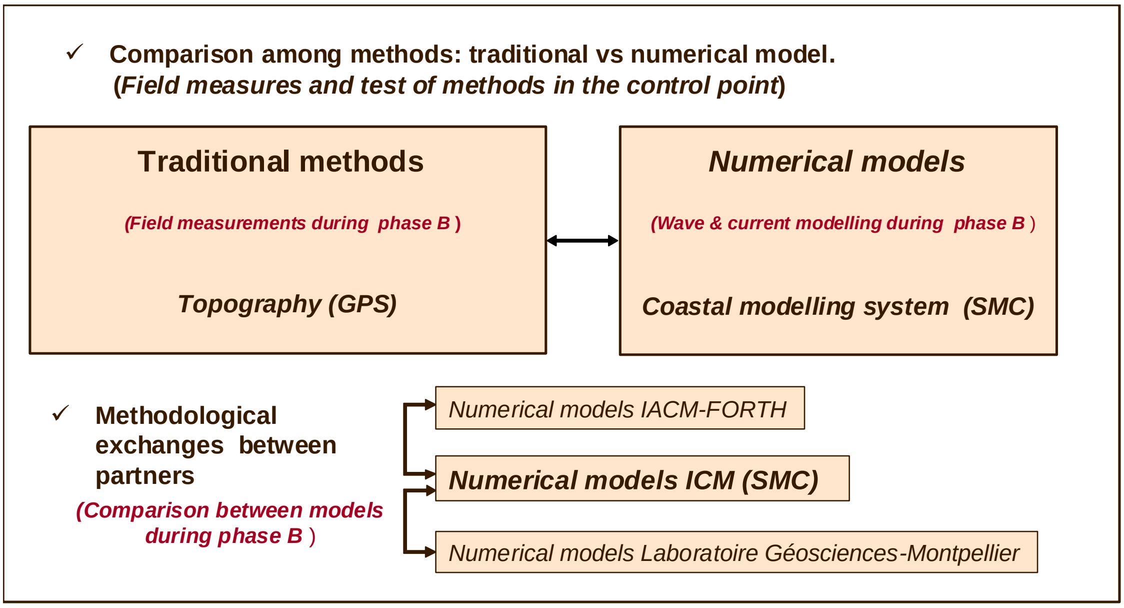

Figure 84: Methodological approach developed during phase B in order to check the accuracy of the method. It includes the acquisition of field data, the test of the method and the methodological exchanges between partners.

Methodological test and evaluation

Previous works show that the process-based models are not completes suitable for detailed modelling of the beach profile evolution close to the shoreline. Van Rijn et al (2003) showed that process-based models providing more accurate results for hydrodynamics than for morphodynamics either at storm or seasonal time scales. But they are very useful in the description of the swash zone and the wave-related sediment transport for shelf-beach protection purposes (Hamm et al, 2002). 2DH hydrodynamic models coupled with sediment transport models can be used to predict nourishment time evolution and to define areas of sand erosion and accumulation close to harbours. Due to their predictive character, they may provide a valuable contribution to the design process (Hamm et al, 2002; Capobianco et al, 2002). Erosion sequences are usually well and reliably reproduced since erosion is dominated by the undertow dynamics under strong wave climates.

For testing the 2DH hydrodynamic and sediment transport models included in the SMC, the results of the models are compared with real data in the Masnou harbour (Maresme, Catalunya). The spatial distribution of sediment transport vectors and the changes in the coastline predicted by the model are compared with the topography and bathymetry obtained with traditional methods.

Field measures

Because numerical models must be periodically verified by field measurements to ensure that each model is producing accurate results, field measurements have been acquired. These data constitute the data input of the numerical models and they will be used for checking the model. The database includes periodical topographies and bathymetries in the study area supported by the Generalitat of Catalunya (March 2006, June 2007, November 2006 and May 2007), long time series of wave climate from National Ports and sediment samples (November 2006 and June 2007, Fig. 85). All of these data have been collected during phase B, although the last bathymetry is still being processed.

The methods used in the topographic and bathymetric surveys are described in the GESA phase B report. They included the use of dGPS and multibeam. The sediment samples have been collected by using a Van-Veen and a vibro-corer in the nearshore. The analysis of long-time series of wave allows defining different wave forcing scenarios which are considered in the hydrodynamic model. Wave data shows two predominant wave directions E-NE and SSW with maximum significant height from the E and ENE (Fig. 85).

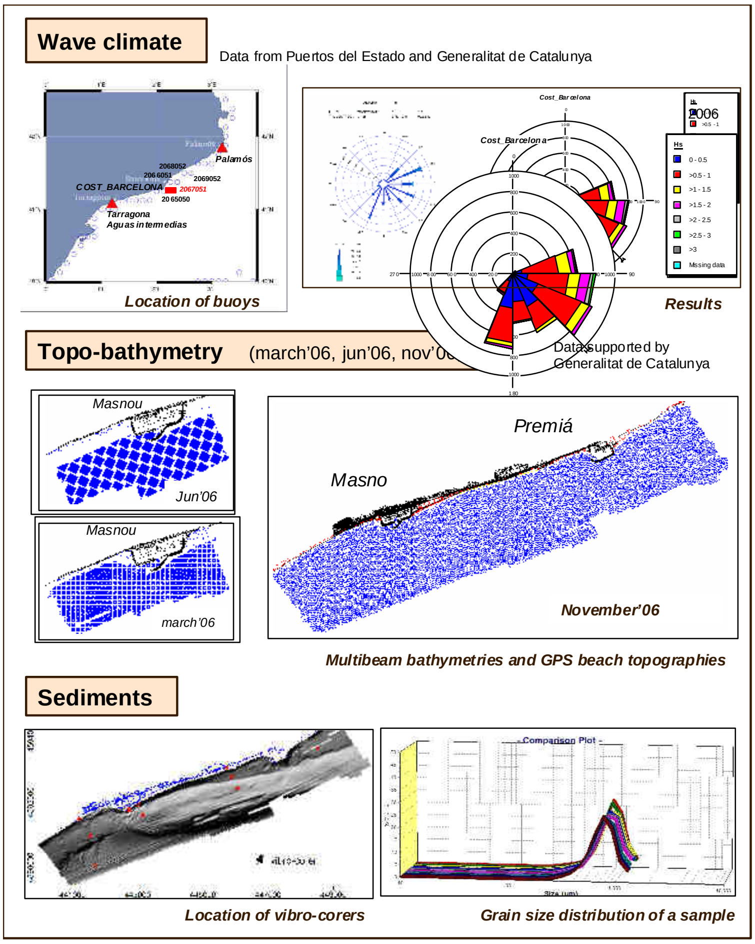

Figure 85: Field measures and data collected during phase B.

Test of methodology

The numerical models included in the Coastal Modelling System (SMC) have been applied for the morphodynamic evolution of coastal areas. The methodological approach considers different phases which include the hydrodynamic and morphodynamic.

In relation to the hydrodynamic, mild slope parabolic model for wave propagation (Kirby and Dalrymple, 1983) and 2DH current model (Basco, 1983; De Vriend et al, 1993) have been applied (see Beachmed-e Hydroreview[1] report for model description) in the Masnou harbour (Maresme, Catalunya). Because different scenarios have been reproduced, an exhaustive analysis of wave climate data during the last year has been performed during this phase B (Tab. 13). It allows describing the hydrodynamic conditions in the study area during the last years when monitoring has been performed with field measures.

Table 13: Wave forcing scenarios defined from long time series of wave data.

Wave direction	Maximum waves			Mean waves	
	ENE	SSW	E	ENE	SSW
Hs (m)	3.5	3.5	3.5	0.5	0.5
T (s)	9	9	9	4	4

The results of the hydrodynamic model show higher waves in areas of the coastline, mainly in the southern beach of the harbour (see example in Fig. 86), in a scenario of stronger conditions (E, Hs: 3.5 m and T: 9s; ENE, Hs: 3.5 m and T: 9s; SSW, Hs: 2.5 m and T: 8s).

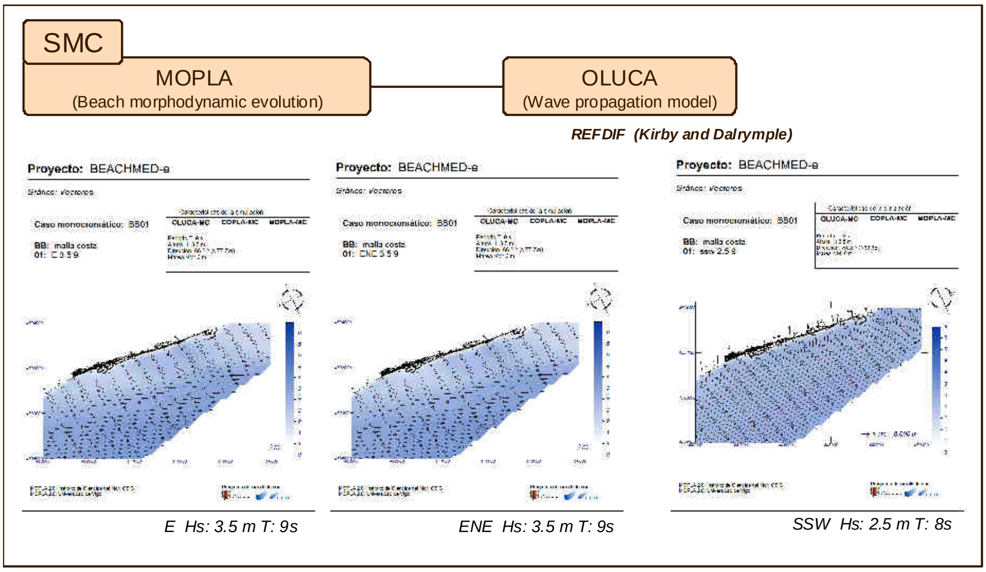

Figure 86: Results of the REF-DIF numerical model. It shows the magnitude and direction of waves. It includes the results obtained during the phase B for maximum waves (E, Hs: 3.5 m and T: 9s; ENE, Hs: 3.5 m and T: 9s; SSW, Hs: 2.5 m and T: 8s).

[1] The Hydroreview group is an "inter-group" that is transversal to different sub-projects gathering partners that are applying or developping Numerical Modelling to coastal studies. This group is headed by Dr. Bouchette, from Beachmed-e' sub-project NAUSICAA (measure 2.2).

These oblique waves induce important longshore currents towards the southern which are stronger in the middle part of the beach. The longshore currents are stronger with higher wave angles (Fig. 87). ENE waves provoke stronger longshore currents which are more important in the northern beach. The longshore currents due to SSW waves are also important mainly in the harbour.

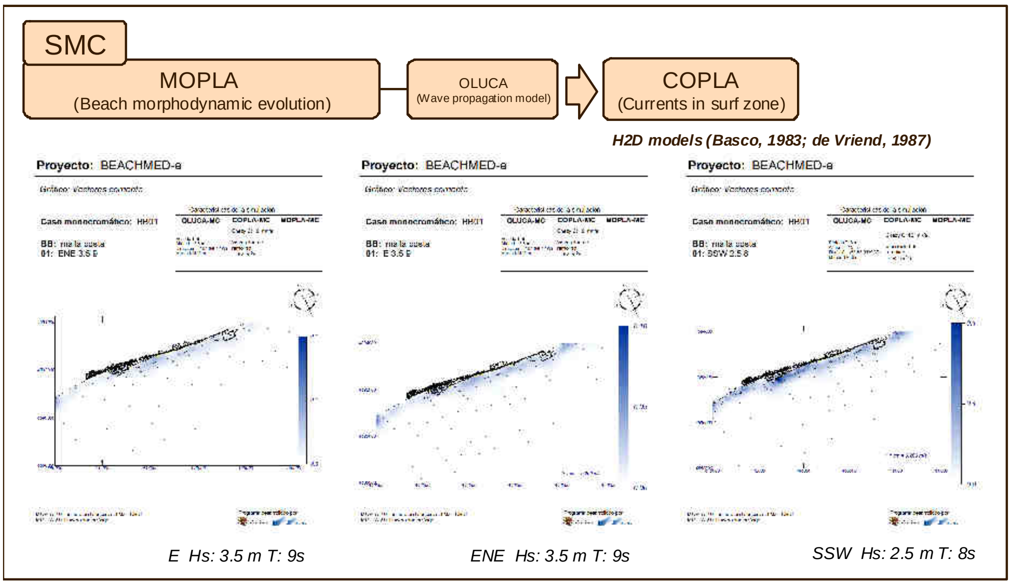

Figure 87: Results of the H2D numerical model. It shows the magnitude and direction of waves-induced currents for different scenarios (E, Hs: 3.5 m and T: 9s; ENE, Hs: 3.5 m and T: 9s; SSW, Hs: 2.5 m and T: 8s).

The output data of the hydrodynamic model constitutes the input dataset for the erosion/sedimentation model (Fig. 88). It defines areas of erosion and accumulation along the coastline. The areas of erosion are more important where waves and currents are stronger.

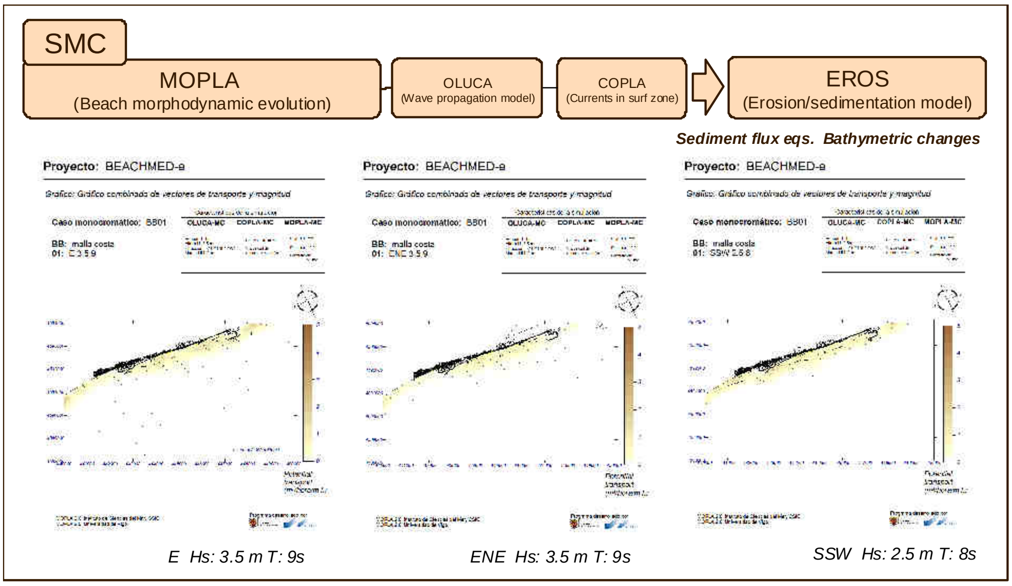

Figure 88: Results of the erosion/sedimentation numerical model. It shows the magnitude and direction of waves-induced currents for different scenarios (E, Hs: 3.5 m and T: 9s; ENE, Hs: 3.5 m and T: 9s; SSW, Hs: 2.5 m and T: 8s).

The results of the numerical model have been compared with the beach topography obtained just after the nourishment (June 2006) and six months after (November 2006). The first tests of the model have shown good results in the prediction of beach evolution. Real data show that coastline regression is more important in the southern area of the harbour where potential transport is lower (Fig. 89). The accumulation of sand in the beach located updrift is predicted by the model according to the stronger currents and a higher sediment transport.

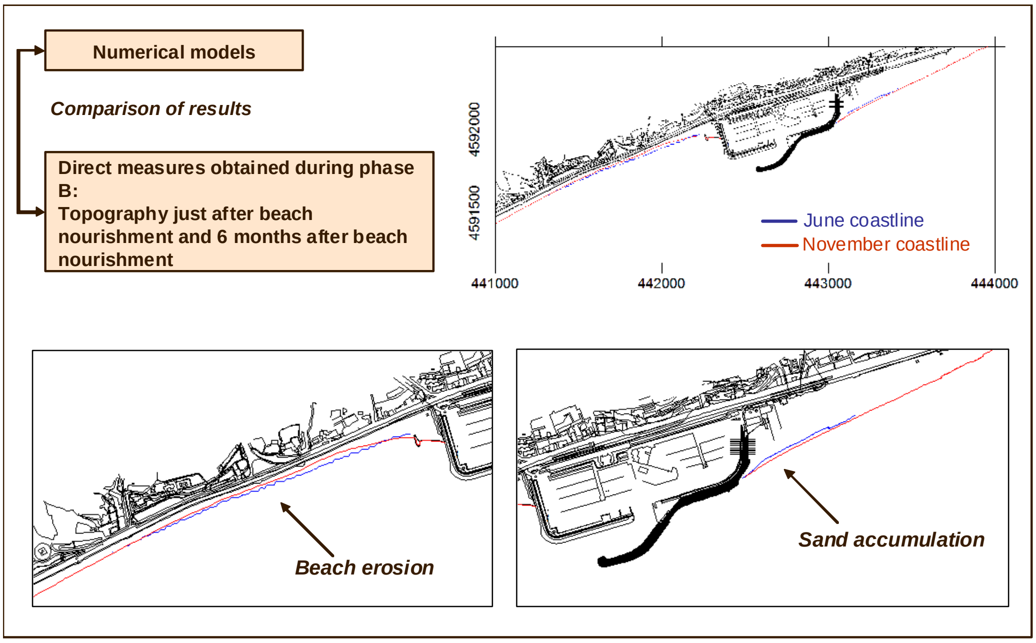

Figure 89: Coastal regression in the southern part of the harbour and sand accumulation in the northern area since the nourishment in April-May 2006.

The future work for the phase C includes the monitoring of a nourishment beach during one year (June 2006-June 2007). The model considers the wave scenarios defined from this year climate wave and its results will be compared with the topography and bathymetry performed one year after nourishment.

There are two partners working with numerical models in this project, ICM and IACM-FORTH. Both of them use models based on the mild slope equation (Lee & Wang, 1992) but with some differences (Fig. 90). ICM uses a model that is based on the mild slope parabolic model for wave propagation. It includes refraction and diffraction but no reflection and needs a little computation time. IACM-FORTH uses the mild slope hyperbolic model which includes the refection but needs a high computation time. There are some works regarding on the differences, advantages and disadvantages between these two models (Lee and Wang, 1992). After a first comparison between the models, the next work during the phase B will be to compare them with real data in order to define their accuracy.

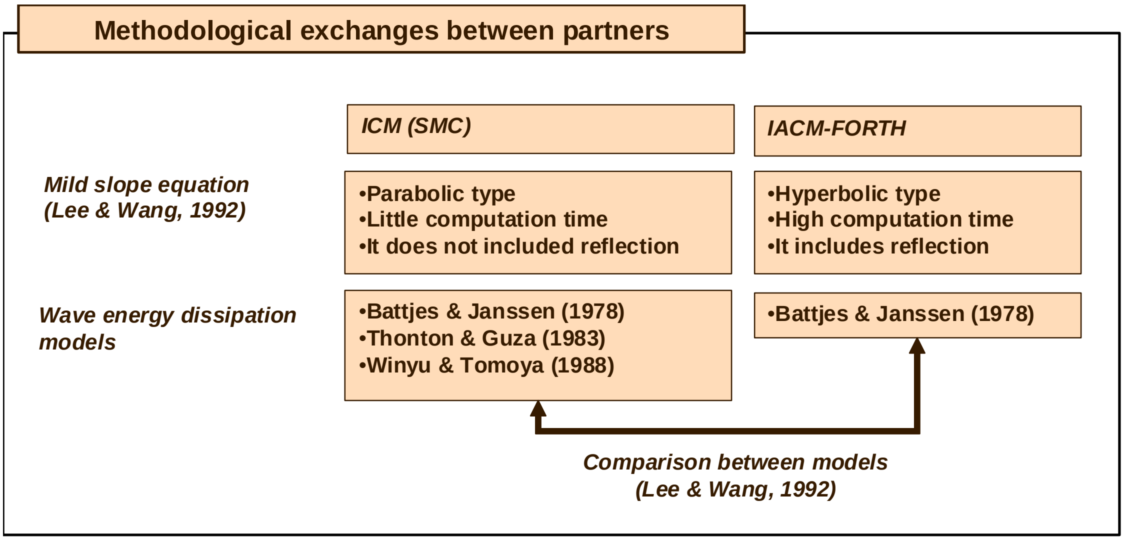

Figure 90: Main results of comparison between the models used by both partners.

The evaluation of the model in the dredge has not been complete positive. The mild slope parabolic model for wave propagation included in the SMC considers a gentle and homogeneous bottom slope (Kirby and Dalrymple, 1983). It is a great restriction on the applicability of this equation for dredged areas where slope is about 1:2 to 9. To resolve it we are working with another partner of the Beachmed Hydroreview Group, the Laboratoire Géosciences-Montpellier. They will test their process-based model in the same study area considering the same input data and scenarios.

References

Abdel-Aziz YI and Karara HM (1971) Direct linear transformation from comparator coordinates into object space coordinates in close-range photogrammetry. In Proc. ASP/UI Symp. Close-Range Photogrammetry, Urbana, IL. pp.1-18.

Albertazzi C, Archetti R, Armaroli C, Ceroni M, Ciavola P, Lamberti A and Medri S (2003) The Coastview Project. In: E. Ozhan (Ed) Proc. of the VI MEDCOAST International Conference on the Mediterranean Coastal Environment, 7 – 10 October 2003. Ravenna. Italy. pp 235 – 246.

Alexander PS and Holman RA (2004) Quantification of nearshore morphology based on video imaging. *Marine Geology*, 208: 101-111.

Basco DR (1983) Surf-Zone Currents. *Coastal Engeneering*, 7: 331-357.

Battjes JA and Janssen JPFM (1978) Energy Loss and set-up due to breaking of random waves. Int. Conf. on Coastal Engineering '78, ASCE. pp. 569-587.

Battjes, JA (1995) Modelling of turbulence in the surf zone. Proc. Symp. Modelling Techniques, California, ASCE, pp. 1050-1061.

Beachmed (2005) Le projet Beachmed : Récupération environnementale et entretien des littoraux en érosion avec l'utilisation des depots sablonneux marins (Convention 2002-01-4.3-I-028) – 3ème cahier technique (phase C). Roma, 324 pp.

Beachmed-e (2007) La gestion stratégique de la defense des littoraux pour un développement soutenable des zones côtieres de la Méditerranée. 1er Cahier Technique Phase A. Regione Lazio. Roma, 152 pp. 2eme Edition.

Borah DK and Balloffet A (1985) Beach evolution caused by littoral frift barrier. *J. of Waterway, Port, Coastal and Ocean Eng*., ASCE 111(4): 645-660.

Briad MHG and Kamphuis JW (1993) Sediment transport in the surf zone: a quasi 3-D numerical model. *Coastal Engineering*, 20:135-156.

Broker I (1995) Coastal area modelling. MAST 68-M Final Workshop. Gdansk, Poland. pp. 2-86 to 2-90.

Broker I, Johnson HK, Zyserman JA, Ronberg JK, Pedersen C, Deigaard R and Fredsoe, J (1995) Coastal profile and coastal area morphodynamic modelling. MAST 68-M Final Workshop. Gdansk, Poland. Pp. 7-12 to 7-16.

Bruun P (1985) Design and Construction of Mounds for Breakwaters and Coastal Protection, Elsevier, New York.

Cáceres AM (2002) El desarrollo de índices e indicadores como ayuda a la gestión de costas. M.Sc.Thesis, ETSECCPB, Universitat Politécnica de Catalunya.

Capobianco M, Hanson H, Larson M, Steetzel H, Stive MJF, Chatelus Y, Aarninkhof S and Karambas T (2002) Nourishment design and evaluation: applicability of model concepts. *Coastal Engineering*, 47 (2): 113-135.

Copeland GJM (1985a) A practical alternative to the «mild-slope» wave equation. *Coastal Engineering*, 9:125-149.

Copeland GJM (1985b) Practical radiation stress calculations connected with equations of wave propagation. *Coastal Engineering*, 9: 195-219.

Cowell PJ, Roy PS and Jones RA (1995) Simulation of large-scale coastal change using a morphological behaviour model. *Marine Geology*, 126: 45-61.

Davidson MA, Aarninkhof SGJ, Van Koningsveld M, Holman RA (2004) Developing coastal video monitoring systems in support of coastal zone management. *Journal of Coastal Research*, SI 39: pp.

Davidson MA, Van Koningsveld M, de Kruif A, Rawson J, Holman R, Lamberti A, Medina R, Kroon A and Aarninkhof S (2007) The CoastView project: Developing video-derived Coastal State Indicators in support of coastal zone management. *Coastal Engineering*, 54 (6-7): 463-475.

De Vriend, HJ, Zyserman J, Nicholson J, Roelvink JA, Pechon P, Southgate HN (1993) Medium-term 2DH coastal area modelling. *Coastal Engineering*, 21: 193-224.

Dean RG (1991) Equilibrium beach profiles: characteristics and applications. *Journal of Coastal Research*, 7: 53-84.

Dean RG (1998) Beach nourishment: a limited review and some recent results. Proc. 26th ICCE, ASCE. pp. 45- 69.

Dean RG (2002) Beach nourishment: Theory and Practice. World Scientific Publishing Co. New Jersey, 399 pp.

Elko NA, Holman RA and Gelfenbaum G (2005) Quantifying the Rapid Evolution of a Nourishment Project with Video Imagery. *J. Coastal Research*, 21 (4): 633-645.

Fraser CS, Baltsavias E and Gruen A (2002b) Processing of IKONOS imagery for sub-metre 3D positioning and building extraction. *ISPRS Journal of Photogrammetry and Remote Sensing*, 56, 177–194.

Fraser CS, Hanley HB and Yamakawa T (2002a) Three-dimensional geopositioning accuracy of IKONOS imagery. *Photogrammetric Record*, 17: 465–479.

Guillén J, Chic O, Ojeda E, Palanques A and Aarnikhoff S (2003) Monitorización de las playas de la ciudad de Barcelona utilizando imágenes de video: evolución de la línea de costa en respuesta a temporales y regeneración artificial (2001-2002). In: M. Lasada & M. Castillo (Eds) VII Jornadas Españolas de Ingeniería de Costas y puertos. Libro de resumenes. pp. 254-256.

Hamm L, Capobianco M, Dette HH, Lechuga A, Spanhoff R and Stive MJF (2002) A summary of European experience with shore nourishment. *Coastal Engineering*, 47 (2): 237-264

Holland KT, Holman RA, Lippmann TC, Stanley J and Plant N (1997) Practical use of video imagery in nearshore oceanographic field studies. *IEEE Journal of Oceanic Engineering*, SI 22 (1): 81-92.

Holman RA and Stanley J (2007) The history and technical capabilities of Argus. *Coastal Engineering*, 54 (6-7): 477-491.

Holman RA, Stanley, J and Ozkan-Haller T (2003) Applying video sensor networks to nearshore environment monitoring. *Oceanography*, 6(3): 78-85.

http://videomonitoring.eu.org/igea

James JR (1975) Techniques in Evaluating Suitability of Borrow Material for Beach Nourishment. U.S. Army Coastal Engineering Research Center, Technical Memorandum, 60, Vicksburg, MS.

Kaichang D, Ruijin M, Jue W and Ron L (2003a) Automatic Shoreline Extraction from High-Resolution IKONOS Satellite Imagery. ASPRS Annual Conference Proceedings. May 2003 Anchorage. Alaska.

Kaichang D, Ruijin M, Jue W and Ron L (2003b) Coastal Mapping and Change Detection Using High-Resolution IKONOS Satellite Imagery. National Conference for Digital Government Research. Boston. MA. pp. 343-346.

Karambas Th V, Southgate HN and Koutitas C (1995) A Boussinesq model for inshore zone sediment transport using an energetics approach. Coastal Dynamics ’95. Gdansk. pp. 841-849.

Karambas ThV (1998) 2DH non-linear dispersive wave modelling and sediment transport in the nearshore zone, Int. Conf. on Coastal Engineering, ASCE. Copenhagen.

Karambas ThV and Bowers EC (1996) Representation of partial wave reflection and transmission for rubble mound coastal structures. Hydrosoft 96, Malaysia.

Karambas ThV and Kriezi EE (1997) Wave Reflection and Transmission for Submerged Monolithic Breakwaters. In: Anagnostopoulos P, Carlomagno GM and Brebbia CA (Eds) Computational Methods and Experimental Measurements. CMEM 97, Computational Mechanics Publications. Southampton, UK and Boston, USA. pp 544-550.

Kirby JT and Dalrymple RA (1983) A Parabolic Equation for the Combined Refraction-Diffraction of Stokes Waves by Mildly Varying Topography. *J. Fluid Mech.*, 136: 543-566.

Koutandos EV, Karambas ThV, Koutitas CG and Prinos PE (2002) Shoreline changes in presence of a floating breakwater. International Conference ‘Protection and Restoration of the Environment VI’., Skiathos, Greece. Vol. I. pp. 403-410.

Larsen J and Dancy H (1983). Open Boundaries in Short Wave Simulations - A New Approach. *Coastal Engineering*, 7: 285-297.

Lee JL and Wang H (1992) Evaluation of Numerical Models on Wave-Current Interactions. Proceedings of the 23th International Conference on Coastal Engineering, ASCE. Venice. pp. 432-446.

Leica (2005) ERDAS Field Guide. Leica Geosystems. Atlanta, Georgia, USA.

Leont’yev IO (1996) Numerical modelling of beach erosion during storm event. *Coastal Engineering*, 29: 187-200.

Leont’yev IO (1997) Short-term changes due to cross-shore structures: a one-line numerical model. *Coastal Engineering*, 31: 59-75.

Leont’yev IO (1999) Modeling of morphological changes due to coastal structures. *Coastal Engineering*, 38: 149-166.

Lesaignoux A (2006) Modélisation et simulations de trains d'ondes LiDAR "vert": application à la détection de faibles lames d'eau en rivière". Master's Thesis, UMII

Medialdea J, Maldonado A and Medialdea T (1989) Mapa Geológico de la Plataforma Continental Española y Zonas Adyacentes (1:200.000). Hoja de Barcelona 35-42E. Instituto Tecnológico Geominero de España.

Milli M and Surace L (2006) Tecniche innovative e tradizionali a confronto nella realizzazione di rilievi batimetrici costieri: un caso di studio. *Bollettino SIFET,* 2/06: 20

Monti C, Guerra F, Balletti C and Miniutti D (1999) Geometric operations in digital images. Atti XVI International Symposium CIPA. Holland.

PCI (2003) OrthoEngine User Guide, PCI Geomatics, Ontario, Canada.

Preti M, Lamberti A, Martinelli L, Albertazzi C and Sammarini S (2005) An effort toward renaturalisation of Igea Marina beach: transformation of 6 emerged barriers into a single low crested structure. In: E. Özhan (Ed) Proc. MedCoast 2005 (Kusadasi, Turkey). pp. 919-930.

Price DM, Chesher TJ and Southgate HN (1995) PISCES: A Morphological Coastal Area Model. Report SR 411. Wallingford, U.K. HR Wallingford.

Roelvink JA, Reniers AJHM and Walstra DJR (1995) Medium term morphodynamic modelling. MAST 68-M Final Workshop., Gdansk, Poland. 7-3 to 7-6.

Stive MJF and Wind HG (1986) Cross-shore flow in the surf zone. *Coastal Engineering* 10: 325-340.

Swales A (2002) Geostatistical estimation of short-term changes in beach morphology and sand budget. *Journal of Coastal Research*, 18(2):338-351.

Tortora P (1991) Calcolo del volume di inerti nel ripascimento artificiale delle spiagge. *Rendiconti Società Geologica Italiana*, 14: 181-184.

Toutin Th (2003a) Block bundle adjustment of Ikonos in-track images. *International Journal of Remote Sensing*, 24: 851–857.

Toutin Th (2003b) Error tracking in IKONOS geometric processing using a 3D parametric modelling. *Photogrammetric Engineering and Remote Sensing*, 69: 43–51.

Toutin Th (2004) Review article: Geometric processing of remote sensing images: models, algorithms and methods. *International Journal of Remote Sensing*, 25,1893–1924

Vail PR (1977) Seismic Recognition of Depositional Facies on Slopes and Rises. *AAPG Bulletin-American Association of Petroleum Geologists*, 61 (5): 837-837.

Van Koningsveld M and Mulder JPM (2004) Sustainable coastal policy developments in The Netherlands. A systematic approach revealed. *Journal of Coastal Research*, 20(2): 375-385.

Van Koningsveld M, Stive MJF, Mulder JPM, De Vriend HJ, Ruessink BG and Dunsbergen DW (2003) Usefulness and effectiveness of coastal research: a matter of perception? *Journal of Coastal Research*, 19: 441-461.

Van Rijn LC, Wasltra DJR, Grasmeijer B, Sutherland J, Pan S and Sierra JP (2003) The predictability of cross-shore bed evolution of sandy beaches at the time scale of storms and seasons using process-based Profile models. *Coastal Engineering*, 47 (3): 295-327.

VLS (2007) Feature Analyst Version 4.1 for Imagine. Reference Manual. Visual Learning Systems Inc. Missoula, USA.

www.airbornehydro.com

www.apat.it

www.optech.ca

www.tenix.com

www.wldelft.nl/argus)

Yamamoto Y, Horikawa K and Tanimoto K (1996) Prediction of shoreline change considering cross-shore sediment transport. Int. Conf. on Coastal Engineering 1996. ASCE. pp. 3405-3418.

Annex

Further information on the project (publications)

Brignone M, Corradi N, Ferrari M, Schiaffino CF. Evaluation of a nourishment programme with a webcam: the case of Levanto (La Spezia, Italy). *Chemistry and Ecology* (special issue CONISMA 2006) (submitted).

Davidson M, Van Koningsveld M, de Kruif A, Rawson J, Holman R, Lamberti A, Medina R, Kroon A and Aarninkhof S (2007) The CoastView project: Developing video-derived Coastal State Indicators in support of coastal zone management. Coastal Engineering, 54 (6-7): 463-475.

Durán R, Alonso B, Bernabeu A, Casas D, Ercilla G, Estrada F, Farran M, Nuez M, Vilas F (2007) Estudio de los depósitos de arena litorales en la costa del Maresme (Catalunya). Abstracts from IV Congreso Internacional de Ciencia y Tecnología Marina "Océanos III Milenio". 23-25 May 2007, Madrid.

Durán R, Bernabeu A, Alonso B, Nuez M, Vilas F, Ercilla G and Moyés M (2007) Seguimiento de la zona de dragado frente al puerto de Masnou (Costa del Maresme, Catalunya). Abstracts from IX Jornadas de Ingeniería de Costas y Puertos. 29-30 May 2007, San Sebastián.

http://videomonitoring.eu.org

http://www.beachmed.it/Beachmede/SousProjets/OPTIMAL/tabid/86/Default.aspx

http://www.geo.unifi.it/ricerca/ponline.php

Jiménez JA, Osorio A, Marino-Tapia I, Davidson M, Medina R, Kroon A, Archetti R, Ciavola P and Aarnikhof SGJ (2007). Beach recreation planning using video-derived coastal state indicators. *Coastal Engineering,* 54 (6-7):*507-521.*

Karambas Th V, Koutandos EV and Kampanis NA. ALS-A coastal engineering model for wave propagation, wave structure interaction and bed morphology evolution. XXXII IAHR Congress, Venice, 2007 (accepted).

Karambas Th V, Koutandos EV and Kampanis NA. Integrated numerical simulation of linear wave propagation, wave induced circulation, sediment transport and beach evolution. J. Maritime Engr., (submitted);

Koutandos EV, Kazolea M, Varsos K and Kampanis NA. The project BEACHMED-e, Water Resources Management: New Approaches and Technologies. European Water Resources Association, Chania (accepted);

Kroon A, Aarninkhof SGJ, Archetti R, Armaroli C, Gonzalez M, Medri S, Osorio A, Aagaard T, Davidson MA, Holman RA and Spanhoff R (2007) Application of remote sensing video systems for coastline management problems. *Coastal Engineering,* 54 (6-7):493-505 .

Minorenti V and La Monica GB Analysis of a coastal ecosystem: a low-cost approach. Geoitalia 2007, Sesto Forum Italiano di Scienze della Terra, Rimini 12-14 Settembre 2007 (accepted)

Minorenti V, Bellotti P and La Monica GB (2007) A non conventional and low-cost technique for realization of orthophoto at large scale in coastal ecosystem. Ecological Complexity and Sustainability. Challenges & Opportunities for 21st Century's Ecology. Beijing 22-26 May 2007. Abstract of Ecosummit 2007, p. 314.

Petrocchi E, Salvatore MC, Casacchia R, La Monica GB and Salvatori RM. High resolution remote sensing for shoreline survey and monitoring. Geoitalia 2007, Sesto Forum Italiano di Scienze della Terra, Rimini 12-14 Settembre 2007 (accepted)

Tortora P. A new numerical model for beach nourishment interventions: application for the scenario of Ladispoli Beach (Latium Coast, Italy). Geoitalia 2007, Sesto Forum Italiano di Scienze della Terra, Rimini 12-14 Settembre 2007 (accepted)